

Université du Québec
Institut National de la Recherche Scientifique
Énergie, Matériaux et Télécommunications

**FABRICATION AND INVESTIGATION OF HETEROJUNCTION SOLAR
CELLS BASED ON NEAR INFRARED QUANTUM DOTS AND ONE
DIMENSIONAL NANOSTRUCTURES**

Par

Belete Atomsa Gonfa

Thèse présentée pour l'obtention du grade de
Philosophiae doctor (Ph.D.)
en sciences de l'énergie et des matériaux

Jury d'évaluation

Président du jury et examineur interne	Luca Razzari INRS-EMT
Examineur externe	Pablo Bianucci Concordia University
Examineur externe	Thomas Szkopek McGill University
Directeur de recherche	Dongling Ma INRS-EMT
Codirecteur de recherche	My Ali El Khakani INRS-EMT

ABSTRACT

Solar cell technology, which harvests the solar energy and converts it to direct current electricity, is a viable alternative to provide clean and renewable energy from an abundant source to meet the energy demand of the growing world population in the future. For a solar cell technology to be applicable practically it has to compete with other sources of energy in terms of cost. Furthermore the power conversion efficiency (PCE) of a solar cell is important. Since the discovery of the photovoltaic effect in 1839 by the French scientist Alexandre- Edmond Becquerel [1], various materials and device structures have been investigated resulting in development of devices of high PCE and even commercialized for practical applications. Among figures of merit, for example, single junction devices have achieved a record PCE of 28.3 % [2] and multijunction devices (4 junctions) have achieved a PCE of 46 % [3]. The most widely commercialized single crystalline silicon solar cells have achieved a record PCE of 25.6 %. However, these solar cells are produced at very high processing cost and it is quite necessary to develop solar cells, which can be produced at lower cost and with reasonable PCE so that they can compete with other sources of energy.

The solar cells investigated by a plethora of researchers so far are classified as different generations based on their cost, PCE, device characteristics, and the nature of the materials involved. While the first generation solar cells, such as single crystalline silicon solar cells, achieved high PCE, their price is high. The second generation solar cells have low cost, but their efficiency is low. The concept of the third generation solar cells is later on proposed towards making low cost and high PCE solar cells. Quantum dots (QDs) based solar cells are considered as promising third generation solar cells candidates. Among QDs synthesized by different techniques, colloidal QDs, which are synthesized in solution, are attractive for applications in solar cells because of their easy, low cost synthesis and their low temperature solution processability into solar cell devices. Moreover, they possess several attributes, which endow them high potential to achieve high PCE. QDs are strong absorbers of light due to their high extinction coefficient and thus thin layer of QDs can be used in designing solar cells. The absorption of photons by QDs can be tuned by varying their size thanks to the quantum confinement effect. Especially near infrared (NIR) QDs are very attractive as they can absorb NIR part of the solar spectrum, which is wasted by other solar cell materials, but yet comprise about 50 % of the solar spectrum, in addition to higher energy photons. QDs also

offer a possibility of utilizing multiple exciton generation (MEG) and extraction of hot carriers in designing very high PCE solar cell devices and intermediate band solar cells, all of which have potential to surpass Shockley-Queisser limit for single junction solar cells. Further considering device stability, recently core-shell QDs attracted attention in solar cells due to the presence of a robust, inorganic shell on the surface.

While designing solar cell devices from QDs, several factors need to be taken into consideration. In devices involving continuous film of QDs, the QDs should be closely packed for efficient mobility of charge carriers through the film and the charge carrier recombination sites should be minimized. To alleviate this problem, combining the QDs with one dimensional (1D) nanostructure to form continuous charge transport pathways is one solution in improving the performance of QD based solar cell devices. Another means of overcoming limited charge carrier diffusion in thick QD film is integrating plasmonic nanoparticles with thinner QD film to increase absorption of light, while maintaining efficient charge carrier extraction.

In the first part of this work, solar cells fabricated by combining colloidal PbS and PbS/CdS core-shell QDs with rutile TiO₂ nanorod arrays (2 and 4 μm long) have been investigated. The general structure of the solar cell devices investigated is fluorine doped tin oxide (FTO)/TiO₂/QDs/interfacial layer/Au. Two types of QDs (PbS and PbS/CdS core-shell) and two types of interfacial layer (Poly(3,4-ethylenedioxythiophene):poly(styrene sulfonate) (PEDOT:PSS) and MoO₃) between the QD film and the back electrode have been investigated. It has been found out that both the processing atmosphere and the interfacial layer influence the performance of the solar cell devices. A maximum PCE of 2.14 % has been achieved under air mass (AM) 1.5 illumination with devices involving PbS/CdS core-shell QDs, 2 μm long TiO₂ nanorod arrays and MoO₃ interfacial layer. Moreover these devices were processed in ambient atmosphere and have shown better performance (by about 40 %) than devices involving PbS QDs processed under inert atmosphere in glove box.

It has been encouraging to demonstrate the use of PbS/CdS core-shell QDs in solar cells with easy processability and better performance compared to the PbS QDs. However, there still remained room for improvement of the performance by further optimization. Accordingly, in the second part, the solar cell devices involving PbS/CdS core-shell QDs have been further optimized and a PCE as high as 4.43 % has been achieved. This PCE has been achieved by utilizing uniform

sputter-deposited TiO₂ seed layer on FTO glass prior to the growth of TiO₂ nanorod arrays, optimizing the length of the TiO₂ nanorod arrays and post deposition mild thermal annealing of the PbS/CdS core-shell QD film under inert atmosphere. The performance of the solar cell devices has been found to depend on the length of TiO₂ nanorod arrays and reach maximum at optimum TiO₂ nanorod array length of about 450 nm.

In the third part, plasmon-enhanced bulk heterojunction (BH) solar cells involving Au nanostars incorporated into NIR PbS/CdS core-shell QD film, which was spin coated onto TiO₂ nanorod arrays film on FTO glass substrate are studied. The effects of the density of the Au nanostars and their location in between the TiO₂ nanorod arrays and the back electrode on the performance of the device were investigated. After optimizing the density and the location of the Au nanostars a PCE of 4.16 % has been achieved. This is about 16 % increase compared to the device without Au nanostars with a PCE of 3.59 %. The improvement in the PCE as a result of Au nanostars incorporation is mainly due to increase in the short circuit current (J_{sc}) (about 26 % in this case). This indicates that the presence of Au nanostars enhances the charge carriers generation by improving the absorption of photons. This was further confirmed by the enhancement of photoresponse, as evidenced by external quantum efficiency (EQE) spectra of the devices.

ACKNOWLEDGEMENTS

First and foremost I would like to express my heartfelt gratitude to my supervisors Prof. Dongling Ma and Prof. My Ali El Khakani for giving me the opportunity to carry out my Ph.D. study under their guidance and for their invaluable advice, encouragement, moral support and constructive criticism throughout my Ph.D. study. Their endless effort in improving the quality of my research project by giving me suggestions and some novel ideas is quite appreciable. The frequent and useful discussions I have had with them at different stages of my research work was among the factors which contributed largely to the success of my research. In general, the contributions they made for the development of my professional career is quite appreciable.

I am also grateful to Prof. Nianqiang Wu for providing me some samples from his group, Prof. Ricardo Izquierdo for kindly allowing me to carry out some experiments in his laboratory, Prof. Shanqing Zhang for letting photoelectrochemical measurements done in his group, and Prof. Ana Tavares for her collaboration for allowing me to use some facilities in her laboratory. Their comments have improved the quality of the articles I wrote for publications.

I also thank Dr. Haiguang Zhao, Dr. Mee Rahn Kim, Nazar Delegan, Dr. Jiangtian Li, Jingxia Qiu and Peng Zheng who have contributed to my research work by carrying out some parts of the experiments involved in my project and discussing about the experiments and results with me. I would also thank them for reading and commenting on the articles.

My gratitude also goes to Dr. Menouer Saidani, Christophe Chabanier, Dr. Riad Nechache and David Aubut for giving me training and their technical help in using some equipment. I thank Jean-Philippe Masse for carrying out TEM measurements for me. I acknowledge all the present and previous members of Prof. Ma's group and Prof. El Khakani's group, who altogether created a conducive and pleasant working environment. These people include Dr. Jianming Zhang, Dr. Guozhu Chen, Fuqiang Ren, Dr. Ibrahima Ka, Dr. Hongyan Liang, Dr. Defa Wang, Dr. Shan Huang, Dr. Stefano Desinan, Dr. Laurentiu Dinca, Dr. Maxime Gougis, Dr. Vincent Le Borgne, Fan Yang, Dr. Xenhe Xu, Yanlong Liu and Deepak Gangadharan. Their help in and outside of the laboratory and their encouragement and moral support are unforgettable. Finally, I would like to thank Dr. Zackaria Mahfoud for his kind help to translate the summary of my thesis to French.

CONTENTS

ABSTRACT.....	I
ACKNOWLEDGEMENTS.....	IV
LIST OF FIGURES	VII
LIST OF CHEMICAL COMPOUNDS, ABBREVIATIONS AND SYMBOLS	IX
LIST OF PUBLICATIONS AND CONFERENCE CONTRIBUTIONS	XII
CHAPTER 1 INTRODUCTION	1
1.1. Historical Development of Solar Cells	2
1.2. Different Generations of Solar Cells.....	3
1.3. Quantum Dots Based Solar Cells.....	4
1.4. Core-shell Quantum Dots in Solar Cells.....	6
1.5. Different Quantum Dot Solar Cell Structures.....	9
1.5.1. Quantum Dots Sensitized Solar Cells	9
1.5.2. Schottky Junction Quantum Dot Solar Cells	10
1.5.3. Bulk Heterojunction Solar Cells Based on Quantum Dot/polymer Hybrid.....	10
1.5.4. Depleted Heterojunction Quantum Dot Solar Cells.....	11
1.5.5. Depleted Bulk Heterojunction Quantum Dot Solar Cells	12
1.6. Plasmon Enhanced Solar Cells	13
1.7. Thesis Objectives and Organization	14
1.7.1. Objectives	14
1.7.2. Thesis Organization	14
CHAPTER 2 LITERATURE REVIEW ON QUANTUM DOT/ONE DIMENSIONAL NANOSTRUCTURES IN SOLAR CELLS	16
2.1. Introduction.....	16
2.2. Techniques of Preparation of Quantum Dot/One Dimensional Nanostructure Hybrids and their Integration into Active Layer of Solar Cell Devices.....	17
2.2.1. Hybridization in Solution Using Pre-synthesized Quantum Dots.....	18
2.2.1.1. Covalent Attachment.....	18
2.2.1.2. Attachment via Van der Waals Force	19
2.2.1.3. Dip Coating.....	20
2.2.1.4. π - π Stacking	21
2.2.1.5. Attachment via Electrostatic Interaction.....	22
2.2.2. Hybridization with In-Situ Synthesized Quantum Dots.....	22

2.2.2.1. Successive Ion Layer Absorption and Reaction (SILAR)	23
2.2.2.2. Chemical Bath Deposition (CBD)	23
2.2.2.3. Electrochemical Method	25
2.2.2.4. Spin Coating.....	25
2.2.2.5. Deposition of Quantum Dots onto One Dimensional Nanostructures by Physical Methods	26
2.3. Charge Transfer Properties in Quantum Dot/One Dimensional Nanostructure Hybrids.....	28
CHAPTER 3 EXPERIMENTAL.....	31
3.1. Chemicals and Materials.....	31
3.2. Synthesis of Nanostructures.....	31
3.2.1. Deposition of TiO ₂ Seed Layer	31
3.2.2. Synthesis of TiO ₂ Nanorod Arrays	32
3.2.3. Synthesis of Quantum Dots.....	33
3.2.3.1. Synthesis of PbS Quantum Dots	33
3.2.3.2. Synthesis of PbS/CdS Core-shell Quantum Dots.....	33
3.2.4. Synthesis of Au Nanostars	34
3.3. Fabrication of Solar Cell Devices	34
3.4. Characterizations.....	35
3.4.1. Characterization of Nanostructures.....	35
3.4.2. Characterization of Solar Cell Devices	36
3.5. Theoretical Calculation	36
CHAPTER 4 RESULTS	37
4.1. Air-processed Depleted Bulk Heterojunction Solar Cells Based on PbS/CdS Core-shell Quantum Dots and TiO ₂ Nanorod Arrays.....	37
4.2. Towards High Efficiency Air-processed Near-infrared Responsive Photovoltaics: Bulk Heterojunction Solar Cells Based on PbS/CdS Core-shell Quantum Dots and TiO ₂ Nanorod Arrays...	49
4.3. Plasmonic Enhancement of the Performance of PbS/CdS Core-shell Quantum Dots/TiO ₂ Nanorod Arrays Bulk Heterojunction Solar Cells	67
CHAPTER 5 CONCLUSIONS AND PERSPECTIVES	92
5.1. Conclusions.....	92
5.2. Perspectives.....	93
REFERENCES	95
RÉSUMÉ	111

LIST OF FIGURES

Figure 1.1. Total world energy consumption by source (2013) [7].....	1
Figure 1.2. Evolution of record PCE values of different generations of solar cells since 1976, retrieved from http://www.nrel.gov/ncpv/images/efficiency_chart.jpg on January 26, 2015; this plot is courtesy of the National Renewable Energy Laboratory, Golden, CO. [24].....	4
Figure 1.3. Schematic illustration of band gap of QDs versus size compared to bulk semiconductor, CdSe in this case [26].....	5
Figure 1.4. Absorption spectra of PbS QDs tuned over a wide range of wavelength [35].	6
Figure 1.5. Different types of core-shell structures and their wave functions [48].....	7
Figure 1.6. Comparison of PL decay of core-shell QDs with the parent QDs [50].....	8
Figure 1.7. Schematic representation of working principles of QDSSCs [27].....	9
Figure 1.8. Device architecture (a) and energy band model (b) of a Schottky QDs solar cell [65].....	10
Figure 1.9. Illustration of polymer-QDs BH device [67].....	11
Figure 1.10. Architecture of DH solar cell device (a) and energy band diagram (b) [39].....	12
Figure 1.11. DBH architecture with porous structured electrode (a) and 1D nanostructure arrays electrode (b) [76].....	12
Figure 2.1. Comparison of charge transport pathways in QDs and QD/1D nanostructure hybrids [8].....	17
Figure 2.2. (a) Schematic illustration of the formation of amide bond linking CdSe QDs to MWCNTs [99] and (b) TEM image of CdSe QDs/MWCNTs nanohybrids synthesized via covalent bonding [96].....	19
Figure 2.3. TEM images of PbS/CdS QD/MWCNTs hybrid [51].....	20
Figure 2.4. SEM showing ZnO nanorod arrays before (a) and after (b) sensitization with CdSe QDs via dip coating [111].....	21
Figure 2.5. (a) Schematic drawing of CdSe QDs attached onto SWCNTs through π - π stacking [115] and (b) TEM image of CdSe QDs linked to SWCNTs through pyridine [118].....	22
Figure 2.6. TEM image of QD/TiO ₂ nanowire hybrid prepared by SILAR technique [122].....	23

Figure 2.7. SEM images of ZnO nanowire arrays (a) and CdSe-CdS co-sensitized ZnO nanowire arrays (b), and TEM (c) and HRTEM (d) images CdSe-CdS co-sensitized ZnO nanowire prepared by a combination of SILAR and CBD techniques [133].....	24
Figure 2.8. SEM images of (a) ZnO nanoneedle arrays and (b) CdSe QDs decorated ZnO nanoneedle arrays via electrochemical technique [134].....	25
Figure 2.9. Cross sectional SEM images showing TiO ₂ nanorod arrays (a) and PbS/CdS core-shell QDs deposited onto the nanorod arrays via layer-by-layer spin coating technique in the fabrication process of DBH solar cells (b) [54].....	26
Figure 2.10. TEM image of PbS QD/Si nanowire nanohybrid prepared by ALD (a) [140] and SEM image of PbS QD/TiO ₂ nanorod arrays/SWCNTs nanohybrid prepared via PLD (b) [138]...	27
Figure 2.11. Schematic illustration of photo induced charge transfer from QDs to 1D nanostructures [145].....	28
Figure 2.12. (a-c) PL emission decays of the PbS QD/TiO ₂ -nanobelt hybrids and (d) charge transfer rate constants for different size PbS QDs [147], and (e) PL emission of CdSe QDs in CdSe QD/SWCNT nanohybrid (increase in amounts of SWCNTs, from a to j) [116].....	29
Figure 2.13. UV-Vis spectra of (a) Trioctylphosphine oxide (TOPO) capped CdSe QDs, (b) MPA capped CdSe QDs, (c) CdSe QD/MWCNT nanohybrids and (d) amine functionalized MWCNTs [99].....	30

LIST OF CHEMICAL COMPOUNDS, ABBREVIATIONS AND SYMBOLS

Chemical Compounds

CdO	cadmium oxide
CdS	cadmium sulfide
CdSe	cadmium selenide
CdTe	cadmium telluride
CuInGaSe ₂	copper indium gallium selenide
HAuCl ₄ .xH ₂ O	tetrachloroauric(III) acid
HCl	hydrochloric acid
MoO ₃	molybdenum oxide
N ₂	nitrogen
O ₂	oxygen
Pb(OAc) ₂ .3H ₂ O	lead acetate trihydrate
PbS	lead sulfide
TiO ₂	titanium dioxide
ZnO	zinc oxide

Abbreviations

(TMS) ₂ S	bis(trimethylsilyl) sulfide
1D	one dimensional
ALD	atomic layer deposition
AM	air mass
BH	bulk heterojunction
CBD	chemical batch deposition
DBH	depleted bulk heterojunction
DH	depleted heterojunction
DMF	N,N-dimethylformamide

EDS	energy dispersive spectroscopy
EQE	external quantum efficiency
FDTD	finite-difference time-domain
FF	fill factor
FTO	fluorine doped tin oxide
HRTEM	high resolution transmission electron microscope
MEG	multiple exciton generation
MPA	mercaptopropionic acid
MWCNT	multi wall carbon nanotube
NIR	near infrared
OA	oleic acid
ODE	1-octadecene
P3HT	poly (3-hexylthiophene)
PCBM	phenyl-C61-butyric acid methyl ester
PCE	power conversion efficiency
PEDOT:PSS	poly(3,4-ethylenedioxythiophene):poly(styrene sulfonate)
PL	photoluminescence
PLD	pulsed layer deposition
PVP	polyvinylpyrrolidone
QD	quantum dot
QDSSC	quantum dot sensitized solar cell
SAED	selected area electron diffraction
SEM	scanning electron microscope
SILAR	successive ion layer absorption and reaction
SWCNT	single wall carbon nanotube
TEM	transmission electron microscope
TGA	thioglycolic acid
TOP	trioctylphosphine

TOPO trioctylphosphine oxide

UV ultraviolet

XRD x-ray diffraction

Symbols

μ micro

E_g band gap

J_{sc} short circuit current

R_s series resistance

R_{sh} shunt resistance

V_{oc} open circuit voltage

η power conversion efficiency

Ω Ohm

LIST OF PUBLICATIONS AND CONFERENCE CONTRIBUTIONS

Journal Publications

1. **B. A. Gonfa**, M. R. Kim, M. A. El Khakani, D. Ma, Plasmonic Enhancement of the Performance of PbS/CdS Core-shell Quantum Dots/TiO₂ Nanorod Arrays Bulk Heterojunction Solar Cells, *to be submitted*.
2. **B. A. Gonfa**, M. R. Kim, N. Deegan, A. C. Tavares, R. Izquierdo, N. Wu, M. A. El Khakani, D. Ma, Towards High-Efficiency Air Processed Solar Cells: the Case Study of Near Infrared PbS/CdS Core-shell Quantum Dots and TiO₂ Nanorod Arrays, *Nanoscale*, 2015. **7**(22): 10039-10049.
3. I. Ka, **B. Gonfa**, V. Le Borgne, D. Ma, M. A. El Khakani, Pulsed Laser Ablation based Synthesis of PbS-QDs Decorated One-Dimensional Nanostructures and their Direct Integration into Highly Efficient Nanohybrid Heterojunctions based Solar Cells., *Adv. Funct. Mater.*, 2014. **24**(26): 4042-4050.
4. H. Zhao, Z. Fan, H. Liang, G. S. Selopal, **B. A. Gonfa**, L. Jin, A. Soudi, D. Cui, F. Enrichi, M. M. Natile, I. Concina, D. Ma, A. O. Govorov, F. Rosei, A. Vomiero, Controlling Photoinduced Electron Transfer from PbS@CdS core@shell Quantum Dots to Metal Oxide Nanostructured Thin Films, *Nanoscale*, 2014. **6**(12):7004-7011.
5. **B. A. Gonfa**, H. Zhao, J. Li, J. Qiu, M. Saidani, S. Zhang, R. Izquierdo, N. Wu, M. A. El Khakani, D. Ma, Air-processed Depleted Bulk Heterojunction Solar Cells based on PbS/CdS Core-shell Quantum Dots and TiO₂ Nanorod Arrays, *Sol. Energ. Mat. Sol. Cells*, 2014. **124**: 67-74.
6. H. Zhao, H. Liang, **B. A. Gonfa**, M. Chaker, T. Ozaki, P. Tijssen, F. Vidal, D. Ma, Investigating Photoinduced Charge Transfer in Double- and Single-Emission PbS@CdS Core@shell Quantum Dots, *Nanoscale*, 2014. **6**(1):215-225. (*Back Cover*)
7. **B. A. Gonfa**, M. A. El Khakani, D. Ma, Quantum Dot/Carbon Nanotube Nanohybrids for Novel Nanostructured Photovoltaic Devices, *Rev. Nanosci. Nanotech.* 2012., **1**(1):22-39.

8. D. Wang, J.K. Baral, H. Zhao, **B. A. Gonfa**, V.V. Truong, M. A. El Khakani, R. Izquierdo, D. Ma, Controlled Fabrication of PbS Quantum-Dot/Carbon-Nanotube Nanoarchitecture and its Significant Contribution to Near-Infrared Photon-to-Current Conversion. *Adv. Funct. Mater.*, 2011. **21**(21): 4010-4018.

Conference Presentations

1. **B. A. Gonfa**, M.R. Kim, N. Deegan, A.C. Tavares, R. Izquierdo, N. Wu, M.A. El Khakani, D. Ma, Ambient Air Processed Near Infrared PbS/CdS Core-shell Quantum Dots/TiO₂ Nanorod Arrays Bulk Heterojunction Solar Cells, *Colloque de Plasma-Québec*, Université de Montréal, Montréal, June 3-5, 2015 (*Poster presentation*)
2. **B. A. Gonfa**, Core@shell Quantum Dots for Future Energy Applications, *Colloque annuel du CQMF*, Auberge Gouverneur, Shawinigan, November 7 and 8, 2013 (*Oral presentation*)
3. G. Chen, H. Zhao, D. Wang, **B. A. Gonfa**, H. Liang, J. Zhang, D. Ma, Rational Design and Realization of Nanostructured Materials for Biomedical and Energy Applications, *Colloque annuel du CQMF*, Auberge Gouverneur, Shawinigan November 14 and 15, 2012 (*Poster presentation*)
4. D. Wang, **B. A. Gonfa**, I. Ka, M. A. El Khakani, D. Ma, Design and Realization of Near-infrared Photoactive Nanomaterials: Hybridizing 0-D PbS Quantum Dots with 1-D Nanostructures, *MRS Conferense, Boston*, November 29 - December 3, 2010 (*Poster presentation*)

CHAPTER 1 INTRODUCTION

According to a report of the basic energy sciences workshop on solar energy utilization, the annual energy consumption of the world population in 2005 was about 4.1×10^{20} J and is expected to double by mid-21st century associated with projected population and economic growth [4, 5]. The major fraction (about 78 %) of the current energy sources of the world is from fossil fuels like petroleum, coal and natural gas [6], courtesy of the annual “Renewables global status” report of 2014. However, the energy sources from the fossil fuels come with environmental impacts, not to mention about their potential to run out with time. Burning of the fossil fuels is associated with emission of CO₂ to the atmosphere, which is one of the greenhouse gases resulting in global warming. In addition, when fossil fuels like coal are burned, they emit SO₂ to the atmosphere that is later converted to sulfuric acid, causing damages to vegetation, buildings, monuments, and statues.

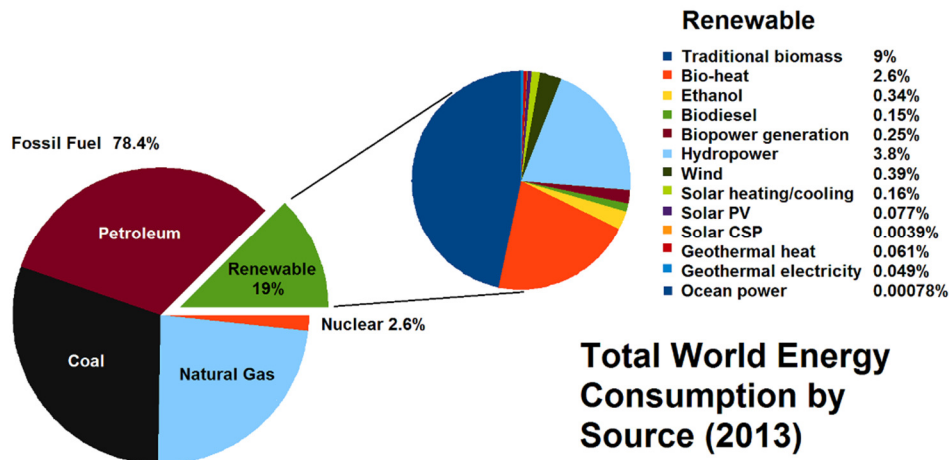


Figure 1.1. Total world energy consumption by source (2013) [7].

Therefore, it is important to look for alternative renewable energy sources with less impact on the environment [8]. Figure 1.1 shows the shares of different sources of energy including fossil fuels and different types of renewables in the overall global energy consumption updated to 2013. Among several potential renewable green energy sources, one very attractive source is the solar energy. The sun emits energy, which is released from fusion of hydrogen via proton-proton chain reaction at very high temperature (~ 16M °C) of its core. The energy released in this process of

conversion of a gram of hydrogen to helium is equivalent to the energy released from combustion of 20 tons of coal [9]. Solar energy flux towards the Earth's surface is about 3×10^{24} J/year, which is about 10,000 times the present energy consumption of the world population [10].

Considering the availability of sunlight in abundance and the need for clean and renewable source of energy, it is inevitable to look for a safe way to collect and utilize the environmental friendly, renewable and cheap solar energy compared to fossil fuels. Among different ways of harvesting solar energy, one very attractive and promising technology is using the solar cell technology, which converts the solar energy to direct current electricity. Solar cells are among the technologies expected to provide cheap, clean and renewable sources of energy for the growing world population in the future [11]. The energy need of the world can then be fulfilled by about 0.1% coverage of the Earth's surface with solar panel of about 10% PCE [10], which is equivalent to the solar energy received by Earth in less than an hour.

1.1. Historical Development of Solar Cells

Solar cell is a device, which converts solar light to electricity by the means of photovoltaic effect. Solar energy has been used by human beings for thousands of years [12]. For example, the energy of the sun was used to keep warm. Buildings were also designed in a way that the walls and the floors collect solar energy during the day and release them as thermal energy during the night. The term photovoltaic, which has been in use in English language since 1849, came from the Greek word photos meaning light and voltaic (the name of the Italian physicist Alessandro Volta after whom the unit of electromotive force, the volt, is named) [13]. In 1839 the French scientist Alexandre-Edmond Becquerel observed that illuminating a conductive solution would create an electric current between electrodes submerged in the solution [1].

In 1876, William Adams discovered that illuminating a junction between selenium and platinum can have a photovoltaic effect [14]. This effect is the basis for modern solar cells. In 1883 inventor Charles Fritts built what many regard as the first true photovoltaic cell using selenium on a thin layer of gold [15]. His solar cell had a PCE of only 1 to 2 %, but represented the beginning of the solar cell technology as we know it today. In 1888 Alexander Stoletov built the first photoelectric cell based on the photoelectric effect, which was discovered by Heinrich Hertz earlier in 1887 and later explained by Albert Einstein in 1905 for which he received the Nobel Prize in physics in

1921. Following the patenting of the modern semiconductor junction solar cell in 1946 by Russell Ohl [16], Bell laboratories developed the first practical solar cell in 1954 using diffused silicon p-n junction, which reached a PCE of about 6% [17].

Since then the solar cell technology has undergone remarkable development in terms of PCE as well as diversity with respect to materials and structure. The commercialization of solar cells has also been realized and the price has decreased and the volume of production increased almost exponentially with time. The highest PCE so far achieved by a single junction solar cell is 28.8 % using GaAs [2]. However, this type of solar cells is expensive due to its high processing cost and is limited to a few areas like space applications. As for Si solar cells, the record PCE of 25.6 % has been achieved in 2014 by the mostly commercialized single junction, single crystalline silicon solar cells with module PCE reaching up to 19.3% [18-20].

Multijunction solar cell devices involving four sub-cells of III-V semiconductors have reached a record PCE of 46 % under concentrated sunlight as high as 508 times [3]. However, achieving high PCE solar cells at low cost so that they can compete with fossil fuels is still a challenge and remains to be the area of focus in solar cell research. The different generations of solar cells are presented in the next subsection.

1.2. Different Generations of Solar Cells

Solar cells are classified into three generations. The first generation of solar cells includes wafer based solar cells, such as, single crystalline silicon solar cells. The solar cells of this generation have achieved high PCE, but their price is high due to the high processing cost to obtain pure, defect-free silicon [8].

The second generation of solar cells includes thin film amorphous silicon, polycrystalline silicon, CuInGaSe₂ and CdTe solar cells, which are less expensive compared to the first generation solar cells but their PCE is relatively low [8].

The implementation of the third generation solar cells involves the development of new materials or structures, which are believed to be cheaper and have potential to lead to high PCE [21, 22]. Colloidal QD based solar cells, which can be processed from solution at low cost, are one example. In general, for solution processable solar cells to be practically applied they have to reach a PCE of 10 % [23]. The record PCE landmarks of different types of solar cells are shown in Figure 1.2.

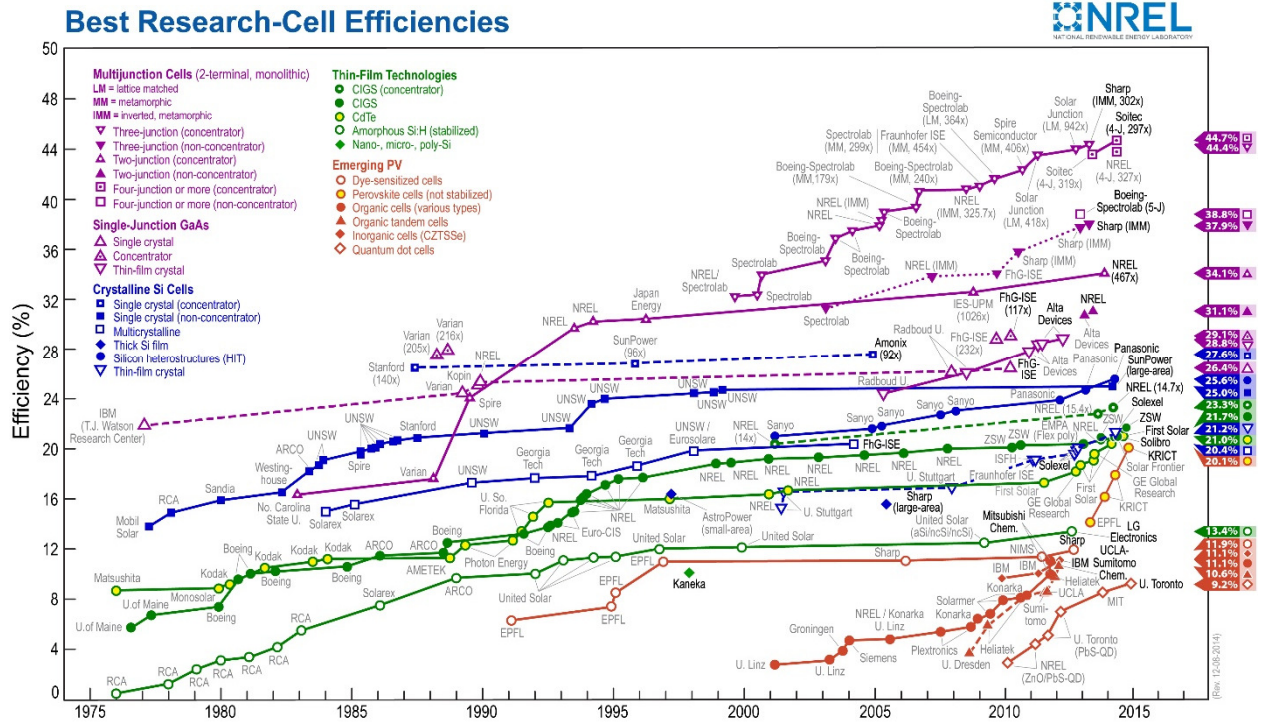


Figure 1.2. Evolution of record PCE values of different generations of solar cells since 1976, retrieved from http://www.nrel.gov/ncpv/images/efficiency_chart.jpg on January 26, 2015; this plot is courtesy of the National Renewable Energy Laboratory, Golden, CO. [24].

1.3. Quantum Dots Based Solar Cells

QDs are semiconductor nanocrystals with confined electrons and holes within the Bohr radius of the material. In QDs the energy levels are discrete, quantized and similar to those of an atom, rather than the continuous bands of bulk semiconductors. As a result QDs are sometimes referred to as “artificial atoms” [25]. Figure 1.3 demonstrates comparison of the band structure of bulk material and QDs of varying sizes.

The energy levels and the band gap of QDs can thus be fine-tuned simply by changing the size of the QDs, not to mention the availability of materials with different chemical composition for choice to synthesize QDs. Accordingly their excitonic absorption peak position can be tuned. Figure 1.4 shows the absorption of PbS QDs tuned over a wide range of wavelength. Among different techniques utilized to make QDs, colloidal synthesis is the cheapest and facile method that can produce monodisperse, high-quality QDs.

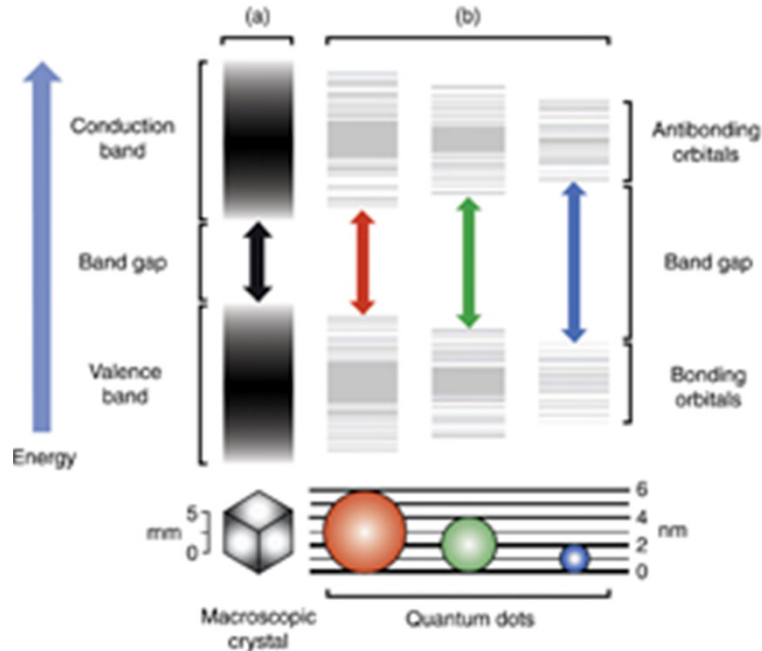


Figure 1.3. Schematic illustration of band gap of QDs versus size compared to bulk semiconductor, CdSe in this case [26].

Colloidal QDs have huge potential for applications in solar cells. The above-mentioned unique tunability of their absorption makes them attractive in designing advanced solar cells as their adjustable band gap allows to efficiently harvest photons from the wide range of the solar spectrum. In addition, they feature low cost and easy synthesis, and solution processability into devices at low temperature, all of high relevance to practical applications [27].

Moreover, QDs possess high extinction coefficient, making them good light absorbers, which in turn allows employment of less amounts of material in construction of solar cell devices. They are also capable of MEG, a phenomenon in which two or more excitons are generated by a single photon of energy at least higher than twice the band gap of the QDs via impact ionization [28-30]. MEG in PbSe QDs has also been practically demonstrated via achieving EQE exceeding 100 % at certain wavelengths [31]. Fast extraction of hot carriers is also possible in solar cell devices involving QDs [32, 33]. QDs can also be used to design intermediate band solar cells [34]. All of these result in increase of the theoretical PCE achievable by QD solar cells compared to other materials and endow them high potential to surpass the Shockley-Queisser limit for single-junction solar cells (about 31 %) [21]. With all these advantages, QDs have been so far investigated in solar cell devices of various architectures.

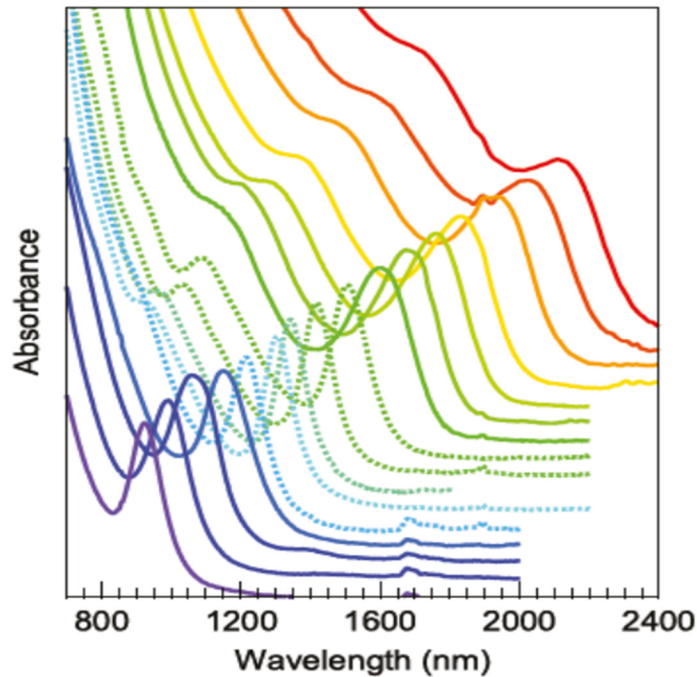


Figure 1.4. Absorption spectra of PbS QDs tuned over a wide range of wavelength [35].

Since efficient light absorption is one of the prerequisites of designing solar cell devices with improved performance, it is important to span the optical absorption of the devices over the whole solar spectrum including the NIR part, which comprises about half of the solar spectrum but wasted by conventional solar cells. This can be achieved by using NIR QDs [36, 37]. The lead chalcogenides PbS and PbSe are very good examples of materials capable of yielding NIR QDs since their band gap can be tuned from IR to UV as they possess large Bohr radius and narrow band gap. In particular, PbS exhibits a small bulk band gap of 0.34 eV and large Bohr radius of 20 nm [38], which means the band gap can be tuned over a large range of energy by controlling particle size due to the quantum confinement effect [39]. Moreover, PbS QDs can be synthesized from earth abundant elements [40].

1.4. Core-shell Quantum Dots in Solar Cells

Even though QDs offer many advantages in designing solar cells, there are associated drawbacks that need to be addressed. Most QDs have limited stability against the environment. They are also sensitive to liquid electrolyte, which is a transport medium for holes via redox process in quantum dot sensitized solar cells (QDSSCs). These electrolytes may be corrosive to the QDs, adversely

affecting their optoelectronic properties. QDs are also sensitive to ligand exchange process, which is done to decrease inter-particle spacing by replacing the long chain ligands with shorter chain ligands so as to increase the charge carriers mobility through the QD film. They are also sensitive to elevated temperature during processing, testing and operation of solar cell devices [41]. Core-shell QDs are believed to offer remedies for these problems endured by the QDs capped only with organic ligands. Core-shell QDs are QDs containing a core dot and an epitaxial shell. The shell passivates the surface defects of the core arising from dangling bonds on the QD surface, which arise due to the partial passivation by organic ligands [42, 43]. These surface defects could act as charge carrier trapping sites or recombination sites, and thus adversely affecting the performance of the ultimate solar cell devices. In addition, thanks to the presence of an inorganic, robust shell, the core-shell QDs possess enhanced chemical, thermal and photochemical stability [44-46].

Depending on the localization of the electron and hole wave functions, which are dictated by the core-to-shell band-edge offset, there are three types of core-shell QDs (Figure 1.5). They are type-I, type-II and quasi-type-II core-shell QDs [47, 48]. Type-I core-shell QDs are the core-shell QDs, in which the band gap of the shell is higher than that of the core with both the conduction and valence band edges of the core located in the band gap of the shell and both the charge carriers - electrons and holes are mainly confined inside the core. Type-II core-shell QDs are those QDs, in which either the conduction band edge or the valence band edge of the core is located in the band gap of the shell allowing confinement of one of the carriers inside the core and the other inside the shell. Quasi-type-II core-shell QDs have intermediate band alignment compared to type-I and type-II and permits the delocalization of one carrier over the entire core-shell structure, while the other is confined either in the core or in the shell.

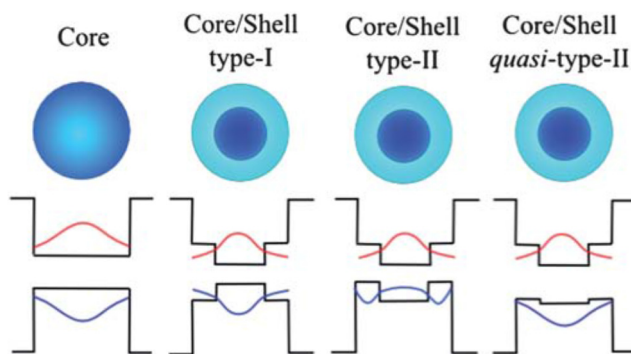


Figure 1.5. Different types of core-shell structures and their wave functions [48].

Core-shell QDs, in general, possess increased exciton lifetime as the nonradiative relaxation process is suppressed due to better surface passivation. For example, with respect to PbS QDs, the corresponding PbS/CdS core-shell QDs show increased lifetime (1.56 μs for PbS/CdS core-shell QDs versus 0.75 μs for PbS QDs), as we previously reported (Figure 1.6). This inhibits phonon emission, resulting in reduced carrier cooling and increased rate of impact ionization, hence the increase of MEG efficiency. For example, it has been demonstrated that thick shell PbSe/CdSe quasi-type-II core-shell QDs can yield nearly a 4-fold increase in the MEG compared to PbSe QDs [49].

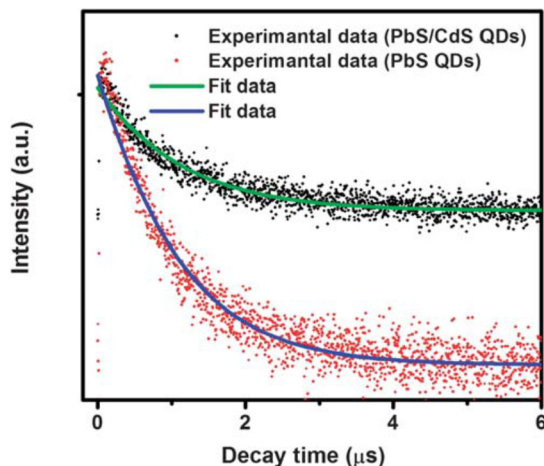


Figure 1.6. Comparison of PL decay of core-shell QDs with the parent QDs [50].

Type I and type II core-shell QDs have been demonstrated to have potential in designing solar cells. For example, the charge transfer process from type I core-shell QDs to electron acceptor materials, such as methyl viologen chloride (MV^{2+}) [51, 52], multi wall carbon nanotubes (MWCNTs) [51], TiO_2 and SnO_2 [53] that can be used in solar cells has been studied by our group and others'. These studies have shown that even if the shell in type I core-shell QDs appears to impose energetic barrier against the transfer of charges from the photoexcited core to the charge acceptors, the advantages they offer in passivating the surface defects and providing protection for the core shouldn't be underestimated. Thin shells can still allow the transfer of charge carriers and the shell thickness can be tuned in such a way that there is a best compromise between charge transfer and surface passivation. Type I core-shell QDs have been applied in heterojunction solar cells solar cells [54-56]. Type-II and quasi Type-II have also been implemented in QDSSCs [57-59] and heterojunction solar cells [60-62].

1.5. Different Quantum Dot Solar Cell Structures

1.5.1. Quantum Dots Sensitized Solar Cells

QDSSCs are analogous to dye sensitized solar cells (DSSCs), with the dye being replaced by QDs as light absorbers. In QDSSCs, a monolayer of QDs is attached to the surface of the mesoporous photoelectrode made of wide band gap semiconductors like TiO_2 or ZnO . Under illumination the photons are absorbed by the QDs, which excite electrons to the conduction band. The electrons are then accepted by the mesoporous electrode driven by conduction band offset and transported to the photoelectrode. The redox electrolyte accepts holes and transports them to the counter electrode. In this way photocurrent is generated, flowing from the counter electrode to the photoelectrode in the external circuit. A schematic illustration of the working principle of QDSSCs is shown in Figure 1.7.

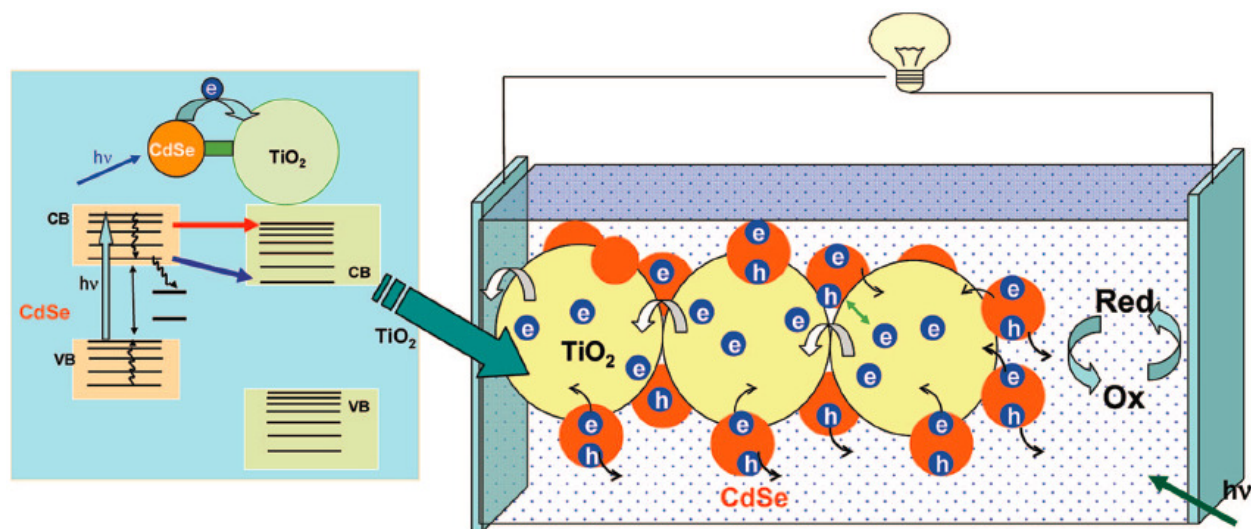


Figure 1.7. Schematic representation of working principles of QDSSCs [27].

To achieve QDSSCs with high performance, a thick mesoporous photoelectrode with adsorbed QDs should be used in principle. However, it is challenging to fully infiltrate the QDs into the thick photoelectrode and thus the photon absorption is limited, resulting in low performance cell. The vulnerability of the QDs to corrosion in the liquid electrolyte represents another problem. So far a PCE as high as 7 % has been reported for QDSSCs [63].

1.5.2. Schottky Junction Quantum Dot Solar Cells

In Schottky junction architecture, the QD film is sandwiched between a transparent conducting electrode and a low work function electrode like aluminum, at which it forms a Schottky contact (Figure 1.8 a). The transport of photogenerated charge carriers is assisted by the presence of a built-in electric field within the depletion layer of the QD film developed due to the Schottky contact.

The performance of Schottky junction QDs solar cells is limited due to the fact that photogeneration of charge carriers occurs in the quasi-neutral region in the illumination side opposite to the Schottky junction and the charge diffusion length in the QD film is limited. This limits the thickness of the QD film that can be used, and thus decreases light absorption. The Fermi-level pinning and charge back recombination at the QDs-low work function metal interface also limits the open circuit voltage (V_{oc}) of the Schottky junction solar cells. So far the highest PCE of 4.5 % has been achieved by this type of solar cells [64].

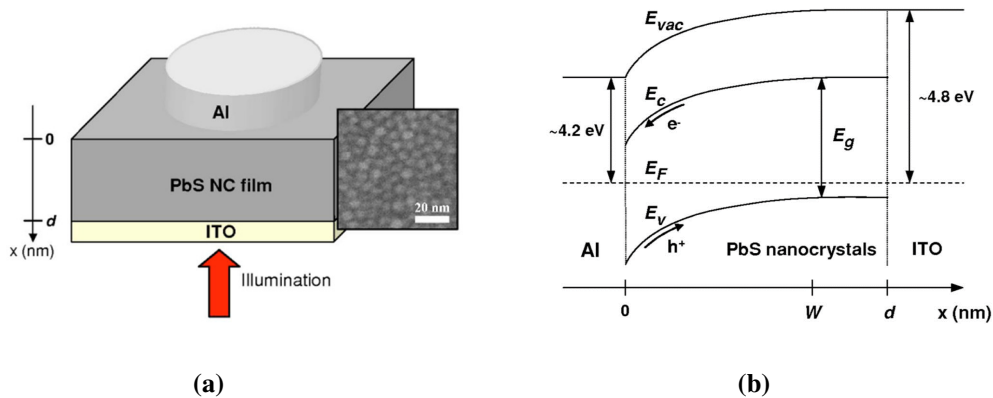


Figure 1.8. Device architecture (a) and energy band model (b) of a Schottky QDs solar cell [65].

1.5.3. Bulk Heterojunction Solar Cells Based on Quantum Dot/polymer Hybrid

The photoactive layer of this type of solar cells is comprised of a nanocomposite formed by blending semiconducting conjugated polymer and QDs (Figure 1.9). The driving force for charge separation and transport in this kind of solar cells is generated by the band alignment of the QDs and the semiconducting polymer as well as the electric field generated due to the difference in work function between two electrodes, the transparent conducting oxide and the low work function backelectrode. The light is absorbed by both the QDs and the semiconducting polymer generating

excitons, which are separated into charge carriers at the polymer-QDs interface. In the particular case illustrated in Figure 1.9, the QDs act as both the electron acceptor and transporter, though not always the case.

In this kind of solar cell architecture, the QDs have to be interconnected to efficiently transport the electrons to an electrode. To enhance the transport of electrons, QDs can be grafted onto MWCNTs and mixed with the polymer making up the photoactive layer [66]. In this case the electrons accepted by and/or photogenerated in the QDs can be transferred to the MWCNTs and transported quickly. As shown in our previous work, this strategy led to higher performance compared to a polymer/phenyl-C61-butyric acid methyl ester (PCBM) solar cell fabricated and tested under similar conditions.

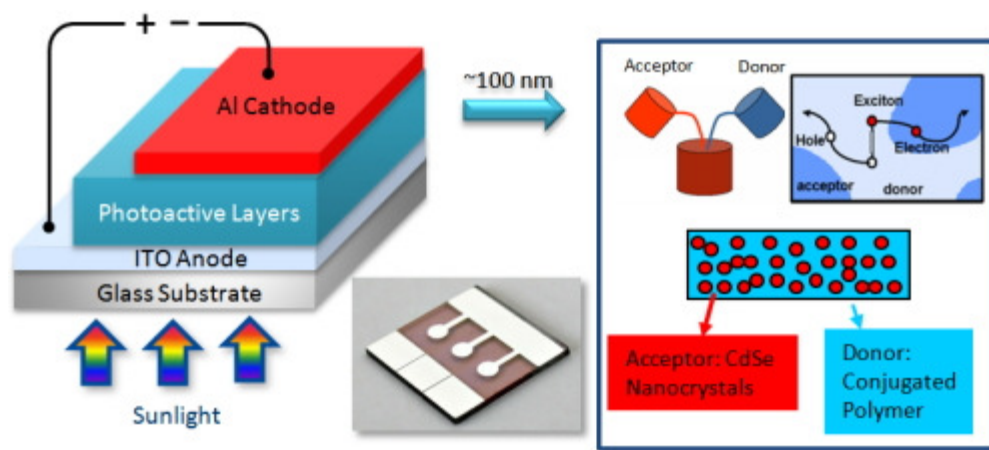


Figure 1.9. Illustration of polymer-QDs BH device [67].

1.5.4. Depleted Heterojunction Quantum Dot Solar Cells

Depleted heterojunction (DH) solar cells have a planar p-n junction configuration, usually involving p-type QD layer and n-type materials like TiO_2 [39], ZnO [68, 69], CdS [70] and PCBM [71]. This architecture overcomes the limitations of Schottky junction solar cells in the sense that the device can be illuminated on the depleted region side so that the charge carriers can be separated and transported more efficiently. An example of DH device structure and the band alignment of the materials involved are shown in Figure 1.10.

Combined with band alignment engineering of the QDs via ligand treatment of the QD film, this solar cell architecture is the highest performing QDs solar cell reported to date with certified PCE of 8.55 % and a laboratory record PCE of 9.2 % [72].

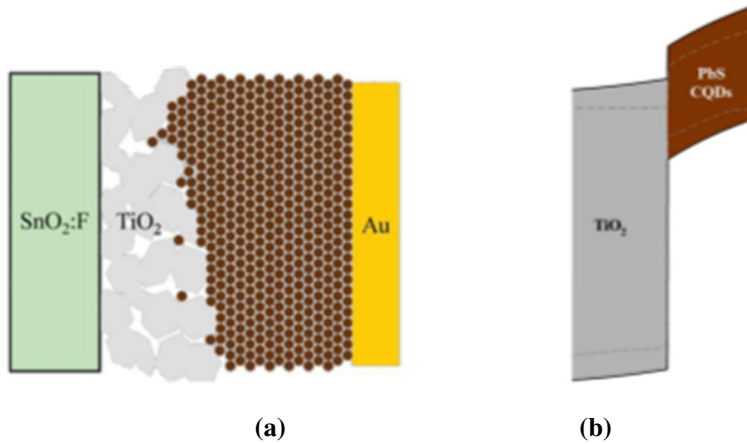


Figure 1.10. Architecture of DH solar cell device (a) and energy band diagram (b) [39].

1.5.5. Depleted Bulk Heterojunction Quantum Dot Solar Cells

This architecture involves porous photoelectrode either as mesoporous film or nanorod/nanowire arrays, in which the QDs are infiltrated forming a three dimensional interpenetrating network of interface between the QDs and the photoelectrode, and hence the depleted region [55, 73-77]. This results in increased interfacial area between the QDs and the photoelectrode, which in turn increases the volume of the depleted region. The schematic representations of the depleted bulk heterojunction (DBH) architectures are shown in Figure 1.11.

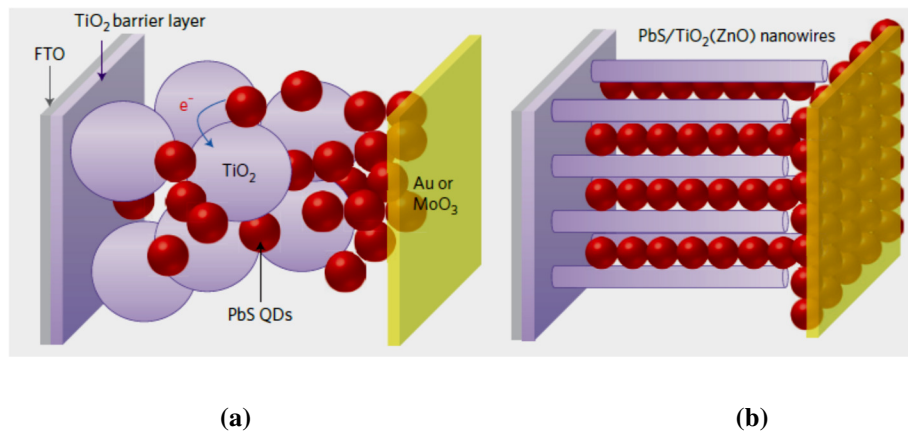


Figure 1.11. DBH architecture with porous structured electrode (a) and 1D nanostructure arrays electrode (b) [76].

This architecture allows the use of more amounts of QDs compared to the planar structures. A high PCE of 6.1 % has been reported for the device of this kind [77], involving TiO₂ nanopillar prepared by lithography. Later on a PCE of 7.3 % has been reported for the device involving solution processed TiO₂ nanowire network converted from ZnO nanorod arrays synthesized by hydrothermal method [78].

1.6. Plasmon Enhanced Solar Cells

Plasmonic materials are materials with oscillation of electron cloud at their surface called plasmons. Metallic nanostructures display the surface plasmon resonance properties, and can scatter incident photons or induce field enhanced absorption in the medium around them [79]. Plasmonic metal nanostructures can be used to enhance the performance of solar cells by enhancing the absorption of light, because of both path length enhancement due to plasmon enhanced light trapping via the scattering and field enhanced absorption phenomena, which leads to increase in photocurrent in thin film solar cells. Since the plasmonic nanostructures increase the optical thickness of the thin film without increasing the physical thickness, they can also enable efficient extraction of hot carriers which is strongly dependent on the physical film thickness of solar cells; the thinner the film the more efficient hot carriers extraction is [80].

Plasmonic enhancement of photocurrents and/or efficiencies have been demonstrated in different types of solar cells, such as silicon solar cells [81, 82], polymer solar cells [83, 84], dye sensitized solar cells [85, 86] and perovskite solar cells [87]. Recently there were also reports on plasmon enhancement of QD based solar cells [88-90]. A plasmonic PCE and J_{sc} enhancements by about 36 % and 19 %, respectively, in PbS QD based solar cells have been reported [89]. Even though the plasmonic nanoparticles are advantageous in enhancing the absorption of photons and thus charge carriers generation, they may also have shortcomings. Among which are introduction of charge carrier recombination sites and parasitic absorption [79]. Therefore, detailed investigation in designing of plasmon enhanced solar cells is required to overcome these side effects and take advantage of the positive aspects of plasmonic materials in improving the performance of solar cell devices.

1.7. Thesis Objectives and Organization

1.7.1. Objectives

Solar cell devices involving colloidal QDs are mainly processed and tested under inert atmosphere due to the sensitivity of QDs to oxidative atmosphere. In this regard the surface nature of the QDs is very important. Since core-shell QDs are believed to be more stable against the environment, it is quite interesting to implement them in solar cells processed in air. On the other hand NIR QDs have the potential to extend the absorption of photons to infrared region of the solar spectrum and thus can be used to design solar cell devices, which can harvest the solar photons efficiently. Therefore two of the aims of this thesis are to i) investigate the use of NIR core-shell QDs, specifically PbS/CdS core-shell QDs in DBH solar cell devices processed in atmospheric air by combining them with TiO₂ nanorod arrays synthesized via low cost, wet chemical synthesis and ii) compare their performance with that of similar, PbS QD based solar cells, which are fabricated in a glove box. The photoactive QD film is prepared via layer-by-layer spin coating followed by ligand exchange.

Since the engineering of device architecture is one of the main factors dictating solar cell performance, it is necessary to design core-shell QD solar cells in a better way to improve the PCE. Moreover, further modification of the properties of the QD film is one way of improving the performance of the devices. Based on these considerations, the thesis also aims at investigating the effect of thin TiO₂ seed layer, TiO₂ nanorod array length, and thermal annealing of PbS/CdS core-shell QDs on the performance of the DBH solar cell devices.

As a means of increasing absorption of light, plasmonic nanoparticles have attracted attention to be employed in different types of solar cell devices. One of the aims of this thesis is to investigate Au nanostars in the DBH device involving the NIR PbS/CdS core-shell QDs. The Au nanostars are incorporated in the QD film and the effect of the location of the Au nanostars in between the TiO₂ nanorod arrays and the backelectrode and the effect of their density on the performance of the DBH solar cell devices are investigated.

1.7.2. Thesis Organization

This thesis is presented in five different chapters including:

Chapter 1 Introduction: This chapter is the introduction to the thesis. It also presents the objectives and the skeleton of the thesis.

Chapter 2 Literature Review: The second chapter is a literature survey of the background underlying the subject of focus of the thesis. A review on QD/1D nanostructure hybrids in solar cell applications is presented.

Chapter 3 Experimental: The experimental chapter presents the procedure for synthesis and characterization of the nanostructures, such as QDs and TiO₂ nanorod arrays. The fabrication and testing process of the solar cell devices are also presented.

Chapter 4 Results and Discussion: This chapter is presented in three different parts. The first part is about the first demonstration of PbS/CdS core-shell QDs in DBH solar cells. The second part focuses on further optimization of the solar cell devices by tuning the length of TiO₂ nanorod arrays and their interface with FTO substrate as well as the PbS/CdS core-shell QDs via thermal treatment in inert atmosphere. The third part of this chapter focuses on the plasmonic enhancement of the performance of the DBH solar cell devices.

Chapter 5 Conclusions and Perspectives: In this part the conclusions drawn based on the analysis of the results and future outlook in this area are presented.

Most of the works in this thesis are done by Belete Atomsa Gonfa. However, some parts are done via collaborations. The measurement of electronic resistance of the TiO₂ nanorod array electrode was performed by Jingxia Qiu, in Prof. Shanqing Zhang's group at Griffith University (Australia) via a photoelectrochemical (PEC) method. The 4 μm long TiO₂ nanorod arrays were synthesized by Dr. Jiangtian Li in Prof. NianqiangWu's group at West Virginia University (USA). The TEM measurements were carried out by Jean-Philippe Masse at Université de Montréal - Ecole polytechnique de Montréal. The TiO₂ seed layer were deposited on FTO glass substrate by Nazar Deegan in Prof. My Ali El Khakani's group. The Au nanostars synthesis and characterization by NAA were done by Dr. Mee Rahn Kim, a former postdoctoral researcher in Prof. Dongling Ma's group. Finite-difference time-domain (FDTD) calculations were performed by Peng Zheng in Prof. NianqiangWu's group.

CHAPTER 2 LITERATURE REVIEW ON QUANTUM DOT/ONE DIMENSIONAL NANOSTRUCTURES IN SOLAR CELLS

In this chapter a literature survey on QD/1D nanostructure nanohybrids and their application in solar cells is presented. In particular, different ways of synthesis of the nanohybrids as well as their integration into solar cells are described and discussed. The charge transfer properties of the nanohybrids are also presented. Some contents of this chapter were published in a review article by our group in 2012 [91].

2.1. Introduction

Nanocomposite materials combining QDs and 1D nanostructures are promising in applications like solar cell devices as they enable to combine the desirable properties of the two sets of materials, resulting in synergetic improvement of performance of the devices. 1D nanostructures, such as nanorods, nanowires and nanotubes, in solar cells provide continuous medium for confined charge transport pathways towards electrodes. This decreases charge transport length and reduces the chance of charge carriers recombination, enhancing the collection efficiency of photo-generated charge carriers. In solar cell devices involving QD/1D nanostructures the QDs mainly serve as light absorbers, whereas the 1D nanostructures serve as scaffold for QDs to avoid their agglomeration (important in devices requiring monolayer of QDs on the surface of 1D nanostructures) and photogenerated charge carrier acceptors and transporters. A schematic comparison of charge transport routes towards electrode in devices involving a QD film and QD/1D nanostructure nanohybrids is shown in Figure 2.1.

The very high charge carrier mobility of 1D nanostructures makes them very useful in designing solar cells, for example, as observed in laser synthesized single wall carbon nanotubes (SWCNTs) [92]. Semiconducting carbon nanotubes (CNTs) show higher electron mobility than any other previously known semiconductors (the highest mobility known for a semiconductor (except for CNTs) at room temperature is $77000 \text{ cm}^2/\text{Vs}$ for InSb [93]). Their electron mobility at room temperature is higher than $10^5 \text{ cm}^2/\text{Vs}$ and is less affected by the increase in temperature. 1D nanostructures of semiconductors also display electron mobility of several orders of magnitude higher compared to that of nanoparticle films [94]. The high surface area of 1D nanostructures is

also very important as this increases the interfacial area with the QDs. Several types of QDs have been combined with different 1D nanostructures, such as CNTs and nanorods/nanowires of n-type semiconductors like TiO₂ and ZnO. QD/1D nanostructure nanohybrids can be prepared by several techniques and integrated into the photoactive layer of solar cell devices of various architectures. Apart from electrodes, usually semiconducting polymers, liquid electrolytes or other charge transport materials have to be involved to complete the device and/or enhance the performance of the devices.

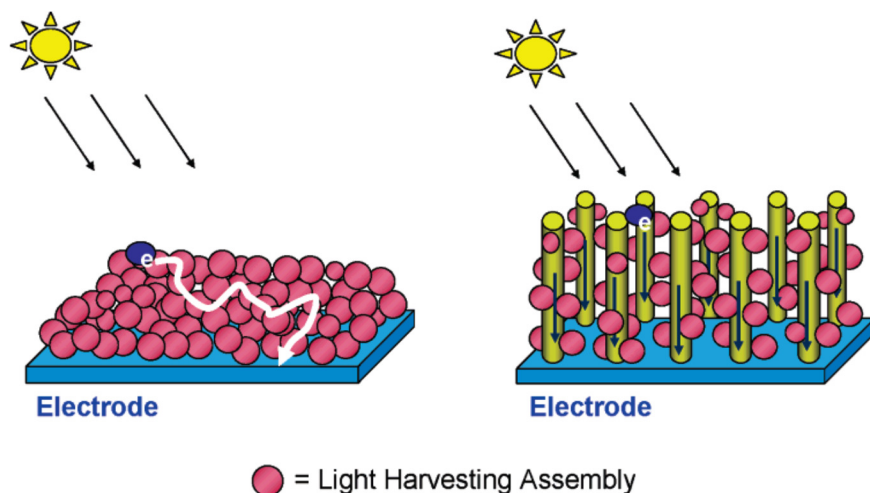


Figure 2.1. Comparison of charge transport pathways in QDs and QD/1D nanostructure hybrids [8].

2.2. Techniques of Preparation of Quantum Dot/One Dimensional Nanostructure Hybrids and their Integration into Active Layer of Solar Cell Devices

The primary purpose of using QDs is to absorb light and generate charge carriers. The 1D nanostructured materials can serve dual purposes - to form a heterojunction with the QDs and to transport charge carriers. To benefit from both advantages of the QDs and 1D nanostructures, development of facile techniques for the integration of QDs with 1D nanostructures according to device requirements is crucial. Depending on the architecture of the solar cell devices to be designed, the QD/1D nanostructure nanohybrids can be prepared by different techniques. This may involve separate hybridization of the QDs to the 1D nanostructures in solution and incorporation into the photoactive layer later on or may be done directly on a substrate as a step in the buildup

of the devices. The QDs may be synthesized separately and subsequently attached to the 1D nanostructures or the QDs can be synthesized in situ in the presence of the 1D nanostructures and anchor to their surface in a single step. The different techniques along with the solar cell architectures they yield are discussed in the next subsections.

2.2.1. Hybridization in Solution Using Pre-synthesized Quantum Dots

Pre-synthesized QDs can be hybridized to 1D nanostructures, such as CNTs, in solution to be integrated into solar cell devices later on. This could involve pre-treatment of the surface of the 1D nanostructures so that they can be linked chemically with the ligands capping the QDs. The ligand capping the QDs can also be changed so as to link them to the 1D nanostructures. The different ways of attachment of QDs to the surface of the 1D nanostructures are discussed below.

2.2.1.1. Covalent Attachment

QDs can be conjugated to 1D nanostructures, such as CNTs through the formation of covalent bonds between functional groups of the CNTs and the end groups of capping ligands of the QDs by, for example, amide bond formation [95-101] or esterification [102]. As demonstrated by Pan *et al.*[99], mercaptopropionic acid (MPA) capped CdSe QDs can be attached to carboxylic group-functionalized MWCNTs (Figure 2.2). The reaction involves intermediary bifunctional molecular linking agents, such as ethylenediamine, which are first attached to the carboxylic acid functionalized CNTs through the formation of the amide bond [99, 100]. The same kind of reaction helps the bonding of this group to the carboxylic group of the capping ligand on the QDs.

Solar cell devices have been constructed on flexible electrodes using CdSe QDs hybridized to SWCNTs via covalent attachment and mixed with regioregular poly (3-octylthiophene) (P3OT) semiconducting polymer to make the active layer of the device [103].

Solar cells involving Si nanoparticles covalently attached to MWCNTs via C-O-Si bond have been studied [104]. These devices involved blends of the Si nanoparticles – MWCNTs nanohybrids and poly (3-hexylthiophene) (P3HT) as active layer and PEDOT:PSS as hole transport layer, which have shown higher PCE than devices involving mixture of the Si nanoparticles, P3HT and MWCNTs without covalent attachment of the Si nanoparticles to the MWCNTs. They have also shown better performance than devices involving only P3HT, mixture of P3HT and MWCNTs, or

mixture of P3HT and Si nanoparticles. This work has clearly demonstrated the importance of close conjugation of QDs to the 1D nanostructures in the performance of the solar cell devices.

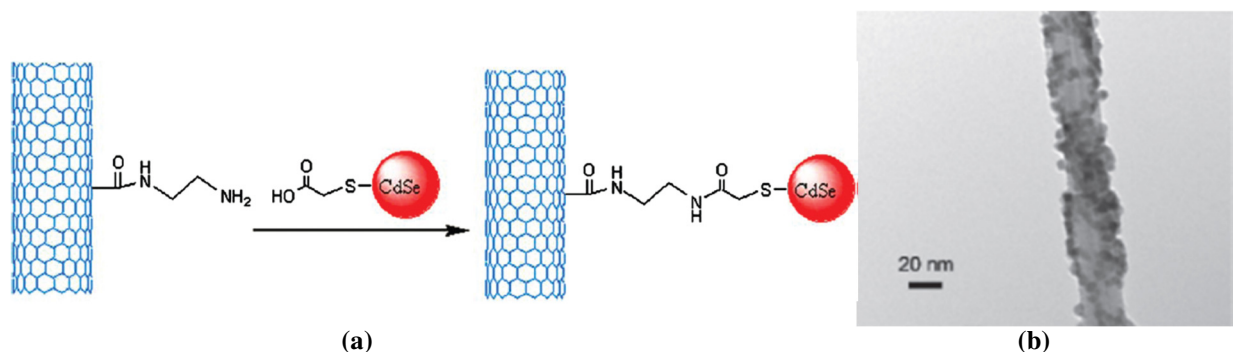


Figure 2.2. (a) Schematic illustration of the formation of amide bond linking CdSe QDs to MWCNTs [99] and (b) TEM image of CdSe QDs/MWCNTs nanohybrids synthesized via covalent bonding [96].

CdS QDs have been attached to crystalline semiconducting polymer nanowires (P3HT) via solvent assisted grafting and ligand exchange and then integrated into the photoactive layer of BH devices [105]. The formation of chemical bonds between the S atoms of the QDs and the C atoms of the polymer is responsible for the attachment of the QDs to the surface of the polymer nanowires as evidenced by X-ray photoelectron spectroscopy studies of the nanohybrids. This approach enhances close interfacial interaction between the inorganic QDs and the semiconducting polymer, increasing the efficiency of charge separation and transport and ultimately the performance of the device.

CdSe/ZnSe core-shell QDs have also been hybridized through complexation of the cations of the QDs to the carboxylic group introduced onto the surface of MWCNTs and used to fabricate solar cell devices [106].

2.2.1.2. Attachment via Van der Waals Force

By simply mixing QDs capped with long chain organic ligands with CNTs, which are also functionalized with long chain organic ligands, the QDs can be attached to the CNTs via hydrophobic interactions between the ligands on the surface of the QDs and the CNTs [51, 66, 107, 108]. Figure 2.3 shows typical TEM images of PbS/CdS core-shell QDs hybridized to MWCNTs in solution via van der Waals force, as reported by our group [51]. The MWCNTs are functionalized with oleyl amine by attaching the oleyl amine ligand to the surface of the MWCNTs via forming amide bond with the carboxylic group on the MWCNT surface induced during the

oxidative treatment of the MWCNTs with HNO_3 . Mixing the oleyl amine capped PbS/CdS QDs with the surface functionalized MWCNTs renders QDs immobilized on the surface of the MWCNTs due to the hydrophobic interaction between the oleyl amine chains present on the surface of both QDs and MWCNTs. It is quite clear from the TEM images that the QDs are closely attached to the MWCNTs.

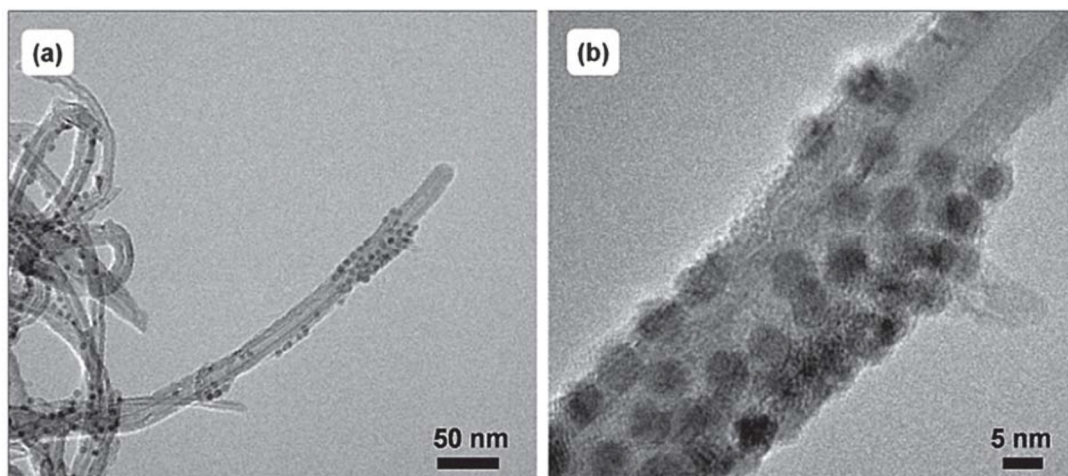


Figure 2.3. TEM images of PbS/CdS QD/MWCNTs hybrid [51].

PbS QD/MWCNT hybrids prepared by this technique have been applied in BH solar cells by blending them with semiconducting polymer (P3HT) and have shown a better performance compared to the control device of P3HT-PCBM prepared under similar conditions [66]. This work has proven the importance of the QD/MWCNTs hybrid in the performance of devices as they combine the enhanced light absorption by QDs with the high electron mobility of the MWCNTs.

2.2.1.3. Dip Coating

Dip coating technique is a simple process in which QDs are infiltrated into 1D nanostructures (arrays or random network) by dipping the substrate covered with the 1D nanostructures into the pre-synthesized QD solution. The long chain ligands capping the QDs are then exchanged with shorter ones by dipping the substrate covered with the QD/1D nanostructure nano hybrids in the solution containing short chain ligands. The amount of QDs adsorbed onto 1D nanostructures can be controlled by adjusting the time the substrate is kept inside the QDs solution and/or by tuning the number of dip coating cycles until the desired loading of the QDs is achieved.

This technique has been used to fabricate DBH solar cell devices involving PbSe QDs and ZnO nanowire arrays on ITO substrate, with N-N'-bis(1-naphthalenyl) -N-N'-bis(phenylbenzidine) (α -NPD) as hole transporter between PbSe QD film and Au back electrode [109]. This DBH device achieved a PCE three times higher than that involving a thin film of ZnO and the same amount of PbSe QDs. The higher performance of the DBH devices was attributed to increased charge collection efficiency due to the interpenetration of the QDs with the nanowires. QDSSCs involving CdSe QDs and ZnO nanorod arrays [110, 111] have also been fabricated by dipping a substrate containing the nanorod arrays in presynthesized CdSe QD solution with the original oleic acid ligand already exchanged with thioglycolic acid (TGA) or MPA. It is believed that the QDs are adsorbed onto the surface of the nanorod arrays via the carboxylate group of the ligands. Figure 2.4 shows ZnO nanorod arrays before and after decoration with CdSe QDs; it is evident that the QDs cover the nanorods surface after dip coating.

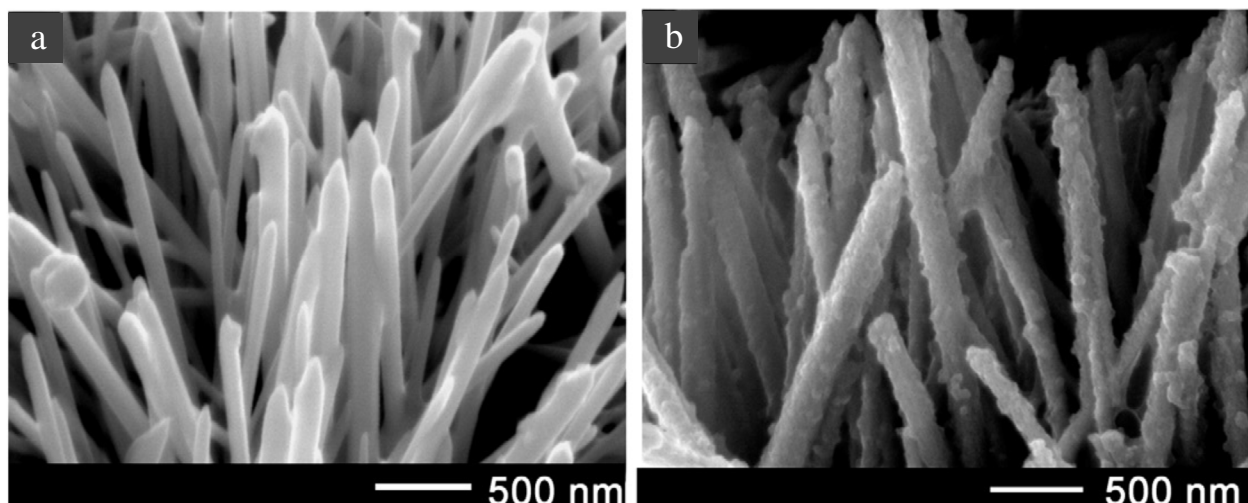


Figure 2.4. SEM showing ZnO nanorod arrays before (a) and after (b) sensitization with CdSe QDs via dip coating [111].

2.2.1.4. π - π Stacking

When QDs are capped with ligands consisting of a conjugated system, they can be hybridized with 1D nanostructures having a conjugated system, such as CNTs, via π - π interactions [112-118]. The conjugated system can be introduced to the surface of the QDs by using ligands containing this system during the synthesis of the QDs or by doing post-synthesis ligand exchange. Figure 2.5

shows schematic illustration of the attachment of QDs to CNTs via π - π stacking and a representative TEM image of QD/CNT nanohybrids involving π - π stacking.

This technique is attractive as it involves self-assembly of the nano hybrid following simple mixing without requiring surface functionalization of the CNTs. As the surface functionalization usually involves surface oxidation of the CNTs, this technique can avoid disruption of the π bonding of the CNTs and preserves the electronic property of the CNTs [97]. This advantage is quite remarkable for SWCNTs, of which optical and electrical properties can be easily negatively affected by cleavage of carbon-carbon double bonds during surface functionalization [119].

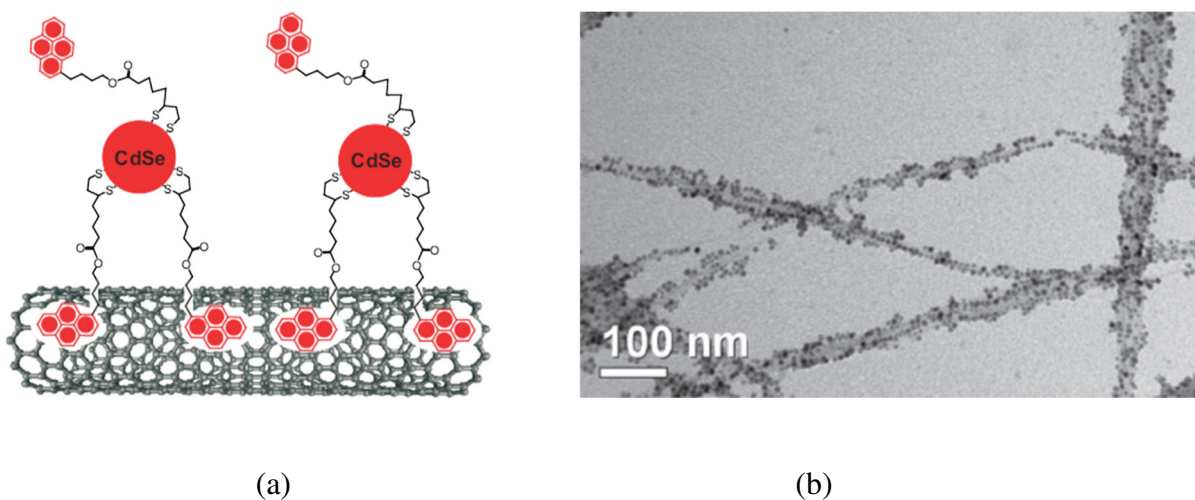


Figure 2.5. (a) Schematic drawing of CdSe QDs attached onto SWCNTs through π - π stacking [116] and (b) TEM image of CdSe QDs linked to SWCNTs through pyridine [118].

2.2.1.5. Attachment via Electrostatic Interaction

QDs can be bound to the surface of the 1D nanostructures via electrostatic interaction due to the opposite surface charges of the QDs and the 1D nanostructures [120, 121]. It has been shown that CNTs (whose surface is functionalized by groups, such as amino, carboxyl or hydroxyl groups) can be linked with CdSe QDs capped by MPA via such an interaction [120].

2.2.2. Hybridization with In-Situ Synthesized Quantum Dots

QDs can also be attached to the surface of the 1D nanostructures by synthesizing the QDs in the presence of the 1D nanostructures. The different techniques involving the direct synthesis of QDs on the surface of 1D nanostructures are presented in the next subsections.

2.2.2.1. Successive Ion Layer Absorption and Reaction (SILAR)

This technique is used to grow/synthesize QDs on the surface of 1D nanostructures on a substrate (arrays or random network) by dipping the substrate alternatively into cationic and anionic precursor solutions of QDs for a number of cycles to achieve a desired size of QDs. The SILAR technique has been mainly used to fabricate QDSSSCs. CdS/CdSe QDs co-sensitized TiO₂ nanowire/nanotube solar cells fabricated by this technique have been studied [122]. In a similar way, NIR PbS/CdS QDs sensitized TiO₂ nanorod array solar cells were fabricated [123]. In other cases, TiO₂ nanorods fabricated by electrospinning [124] and branched TiO₂ nanostructure arrays prepared via hydrothermal synthesis [125] were sensitized by CdS QDs using the same approach. Figure 2.6 shows a representative TEM image of QD/1D nanostructure nanohybrid prepared by this technique.

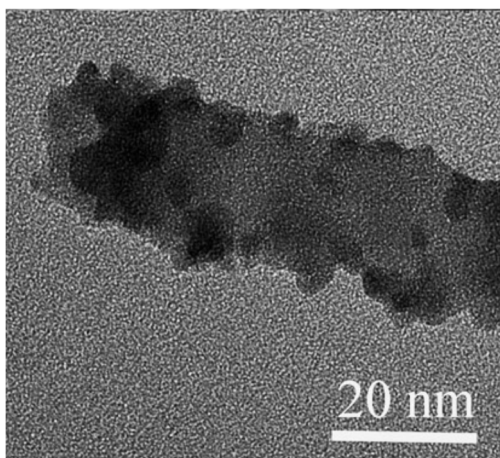


Figure 2.6. TEM image of QD/TiO₂ nanowire hybrid prepared by SILAR technique [122].

2.2.2.2. Chemical Bath Deposition (CBD)

CBD is a technique, in which a substrate with 1D nanostructures (electrode) is immersed in a solution containing all the precursors of QDs that are allowed to react and to directly form QDs on the surface of the 1D nanostructures at elevated reaction temperature [126-128]. This technique is simple, cheap and can also in principle yield high coverage of QDs on the surface of the 1D nanostructures. The size of the QDs may be controlled by controlling the reaction time and performing successive steps of the CBD process. QDSSCs involving CdS QDs and TiO₂ nanowire arrays have been built by this technique [129].

In some cases, direct synthesis of QDs on the surface of 1D nanostructures by the CBD requires chemical modification or functionalization of the surface of the 1D nanostructures. This strategy is mainly realized with CNTs in solution. The surface of the CNTs is modified in such a way that the functional groups serve as specific nucleation site for the growth of QDs [130]. With this technique, ZnO nanocrystals were anchored onto MWCNTs to make UV photovoltaic cells [131]. The CBD and SILAR techniques can also be used in combination by first growing QDs on 1D nanostructures via SILAR followed by over coating with thin layer of another semiconductor material via CBD method. For example, QDSSCs involving CdS/CdSe QDs stabilized by ZnS and ZnO nanowire arrays or Si/ZnO branched hierarchical structures were fabricated by the combination of these two techniques [132]. CdSe sensitized solar cells have also been studied by depositing the CdSe via CBD onto ZnO nanowire arrays pre-coated with CdS by SILAR technique (Figure 2.7) [133].

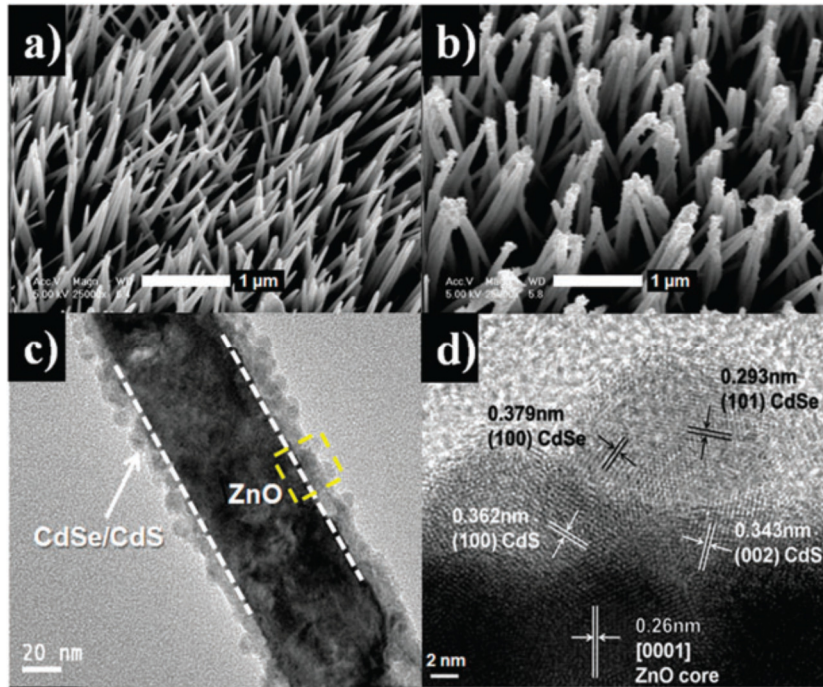


Figure 2.7. SEM images of ZnO nanowire arrays (a) and CdSe-CdS co-sensitized ZnO nanowire arrays (b), and TEM (c) and HRTEM (d) images CdSe-CdS co-sensitized ZnO nanowire prepared by a combination of SILAR and CBD techniques [133].

2.2.2.3. Electrochemical Method

An electrochemical method of synthesis of QDs on the surface of 1D nanostructures is a method in which a two - electrode electrochemical cell is used where the 1D nanostructures serve as the cathode; whereas the other electrode is a counter electrode, for example platinum. The application of constant voltage through the electrolyte solution containing the anion and the cationic complex of the elements constituting the QDs results in the deposition of the QDs on the surface of the 1D nanostructures. CdSe QDs have been deposited onto ZnO nanoneedle arrays electrochemically and applied in QDSSCs [134]. The SEM images of the nanoneedle arrays and the CdSe QDs hybridized nanoneedle arrays are shown in Figure 2.8. CdS QDs sensitized solar cells involving vertically aligned CNTs have also been fabricated by this technique [135].

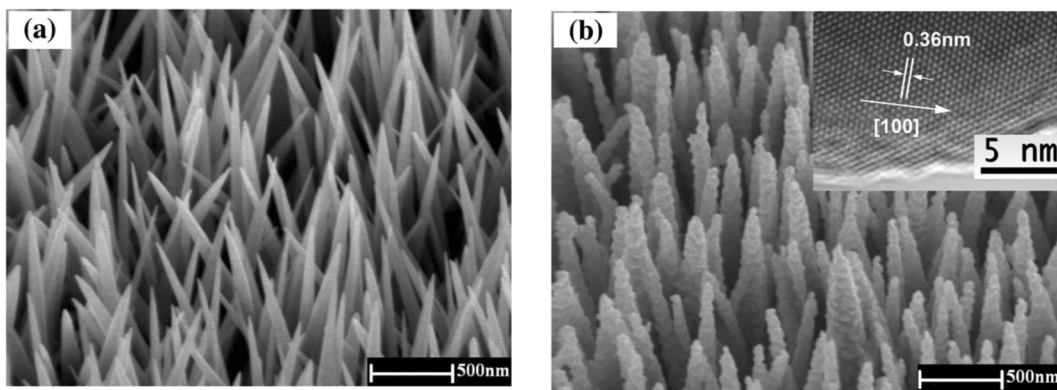


Figure 2.8. SEM images of (a) ZnO nanoneedle arrays and (b) CdSe QDs decorated ZnO nanoneedle arrays via electrochemical technique [134].

2.2.2.4. Spin Coating

Spin coating technique has been widely used to deposit pre-synthesized QDs onto the surface of 1D nanostructures on a substrate for the fabrication of devices, such as DBH solar cells. These devices involve a relatively thick, continuous film of QDs, unlike QDSSCs that require coverage of the surface of 1D nanostructures by a single layer of QDs. Spin coating is usually done in several steps, named “layer-by-layer” deposition. Following deposition, each QD layer is usually first treated with short chain ligands so that they can replace the original long chain ligands for more efficient charge transport, before the next QD layer is deposited by spin coating.

This method has been used to design PbS QDs and PbS/CdS core-shell QDs solar cells involving TiO₂ and ZnO nanorod/nanowire arrays [55, 74, 75, 77, 78]. PbS QDs have also been spin coated on interconnected TiO₂ nanowire networks [136]. This technique so far is the one, which led to the highest PCE among all QD-based solar cells. Figure 2.9 shows comparison of the cross sectional SEM images of TiO₂ nanorod arrays before and after the deposition of PbS/CdS core-shell QDs via layer-by-layer spin coating, with the long chain oleic acid ligand exchanged with 3-MPA for each layer.

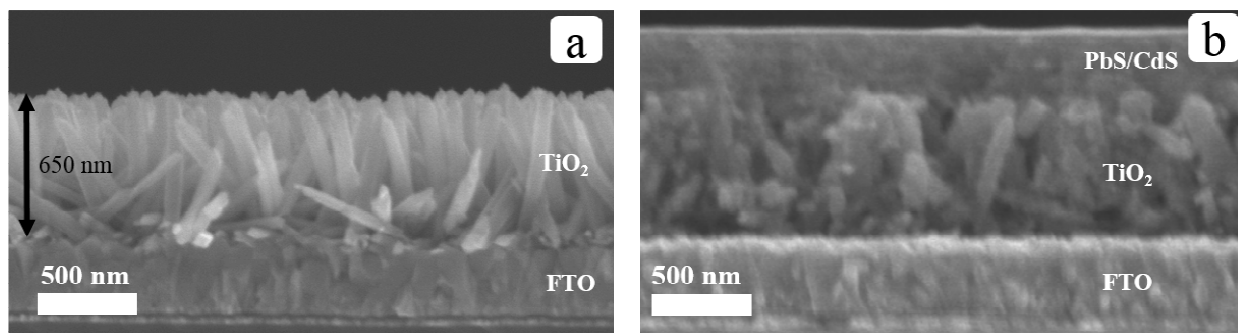


Figure 2.9. Cross sectional SEM images showing TiO₂ nanorod arrays (a) and PbS/CdS core-shell QDs deposited onto the nanorod arrays via layer-by-layer spin coating technique in the fabrication process of DBH solar cells (b) [54].

In another case, PbS QDs and CdSe nanotetrapods are dispersed in a solution and deposited together on a photoelectrode by layer-by-layer spin coating followed by ligand exchange to build DBH solar cell devices [137]. This type of devices involving both the PbS QDs and CdSe nanotetrapods has shown a PCE as high as 5.72 %, which is higher than those achieved by devices involving mixture of PbS and CdSe QDs or just PbS QDs in the active layer, fabricated under similar conditions.

2.2.2.5. Deposition of Quantum Dots onto One Dimensional Nanostructures by Physical Methods

QDs can also be directly grown on 1D nanostructures by physical techniques, such as pulsed layer deposition (PLD) [138, 139], atomic layer deposition (ALD) [140], electron beam evaporation [141, 142] and thermal evaporation [143].

In particular, it has recently been reported that high PCE solar cells can be constructed via physical deposition of PbS QDs onto TiO₂ nanorod arrays and TiO₂ nanorod arrays-SWCNTs hybrid through PLD (Figure 2.10 b) [138]. A PCE of 5.31% has been achieved by this approach.

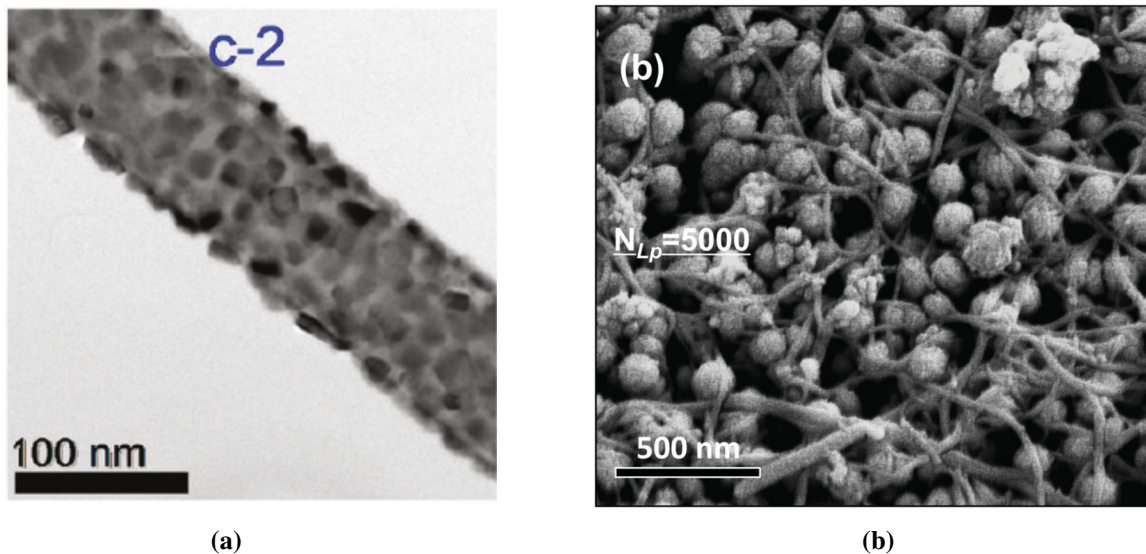


Figure 2.10. TEM image of PbS QD/Si nanowire nanostructure prepared by ALD (a) [140] and SEM image of PbS QD/TiO₂ nanorod arrays/SWCNTs nanostructure prepared via PLD (b)[138].

Techniques, such as CBD, SILAR and PLD, which involve in-situ synthesis of QDs on the surface of 1D nanostructures, are advantageous in the sense that they promise good surface coverage and better infiltration of the QDs into the nanostructures as they are based on the synthesis of QDs from small species. These techniques yield nanostructures with direct contact between the QDs and the 1D nanostructures, which allow efficient charge transfer from the QDs to the 1D nanostructures, since the shorter the distance the more efficient the charge transfer is [121]. The QDs are also not capped with any ligand in these cases, which has its own advantage and shortcomings. While the absence of ligands allows the QDs to be very close physically to 1D nanostructures, the surface dangling bonds/defects of the QDs may not be well passivated, resulting in charge carriers recombination at the surface [144]. Synthesis of QDs with defined size distribution is also challenging by these techniques, which, however, can be routinely achieved by wet chemical method involving synthesis of QDs in an organic phase.

2.3. Charge Transfer Properties in Quantum Dot/One Dimensional Nanostructure Hybrids

To get good performance solar cell devices involving QDs and 1D nanostructures, efficient photogenerated charge transfer from the QDs to the 1D nanostructures is a prerequisite. For this to happen matching of the band energy of the QDs with that of the 1D nanostructures is necessary. This can be achieved by designing the hybrid material so that the bottom level of conduction of the QDs is higher in energy than the Fermi level or the bottom level of the conduction band of the 1D nanostructures. Figure 2.11 schematically illustrates the charge transfer processes in QD/1D nanostructure hybrid.

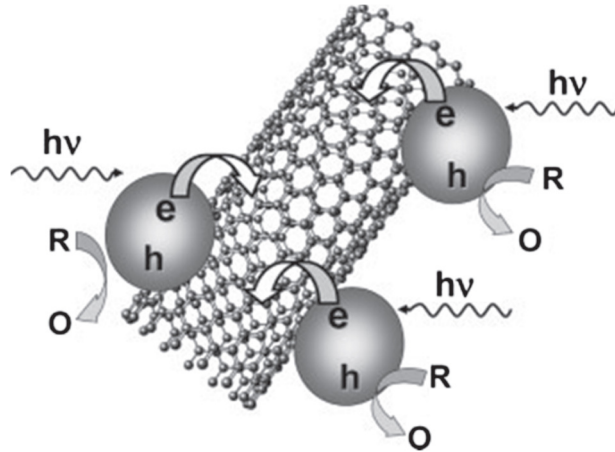


Figure 2.11. Schematic illustration of photo induced charge transfer from QDs to 1D nanostructures [145].

The charge transfer properties from the QDs to the 1D nanostructures are often evaluated by the quenching of the photoluminescence (PL) emission (Figure 2.12 e) of the QDs upon hybridization to the 1D nanostructures as well as a decrease in PL emission decay time of the QDs. The charge transfer efficiency from QDs to 1D nanostructures can be quantitatively determined from the PL emission decay time of the pristine QDs (τ_{QD}) and QDs in the QD/1D nanostructure hybrids ($\tau_{nanohybrid}$) according to the equation:

$$\eta = 1 - (\tau_{nanohybrid} / \tau_{QD}) \quad [146].$$

As reported by our group, the charge transfer from PbS QDs to TiO₂ nanobelts, studied by quenching of PL emission and change in PL decay time, depends on the size of the QDs (Figure 2.12) [147]. The charge transfer efficiency from smaller QDs to the nanobelts is higher than that from bigger ones (Figure 2.12 d). A threshold size of PbS QDs exists, beyond which no electron

can be injected to the TiO₂ nanobelts upon photoexcitation. This is because as the size of the PbS QDs increases, the minimum of the conduction band level decreases, reducing the charge transfer efficiency and eventually completely prohibiting charge transfer as the conduction band minimum of the QDs becomes lower than that of the TiO₂ nanobelts.

In the charge transfer study [147], it has been demonstrated that the threshold band gap of the PbS QDs (with emission peak at about 1480 nm) capable of injecting the electrons to TiO₂ nanobelts is less than those (with emission peak at about 1090 nm) capable of injecting electrons to TiO₂ nanoparticles, which allows extension of the wavelength of photons inducing the charge transfer further into the NIR region to around 1400 nm that represents an important increment of about 300 nm.

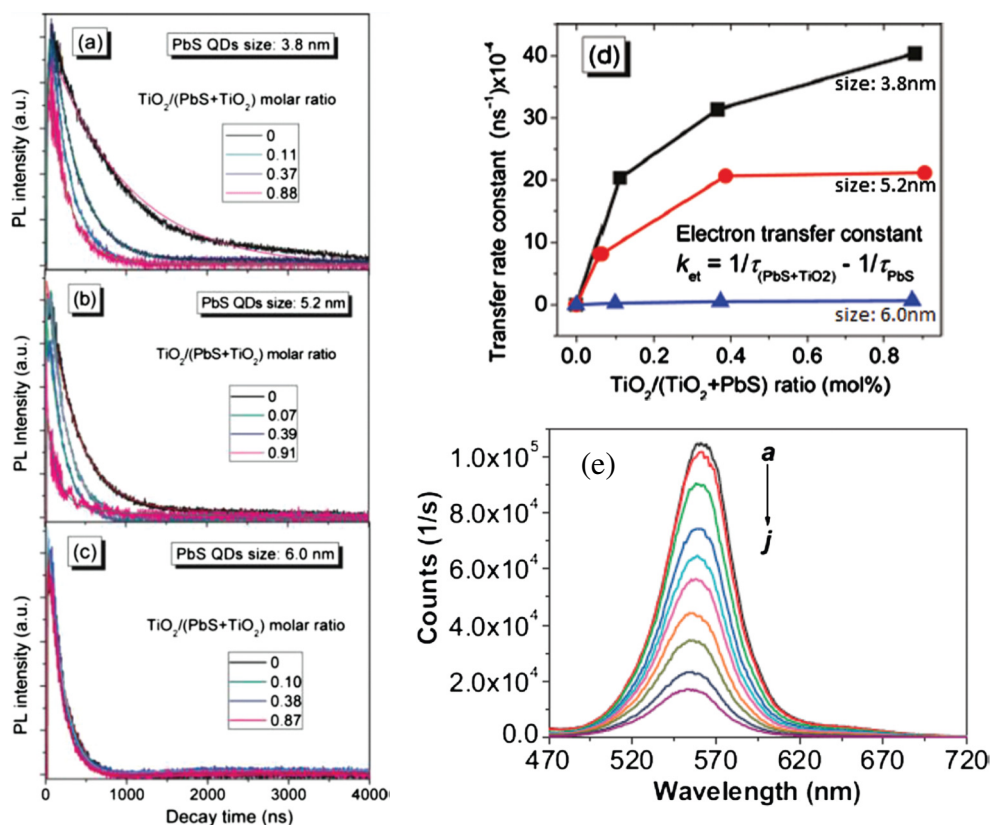


Figure 2.12. (a-c) PL emission decays of the PbS QD/TiO₂-nanobelt hybrids and (d) charge transfer rate constants for different size PbS QDs [147], and (e) PL emission of CdSe QDs in CdSe QD/SWCNT nanohybrid (increase in amounts of SWCNTs, from a to j) [116].

Similarly, PL emission decay studies have confirmed the occurrence of photoexcited charge transfer from CdSe QDs to ZnO nanorod arrays [110]. The charge transfer properties of core-shell QDs hybridized to 1D nanostructures have also been studied [51, 106].

The charge transfer from QDs to 1D nanostructures also depends on the distance between QDs and the 1D nanostructures (i.e., the length of the ligands linking the QDs to the 1D nanostructures) and the nature of ligands (or surface coating) as well. Shorter ligands would help achieving more efficient charge transfer [121, 148]. For example, Si et al. have found out that the electron transfer decreases with increase in the ligand chain length of the QDs [121]. In the cases where longer ligands are involved, the energy transfer, instead of electron transfer, may dominate. Silica coating on CNTs before their conjugation to QDs has also been found to preserve the PL emission of QDs by electronically isolating the QDs from the CNTs [149, 150].

QD/1D nanostructure nanohybrids, such as QD/CNT nanohybrids have also been characterized by absorption spectroscopy, showing distinct excitonic absorption peaks belonging to QDs. The position of the peak depends on the type and size of QDs. Figure 2.13 shows UV-visible absorption spectra of CdSe QDs, CdSe QD/MWCNT nanohybrid and amine functionalized MWCNTs indicating excitonic absorption peaks of the QDs before and after attachment to MWCNTs. Transient absorption spectroscopy has also been used to study charge carrier dynamics in nanomaterials. They are very useful to understand the charge transfer in QD/1D nanostructures nanohybrids [151, 152].

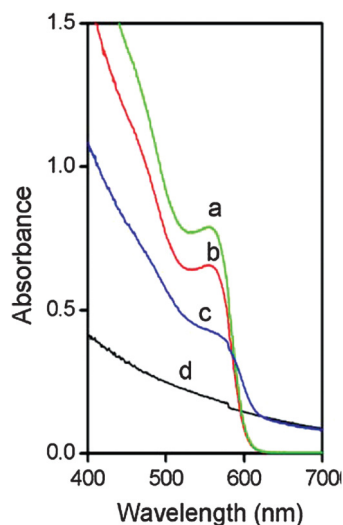


Figure 2.13. UV-Vis spectra of (a) Trioctylphosphine oxide (TOPO) capped CdSe QDs, (b) MPA capped CdSe QDs, (c) CdSe QD/MWCNT nanohybrids and (d) amine functionalized MWCNTs [99].

CHAPTER 3 EXPERIMENTAL

This chapter presents the synthesis techniques of various nanostructures, such as TiO₂ nanorod arrays, PbS QDs, PbS/CdS core-shell QDs and Au nanostars, and their integration into heterojunction solar cell devices. The characterization techniques used to study the properties of the nanostructures and the solar cell devices are also presented.

3.1. Chemicals and Materials

Titanium (IV) butoxide (reagent grade, 97%), tetra-tert-butoxy titanate (deposition grade), concentrated HCl (ACS reagent, ca. 37%), NaNO₃ (ACS reagent, ≥99.0%), Pb(OAc)₂·3H₂O (≥99.99%), oleic acid (OA) (≥99% (GC)), 1-octadecene (ODE) (technical grade, 90%), bis(trimethylsilyl) sulfide (synthesis grade), trioctylphosphine (technical grade, 90%), methanol (anhydrous, 99.8%), CdO (≥99.99% trace metals basis), octane (puriss. p.a., ≥99.0% (GC)), decane (anhydrous, ≥99%), TGA (≥98%) 3-MPA (≥99%), MoO₃ powder (ACS reagent, ≥99.5%), HAuCl₄·xH₂O (99.999% trace metals basis), trisodium citrate (meets USP testing specifications), polyvinylpyrrolidone (PVP) (molecular weight=10,000 g/mole), and N,N-dimethylformamide (DMF) (anhydrous, 99.8%) were purchased from Sigma Aldrich and used as received without any purification. OLED grade PEDOT:PSS was purchased from Clevios™ and Au pellets (99.9 %) from Kurt J. Lesker. FTO glass substrates (TEC 15, R=12-14 Ohm/sq) were purchased from MTI corporation. Hexane (certified ACS) and toluene (certified ACS) were purchased from Fisher Scientific Company.

3.2. Synthesis of Nanostructures

3.2.1. Deposition of TiO₂ Seed Layer

A ~40 nm thick TiO₂ seed layer was deposited on a cleaned FTO glass substrate by sputtering. The deposition was done by sputtering a TiO₂ target (3 inch in diameter) using an RF (13.56 MHz) magnetron sputtering system at a constant power density of 7.7 W/cm². Prior to deposition, the chamber was cryo-pumped to a base pressure of 2 × 10⁻⁸ Torr. High purity Ar (99.999 %) and O₂ (99.995 %) gases were then introduced into the chamber. The gas flow rates were monitored to keep a constant pressure of 1.4 mTorr in the chamber during the sputter-deposition process. In

order to counteract sputtering effect on deposited TiO₂ film stoichiometry, the relative oxygen mass flow rate ratio (i.e.; [O₂]/([O₂]+[Ar])) was kept at 15 %. The FTO glass substrates were mounted on a holder located off-axis at a distance of 20 cm from the target, and heated by a quartz lamp heater of which temperature was kept constant at 300 °C during deposition (which corresponds to an on-substrate temperature of ~200 °C). The thickness of the TiO₂ films was *in-situ* monitored by means of a calibrated quartz-crystal microbalance and *ex-situ* measured through cross-section scanning electron microscopy (SEM) observations. No post acceleration voltage was intentionally applied to the substrates during the sputter-deposition process (they were nonetheless subjected to a built-in plasma sheath bias of ~ -13 V during their growth).

3.2.2. Synthesis of TiO₂ Nanorod Arrays

Vertically aligned TiO₂ nanorod arrays of different length (100 nm to 2 μm) were grown by hydrothermal technique on plain FTO glass substrates as well as on FTO glass substrates covered by the seed layer [153, 154]. First FTO glass substrates were cleaned by sonicating in isopropanol, ethanol and pure water for 15 minutes each before drying under airflow. The precursor solution for the growth of TiO₂ nanorod arrays was prepared by dissolving 1 ml of titanium (IV) butoxide, added dropwise while stirring, in a mixture of 20 ml of pure water and 20 ml of concentrated HCl (ca. 37%). Two FTO glass substrates (1 inch by 1 inch) were placed at an angle in a 23 ml Teflon cup with the conducting sides facing the wall and 12 ml of the precursor solution was added. The Teflon cup was placed inside a stainless steel autoclave, which was then sealed tightly and put in a preheated oven at 150 °C. The autoclave was kept at 150 °C for 1 hour to 20 hours to obtain TiO₂ nanorods of different length. Finally, the autoclave was cooled down naturally in air to room temperature. The FTO substrates with the grown TiO₂ nanorod arrays were then taken out and washed thoroughly with dilute HCl solution first, then with pure water, and subsequently dried under air flow followed by heating at 80 °C for 30 minutes in an oven. The growth of TiO₂ nanorod arrays was evident visually as white film could be observed on the FTO glass. The TiO₂ nanorod arrays were found to grow faster on the FTO substrate covered with the TiO₂ seed layer, under otherwise similar conditions.

TiO₂ nanorod arrays of 4 μm length were grown on plain FTO substrate via hydrothermal method from reference [155]. Typically, 0.75 ml of tetra-tertbutoxy titanate was dissolved in 60 ml of 6 M HCl, and the solution was transferred into a steel lined Teflon autoclave with a volume of 120

mL, where FTO substrates were placed in a Teflon holder. The autoclave was maintained at 150 °C for 20 h and the coated FTO substrate was washed several times with deionized water and ethanol and dried in air.

3.2.3. Synthesis of Quantum Dots

3.2.3.1. Synthesis of PbS Quantum Dots

PbS QDs were synthesized using a modified procedure from references [40, 156]. In the typical procedure 760 mg of $\text{Pb}(\text{OAc})_2 \cdot 3\text{H}_2\text{O}$, 2.4 ml of OA and 15 ml of ODE were added to a 50 ml three neck round bottom flask. The mixture was heated to 150 °C for 1 h while stirring and purging with N_2 flow. It was then cooled under vacuum to 130 °C and the N_2 flow was recovered. Subsequently, 2 ml of mixture of bis (trimethylsilyl) sulfide and trioctylphosphine (1:10 volume ratio) was quickly injected into the flask and the reaction temperature was decreased to 100 °C quickly. The reaction was allowed to last for 5 minutes and then stopped by quenching with cold water. The QDs were precipitated by centrifugation and then re-dispersed in cold toluene. After keeping the QD dispersion at 4 °C for two days, the QD dispersion was centrifuged at 8000 rpm for 30 minutes and the sediment was discarded. Following methanol addition, it was centrifuged at 3000 rpm for about 5 minutes. After removing the supernatant, the QDs sediment was dispersed in toluene. This purification step was repeated one more time. Finally, the QDs were dispersed in mixture of octane and decane (3:1 ratio by volume) at concentration of 37.5 mg/ml for making solar cells or the QDs were dispersed in toluene for the further synthesis of PbS/CdS core-shell QDs.

3.2.3.2. Synthesis of PbS/CdS Core-shell Quantum Dots

PbS/CdS core-shell QDs were synthesized from PbS QDs and Cd precursor via cation exchange technique following a procedure from reference [157]. The Cd precursor was first prepared by heating a mixture of CdO (25 mg), OA (24 mL) and ODE (40 mL) to 255 °C under N_2 for 20 min while stirring. The obtained clear solution was cooled to 155 °C under vacuum for 15 min and the N_2 flux was restored. PbS QDs solution in toluene (20 mL, absorbance: ~12 at the first excitonic absorption peak) was further diluted to 150 ml by toluene in round bottom flask and bubbled with N_2 for 30 min and heated rapidly to 90 °C. While stirring, the Cd/OA mixture was injected and the reaction was carried out at 90 °C for about 30 minutes and stopped by submerging the round

bottom flask in cold water. The PbS/CdS core-shell QDs were purified 3 times using methanol and suspended in mixture of octane and decane (3:1 volume ratio) with QD concentration adjusted to 37.5 mg/ml for solar cell fabrication.

3.2.4. Synthesis of Au Nanostars

Au nanostars were synthesized with a modified procedure from references [158-160]. Typically, Au seed solution was first prepared by diluting 1.058 mL of 104 mM HAuCl₄ aqueous solution with 125 mL of water in three neck round bottom flask and then heated to boiling while stirring. This was followed by the injection of a separate solution prepared by dissolving 0.32 g trisodium citrate in 32 mL water. The mixture solution was then boiled for 15 min and cooled to room temperature. After this, 3.2 g of PVP (molecular weight=10,000 g/mole) was added and the solution was continuously stirred overnight at room temperature, which resulted in Au seed formation. The PVP coated Au seeds were then centrifuged out of the reaction solution and dispersed in ethanol with concentration adjusted to about 4 mM from absorption measurement. The Au nanostars were prepared from the Au seed solution. Accordingly, 0.1 mL of HAuCl₄ solution in DMF (104 mM) was mixed with 30 mL PVP solution in DMF (10 mM) in a three neck round bottom flask. Then 0.1 mL of PVP coated Au seed solution (~ 4 mM) was added rapidly and stirred for 3 hours at room temperature. Finally the Au nanostars were sedimented by centrifugation and redispersed in anhydrous ethanol. The concentration of the Au nanostars was determined by nuclear activation analysis.

3.3. Fabrication of Solar Cell Devices

DBH solar cells were fabricated by spin coating QD solution layer by layer on the film of TiO₂ nanorod arrays grown on FTO substrates. Each layer was spin coated by dispensing 200 µL of the QDs solution on a 1 inch by 1 inch substrate and rotating at 2500 rpm for 10 seconds. Ligand exchange was performed on each layer by treating it with a solution of TGA or 3-MPA in methanol (1:9) for 1 minute followed by spinning at 2500 rpm for 10 seconds. The layer was then washed with methanol and hexane by spinning at 2500 rpm for 10 seconds. Such ligand exchange procedure was repeated three times for each layer.

The spin coating of the QD film was done in a glove box for devices involving PbS QDs and in ambient air for those involving PbS/CdS core-shell QDs. For studying annealing effect, devices

were kept in a tubular furnace at 110 °C under N₂ flow for 30 min. For devices involving Au nanostars, the Au nanostars were deposited on a layer of QD film, which is formed after 2, 3 or 4 spin coating cycles, by spin coating different concentrations of Au nanostars in ethanol at 1000 rpm for 1 min. Then the QDs spin coating and ligand exchange were continued until the desired number of layers was reached.

On some devices, a final layer of PEDOT:PSS was deposited by dispensing 500 μL of its solution (1.3 % by weight in water) and spin coating at 2500 rpm for 1 minute. On some others, ~20 nm thick MoO₃ layer was deposited by thermal evaporation of MoO₃ powder. Finally ~ 40 nm thick gold electrodes were deposited by thermal evaporation of Au pellets from alumina coated tungsten wire baskets through a shadow mask of 4 by 4 circular arrays with circular aperture of 4 mm in diameter, resulting in photoactive area of about 0.13 cm². The pressure in the vacuum chamber was set at < 10⁻⁶ mbar and the distance between the source and the sample was ~ 22.5 cm.

3.4. Characterizations

3.4.1. Characterization of Nanostructures

SEM images were taken with a JEOL JSM-6300F SEM equipped with EDS. TEM, HRTEM images and selected area electron diffraction (SAED) pattern were taken by a JEOL 2100F TEM. The X-ray diffraction (XRD) patterns were acquired using a Philips X'pert diffractometer using Cu-Kα radiation source.

The electronic resistance of the rutile TiO₂ nanorod array electrode was measured by a PEC method at 25°C in 0.10 M NaNO₃ solution in a three-electrode cell. In particular, the TiO₂ nanorod working electrode was mounted in a special holder with an area of 0.78 cm² exposed to UV illumination via a quartz window. A scanning potentiostat (PAR 362, Princeton) was used to conduct the linear sweep voltammetry (LSV) measurements. The light source was a 150 W xenon lamp (Trusttech, Beijing, China) with regulated optical output and an UV-band-pass filter (UG-5, Schott). The output UV light intensity was measured at 365 nm wavelength using a UV irradiance meter (UV-A, Instruments of Beijing Normal University, China).

Absorption and extinction spectra were recorded using a Cary 5000 UV-Vis-NIR spectrophotometer (Varian) including integrating sphere accessory. Fluorescence spectra were acquired with a Fluorolog®-3 system (Horiba Jobin Yvon) with excitation wavelength of 670 nm.

3.4.2. Characterization of Solar Cell Devices

Solar cell devices were characterized by conducting current-voltage (I-V) measurements using an Agilent B2901A instrument in ambient atmosphere in dark and under calibrated AM1.5 simulated sunlight from an Oriel Sol3A Class AAA Solar Simulator (Oriel Instruments, Newport Corporation). Some of the solar cells were characterized by performing current-voltage measurement using a Keithley 2400 programmable voltage source meter in dark and under illumination with an AM1.5 solar simulator comprised of a 150 W xenon lamp with a filter (Oriel) and calibrated to an intensity of $100 \text{ mW}\cdot\text{cm}^{-2}$. EQE of the solar cell devices was measured using Oriel® IQE-200™ quantum efficiency measurement system, by scanning from 380 nm to 1250 nm with a 10 nm resolution.

3.5. Theoretical Calculation

Optiwave FDTD simulation was used to calculate the extinction and electromagnetic field distribution of a Au nanostar. An Au nanostar with five tips in each of two orthogonal planes was modelled. The refractive index of Au was extracted from the data of Palik [161] The simulation cell was created with a grid size resolution of 1 nm. For the simulation of the electric field distribution around the Au nanostar in the QD film, a polarized Gaussian modulated continuous wave centered at 980 nm (close to the first excitonic absorption peak of the QD film) was used as the input light source.

CHAPTER 4 RESULTS

The results section is presented in three different parts, each corresponding to different articles. The first part is about the first demonstration of PbS/CdS core-shell QDs in DBH solar cells. The second part focuses on further optimization of the solar cell devices by tuning the length of TiO₂ nanorod arrays and their interface with FTO substrate as well as the PbS/CdS core-shell QDs via thermal treatment in inert atmosphere. The third part of this chapter focuses on plasmonic enhancement of the performance of the DBH solar cell devices.

4.1. Air-processed Depleted Bulk Heterojunction Solar Cells Based on PbS/CdS Core-shell Quantum Dots and TiO₂ Nanorod Arrays

Belete Atomsa Gonfa, Haiguang Zhao, Jiangtian Li, Jingxia Qiu, Menouer Saidani, Shanqing Zhang, Ricardo Izquierdo, Nianqiang Wu, My Ali El Khakani, and Dongling Ma

Sol. Energ. Mat. Sol. Cells **124** (2014) 67-74.

Colloidal QD based solar cells are a subject of considerable research interest due to their potential to achieve high PCE devices at low cost. NIR QDs in solar cells are even more interesting as they enable the extension of light absorption into the NIR part of the solar spectrum. In particular, core-shell QDs are promising as they offer better stability and good surface passivation reducing recombination losses, which is critical in increasing the PCE of the devices. On the other hand 1D nanostructures look very interesting in solar cells application considering their enhanced charge transport.

In this section, the investigation of NIR PbS/CdS core-shell QDs in DBH solar cells is presented. Processability of the PbS/CdS core-shell QDs into solar cells in ambient atmosphere with enhanced performance compared to the PbS QDs solar cells processed under inert atmosphere in a glove box is demonstrated.

Cet article a dû être retiré de la version électronique en raison de restrictions liées au droit d'auteur.

Vous pouvez le consulter à l'adresse suivante :

DOI : <http://dx.doi.org/10.1016/j.solmat.2014.01.037>

Supporting Information for

**Air-processed Depleted Bulk Heterojunction Solar Cells Based on PbS/CdS
Core-shell Quantum Dots and TiO₂ Nanorod Arrays**

Belete Atomsa Gonfa¹, Haiguang Zhao¹, Jiangtian Li², Jingxia Qiu³, Menouer Saidani⁴,
Shanqing Zhang³, Ricardo Izquierdo⁴, Nianqiang Wu², My Ali El Khakani¹, and Dongling Ma^{1,*}

¹Institut National de la Recherche Scientifique (INRS), Centre-Énergie, Matériaux et
Télécommunications, 1650 Boulevard Lionel-Boulet, Varennes, QC, Canada J3X 1S2

²Department of Mechanical and Aerospace engineering, West Virginia University, Morgantown,
WV, 26506-6106, USA

³Environmental Futures Centre, Griffith School of Environment, Gold Coast Campus, Griffith
University, QLD 4222, Australia

⁴Département d'informatique, University of Quebec at Montreal (UQAM), Case postale 8888,
succursale Centre-ville, Montréal, Québec H3C 3P8, Canada

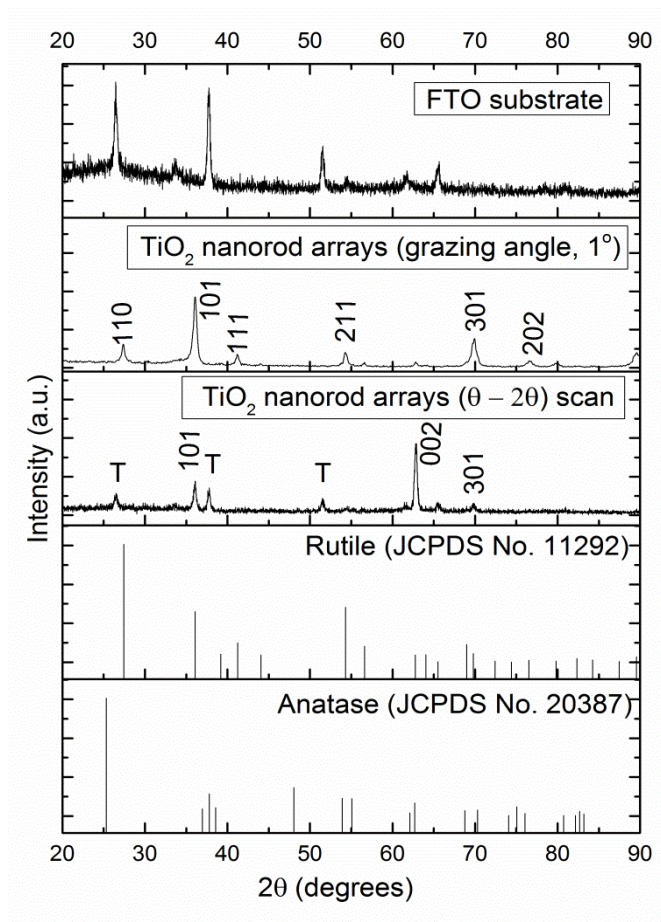


Figure S1. XRD patterns of the as-grown TiO₂ nanorod arrays compared with that of FTO glass substrate and standard rutile and anatase patterns. T denotes peaks corresponding to SnO₂.

Table S1. J-V characteristics of devices fabricated with different number of deposition cycles of QDs.

S.No.	QDs	Ligand used for exchange	No. of spin coating cycles	Interfacial layer	J _{sc} (mA/cm ²)	V _{oc} (mV)	FF (%)	η (%)	Spin coating environment
1	PbS	TGA	3	PEDOT:PSS	3.1	413	33.5	0.43	Air
2	PbS	TGA	6	PEDOT:PSS	4.5	427	36	0.70	Air
3	PbS	TGA	10	PEDOT:PSS	2.7	442	33	0.40	Air

Table S2. J-V characteristics of devices involving different ligands.

S.No.	QDs	Ligand used for exchange	No. of spin coating cycles	interfacial layer	J_{sc} (mA/cm ²)	V_{oc} (mV)	FF (%)	η (%)	Spin coating environment
1	PbS	3 - MPA	6	PEDOT:PSS	5.61	446	42	1.05	Glovebox atmosphere (N ₂)
2	PbS	TGA	6	PEDOT:PSS	6.14	425	44	1.16	Glovebox atmosphere (N ₂)
3	PbS	3 - MPA	6	MoO ₃	7.94	497	39	1.53	Glovebox atmosphere (N ₂)
4	PbS	TGA	6	MoO ₃	8.15	487	37	1.47	Glovebox atmosphere (N ₂)
5	PbS/CdS	3-MPA	6	PEDOT:PSS	5.61	423	44	1.05	Air
6	PbS/CdS	TGA	6	PEDOT:PSS	5.31	428	43	0.97	Air

4.2. Towards High Efficiency Air-processed Near-infrared Responsive Photovoltaics: Bulk Heterojunction Solar Cells Based on PbS/CdS Core-shell Quantum Dots and TiO₂ Nanorod Arrays

Belete Atomsa Gonfa, Mee Rahn Kim, Nazar Delegan, Ana C. Tavares, Ricardo Izquierdo, Nianqiang Wu, My Ali El Khakani, and Dongling Ma

Nanoscale **7** (2015) 10039-10049.

Even though the use and advantages of PbS/CdS core-shell QDs in solar cells have been demonstrated in the previous section, the PCE is not very high and needs to be further improved by materials and device optimizations. This section presents the further optimizations done on the devices towards improved performance. The optimizations involve the study of the effect of uniform, sputter deposited TiO₂ seed layer on FTO substrate before the growth TiO₂ nanorod arrays, different length of TiO₂ nanorod arrays, and mild thermal annealing treatment of the QD film in N₂ atmosphere.

By using the TiO₂ seed layer to modify the TiO₂ nanorod/FTO interface and performing mild thermal annealing of the QD film under N₂, a PCE as high as 4.43 % under AM 1.5 illumination has been achieved using an optimal TiO₂ nanorod length of ~450 nm. The photoresponse extended to wavelengths of ≥ 1200 nm.

Cet article a dû être retiré de la version électronique en raison de restrictions liées au droit d'auteur.

Vous pouvez le consulter à l'adresse suivante :

DOI: 10.1039/c5nr02371h

Supporting information for:

**Towards high efficiency air-processed near-infrared responsive
photovoltaics: bulk heterojunction solar cells based on PbS/CdS core-
shell quantum dots and TiO₂ nanorod arrays**

Belete Atomsa Gonfa^a, Mee Rahn Kim^a, Nazar Delegan^a, Ana C. Tavares^a, Ricardo Izquierdo^b,
Nianqiang Wu^c, My Ali El Khakani^a, and Dongling Ma^{*a}

^aInstitut National de la Recherche Scientifique (INRS), Centre-Énergie, Matériaux et
Télécommunications, 1650 Boulevard Lionel-Boulet, Varennes, QC, Canada J3X 1S2

^bDépartement d'informatique, University of Quebec at Montreal (UQAM), Case postale 8888,
succursale Centre-ville, Montréal, Québec H3C 3P8, Canada

^cDepartment of Mechanical and Aerospace Engineering, West Virginia University, Morgantown,
WV 26506-6106, USA

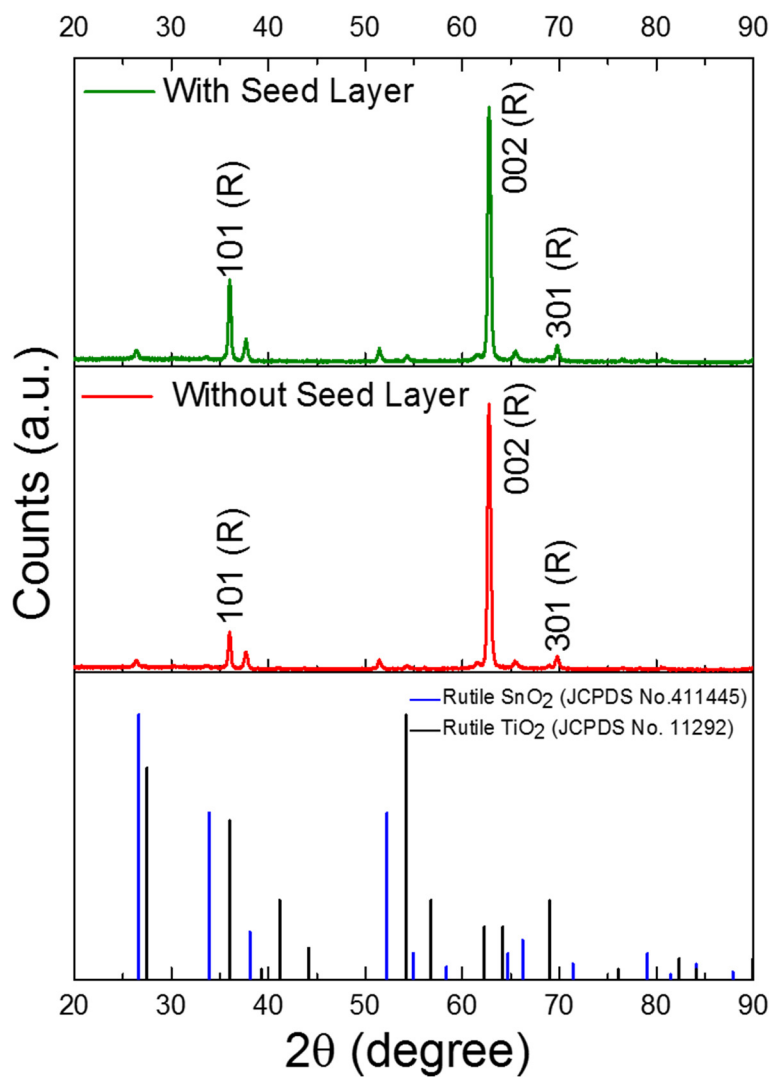


Figure S1. XRD patterns of 2 μm -long TiO₂ nanorod arrays grown on FTO with and without a seed layer, compared with JCPDS files of rutile SnO₂ and rutile TiO₂. R refers to rutile TiO₂.

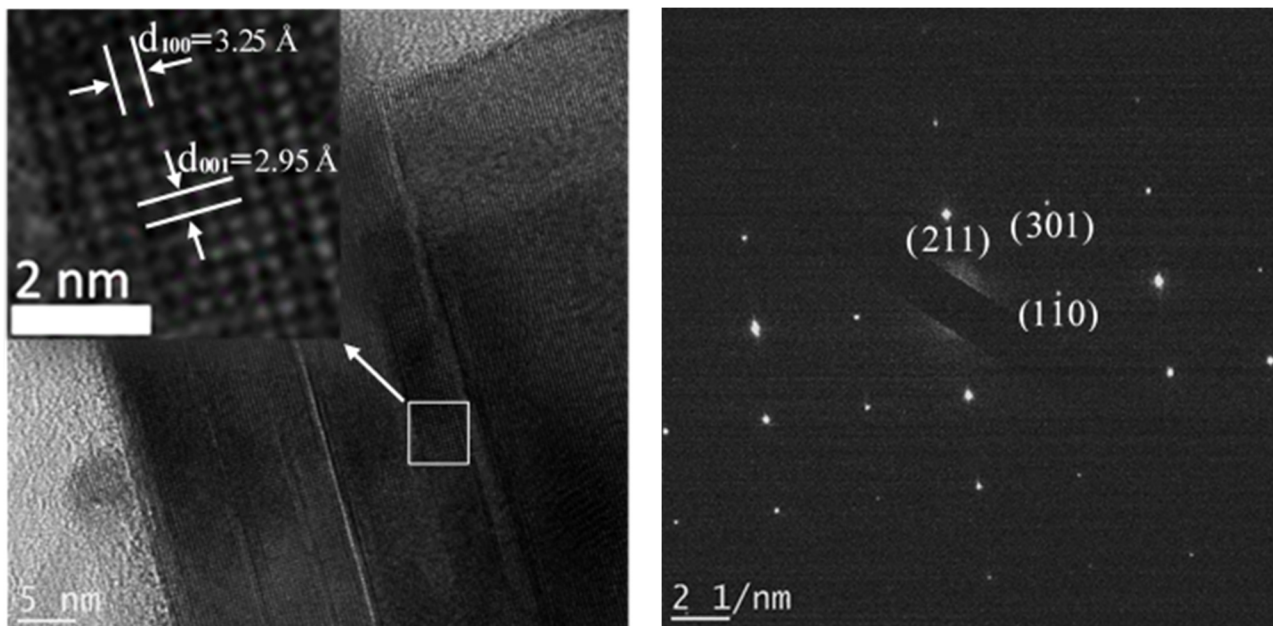


Figure S2. HRTEM images and SAED pattern of a TiO₂ nanorod.

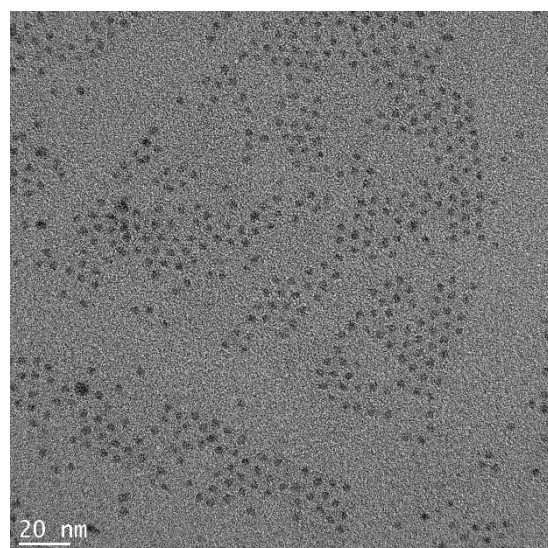


Figure S3. Low magnification TEM image of PbS/CdS core-shell QDs.

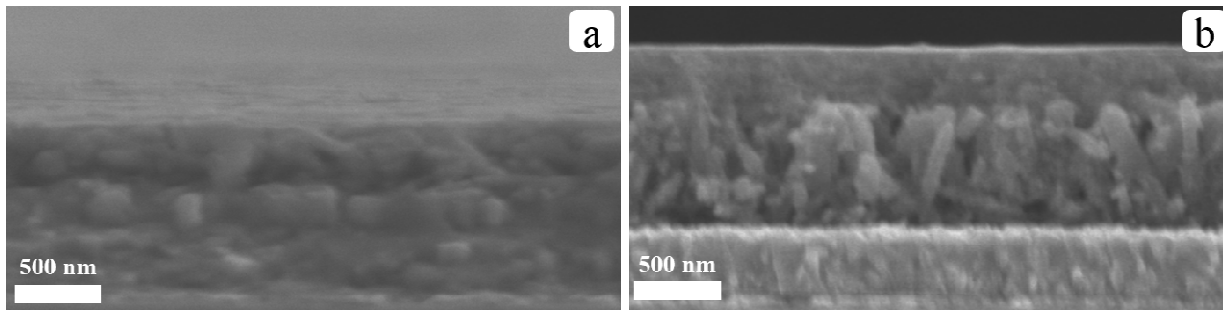


Figure S4. Cross-sectional SEM images of PbS/CdS core-shell QDs spin coated on (a) 250 nm TiO₂ nanorod arrays grown on seed/FTO glass substrate and (b) 650 nm TiO₂ nanorod arrays grown on FTO glass substrate.

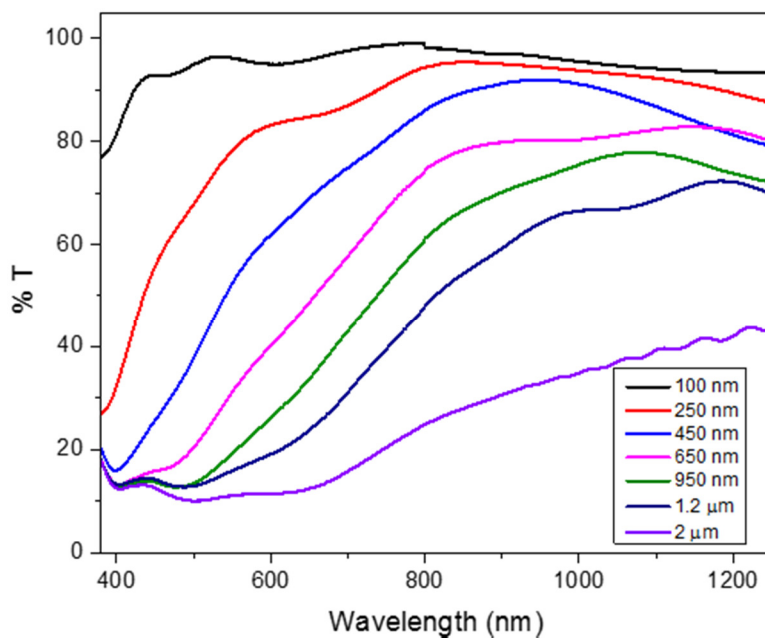


Figure S5. Optical transmittance of TiO₂ nanorod arrays of different length grown on seed/FTO substrate.

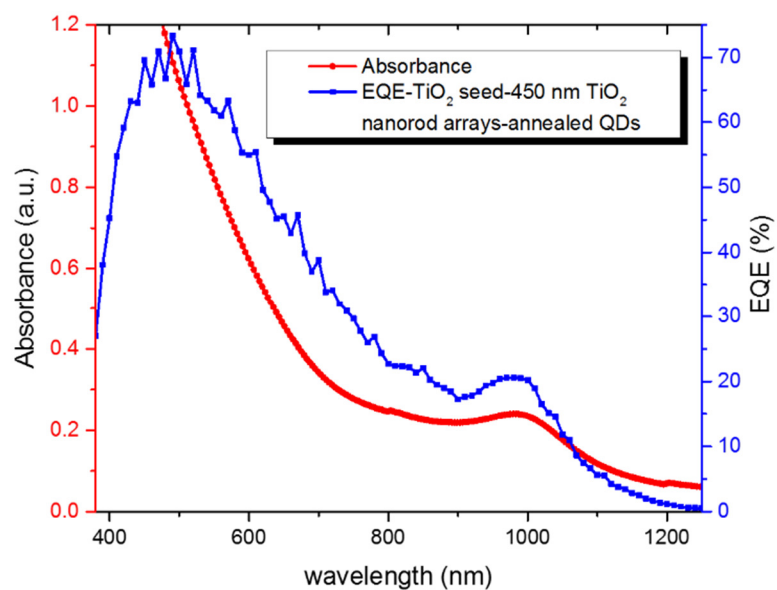


Figure S6. EQE spectrum of the device involving 450 nm TiO_2 nanorod arrays grown on seed/FTO glass substrate and annealed in N_2 atmosphere, compared with the absorption spectrum of annealed PbS/CdS core-shell QDs on quartz.

Table S1. Performance of bulk heterojunction solar cell devices fabricated using TiO₂ nanorod arrays of different length grown on bare FTO substrate.

TiO ₂ nanorod array length	J _{sc} (mA/cm ²)	V _{oc} (mV)	FF (%)	η (%)
100 nm	12.20 (11.36 ± 0.60)	549 (513 ± 19)	44 (39 ± 2.9)	2.66 (2.46 ± 0.19)
250 nm	13.93 (13.38 ± 0.29)	537 (517 ± 14)	48 (45 ± 2.0)	3.45 (3.19 ± 0.21)
450 nm	13.74 (12.77 ± 0.43)	543 (523 ± 10)	50 (46 ± 2.4)	3.56 (3.25 ± 0.22)
650 nm	13.68 (13.29 ± 0.31)	537 (516 ± 13)	47 (43 ± 2.4)	3.34 (3.11 ± 0.21)
950 nm	13.95 (13.55 ± 0.30)	507 (477 ± 19)	45 (43 ± 2.0)	3.16 (2.85 ± 0.27)
1.2 μm	13.21 (12.73 ± 0.39)	497 (474 ± 14)	43 (39 ± 2.1)	2.69 (2.34 ± 0.25)
2 μm	13.87 (13.04 ± 0.58)	495 (478 ± 11)	37 (33 ± 2.4)	2.41 (2.02 ± 0.19)

Table S2. Performance of bulk heterojunction solar cell devices fabricated using 450 nm-long TiO₂ nanorod arrays grown on the bare FTO and seed/FTO substrates, before and after annealing.

Seed	Annealing	J _{sc} (mA/cm ²)	V _{oc} (mV)	FF (%)	η (%)
No	No	13.74 (12.77 ± 0.43)	543 (523 ± 10)	50 (46 ± 2.4)	3.56 (3.25 ± 0.22)
No	In N ₂	17.69 (17.00 ± 0.37)	493 (481 ± 7)	49 (45 ± 2.4)	4.13 (3.93 ± 0.13)
Yes	No	13.68 (13.29 ± 0.28)	547 (537 ± 6)	52 (48 ± 2.2)	3.76 (3.55 ± 0.17)
Yes	In N ₂	17.75 (16.83 ± 0.43)	519 (506 ± 10)	50 (46 ± 2.7)	4.43 (4.28 ± 0.12)

4.3. Plasmonic Enhancement of the Performance of PbS/CdS Core-shell Quantum Dots/TiO₂ Nanorod Arrays Bulk Heterojunction Solar Cells

Belete Atomsa Gonfa, Mee Rahn Kim, Peng Zheng, Nianqiang Wu, My Ali El Khakani, and Dongling Ma

to be submitted

Plasmonic nanoparticles can be incorporated into QD based solar cells to enhance photon absorption, and thus contribute to PCE enhancement. Therefore, it is quite interesting to combine plasmonic nanoparticles with the NIR PbS/CdS core-shell QDs in designing solar cells.

In this part, the investigation of plasmon enhanced, DBH solar cells involving Au nanostars incorporated into NIR PbS/CdS core-shell QD film, which was spin coated onto TiO₂ nanorod arrays film on FTO glass substrate, is presented. After optimizing the density and location of the Au nanostars in the QD film, a PCE of 4.16 % has been achieved, which is about 16 % increase compared to the control device without the Au nanostars. This increase in the PCE is attributed to plasmonic enhancement of light absorption, which increases charge carrier generation in the QDs as evidenced by the increase in the J_{sc} (about 26 % in this case) and EQE.

Plasmonic Enhancement of the Performance of PbS/CdS Core-shell Quantum Dots/TiO₂ Nanorod Arrays Bulk Heterojunction Solar Cells

Belete Atomsa Gonfa¹, Mee Rahn Kim¹, Peng Zheng², Nianqiang Wu², My Ali El Khakani¹, and
Dongling Ma^{1,*}

¹Institut National de la Recherche Scientifique (INRS), Centre-Énergie, Matériaux et
Télécommunications, 1650 Boulevard Lionel-Boulet, Varennes, QC, Canada J3X 1S2

²Department of Mechanical and Aerospace Engineering, West Virginia University, Morgantown,
WV 26506-6106, USA

*Corresponding Author: e-mail: ma@emt.inrs.ca

Phone : (514) 228-6920

Fax : (450) 929-8102

Abstract

Integrating appropriate plasmonic nanostructures into colloidal quantum dot (QD) based solar cells is an attractive strategy in improving their power conversion efficiency (PCE). Such manipulation allows enhanced photon absorption by QDs and, therefore, more charge carrier generation. In this work we report the investigation of plasmon enhanced bulk heterojunction solar cells involving Au nanostars incorporated into a near infrared PbS/CdS core-shell QD film spin coated onto TiO₂ nanorod arrays. The rationale behind choosing the Au nanostars is based on their strong light scattering capability as well as near field enhancement of absorption in the surrounding QD film, as supported by finite-difference time-domain calculations. The effect of the density and location of the Au nanostars in the QD film on device performance was studied in detail and optimal parameters were identified. Following such parameter optimization, a PCE of 4.16 % has been achieved, which was about 16 % higher than that (PCE: 3.59 %) of the control device without Au nanostars. This increase in the PCE was found to be mainly due to the increase in short circuit current (J_{sc}) (about 26 % in this case), suggesting that the presence of Au nanostars enhances the charge carrier generation via improving photon absorption. This was further confirmed by the enhancement of photoresponse as evidenced by the increase of external quantum efficiency mainly in the surface plasmon resonance (SPR) spectral region of the Au nanostars. Theoretical calculations were carried out to simulate the local electric field distribution around the Au nanostars embedded in the QD film. Correlating the experimental and calculation results clearly suggest that enhanced J_{sc} and PCE of the solar cells involving the Au nanostars is due to enhanced absorption via the field enhanced absorption and scattering as a result of the Au nanostars incorporation.

Key Words: Quantum dots, PbS/CdS core-shell quantum dots, TiO₂ nanorods, plasmonic nanoparticles, surface plasmon resonance, Au nanostars, bulk heterojunction solar cells

1. Introduction

Colloidal quantum dot (QD) based solar cells have recently attracted considerable research interest due to their low cost solution processability and great potential to achieve high power conversion efficiency (PCE) [1]. Even though large progress was made in early years following demonstration of the first QD based solar cell reported in 1998 with estimated PCE of about 0.08 % under white light illumination [2], the PCE needed further improvement. Various strategies have been

extensively explored and implemented in the past several years, leading to significant improvement in the PCE of colloidal QD based solar cells. Up to date, a lab-record PCE of ~9.2 % [3-5] has been achieved with the highest certified PCE of 8.55 % [5]. These high efficiencies were achieved by heterojunction solar cells involving PbS QDs, and ZnO or TiO₂ photoelectrodes. These prominent recent advances have been made mainly by engineering device architecture, and by improving charge carrier transport and extraction in the QD film through improving surface passivation of the QDs and decreasing the inter-dot distance [6]. In particular, the concept of bulk heterojunction solar cells allows the use of a relatively thick layer of QDs to maximize light absorption without decreasing charge carrier collection. Since efficient photogeneration of charge carriers and efficient charge transport and collection are required for the ultimate high performance of solar cells, it is important to enhance all these processes simultaneously without compromising each other. The efficient realization of these processes largely depends on the thickness and quality of the QD film.

In bulk heterojunction solar cells, the thickness of the QD film that can be used is limited. It is because the depletion width of the QD film is in general limited and furthermore, the overall thickness of the active QD layer should be less than the sum of the depletion width and charge diffusion length in the QD film, which is about 250 nm in the case of PbS QDs [7]. This compromises light absorption and hence the amount of photogenerated charge carriers. Although the use of a thick QD film enables absorption of more photons, it compromises charge carriers collection. Such a trade-off between charge carrier generation and charge carrier collection leads to the limitation of the PCE. This issue, however, may be alleviated by using plasmonic nanoparticles, which can enhance the absorption of light by a thin QD film [8].

Surface plasmon resonance (SPR) is the oscillation of free electrons on the surface of a metal in response to an applied electromagnetic field. Localized surface plasmon resonance (LSPR) are SPR confined in metal nanoparticles with size less than or comparable to the exciting wavelength. For some noble metals like Au the LSPR occurs in visible range[9]. LSPR mode depends on the size and shape of the metal nanoparticle as well as the refractive index or dielectric constant of the medium around them. LSPR significantly enhances the electric field around the nanoparticle and photon absorption in the medium around them in close proximity, for example, QD film [10, 11]. The plasmonic nanoparticles can also act as light scattering centers, increasing optical path length in the active absorbing medium of solar cells, which will result in enhanced photoresponse and

increased PCE [12]. Plasmonic nanoparticles can also increase absorption of light and exciton generation as well as exciton dissociation via local electric field enhancement and the interaction between plasmons and photogenerated excitons [13]. In addition to offering a new opportunity to overcome the aforementioned limit, the implementation of plasmonics in solar cells could also be an effective way to address one of the present challenges in solar cell technology, which is decreasing semiconductor material cost through using thinner films, while without sacrificing solar cell performance. This strategy may also allow designing of devices that take advantage of hot-carriers [14]. On the other hand, it has to be realized that the introduction of plasmonic nanoparticles may have negative effects on solar cell performance since they may behave as charge carrier recombination centers as well. Therefore, to fulfil the high potential of plasmonic nanoparticles in solar cell applications rational designing, realization and systematic investigation of plasmon enhanced solar cells are required. Even though plasmonic nanoparticles have been studied in different types of solar cells [13, 15-17], their investigation in QD based solar cells remains rare [6]. It was recently demonstrated that plasmonic nanoparticles can be integrated into PbS QD based heterojunction solar cells to enhance the device performance [18, 19]. However, plasmonic enhancement in near infrared (NIR) core-shell QD based solar cells has not been yet reported. Following the demonstration of the use of PbS/CdS core-shell QDs in solar cells with enhanced performance and easier processability in ambient air in our recent works [20, 21], it is highly interesting to explore the use of plasmonic nanoparticles in our PbS/CdS core-shell QD solar cells.

In this work, plasmon enhanced bulk heterojunction solar cells involving Au nanostars, PbS/CdS core-shell QDs and TiO₂ nanorod arrays are investigated. The optimal incorporation of the Au nanostars enhanced the PCE and the short circuit current (J_{sc}) of the devices due to the enhancement of photon absorption upon the introduction of the Au nanostars, as supported by external quantum efficiency (EQE) and optical absorption measurements. It was found that the effect of the Au nanostars on the device performance depends on the density of the Au nanostars in the film as well as their location in the QD film.

2. Materials and Methods

2.1. Chemicals and Materials

Titanium (IV) butoxide (reagent grade, 97%), concentrated HCl (ACS reagent, ca. 37%), $\text{Pb}(\text{OAc})_2 \cdot 3\text{H}_2\text{O}$ ($\geq 99.99\%$), oleic acid (OA) ($\geq 99\%$ (GC)), 1-octadecene (ODE) (technical grade, 90%), bis(trimethylsilyl) sulfide (synthesis grade), trioctylphosphine (technical grade, 90%), methanol (anhydrous, 99.8%), CdO ($\geq 99.99\%$ trace metals basis), octane (puriss. p.a., $\geq 99.0\%$ (GC)), decane (anhydrous, $\geq 99\%$), 3-mercaptopropionic acid ($\geq 99\%$), MoO_3 powder (ACS reagent, $\geq 99.5\%$), $\text{HAuCl}_4 \cdot x\text{H}_2\text{O}$ (99.999% trace metals basis), trisodium citrate (meets USP testing specifications), polyvinylpyrrolidone (PVP) (average molecular weight=10000 gm/mole), and N,N-dimethylformamide (DMF) (anhydrous, 99.8%) were purchased from Sigma Aldrich and used as received without any purification. FTO glass substrates (TEC 15, R=12-14 Ohm/sq) were purchased from MTI corporation. Hexane (certified ACS) and toluene (certified ACS) were purchased from Fisher Scientific Company.

2.2. Synthesis of Nanostructures

TiO_2 nanorod arrays and PbS/CdS core-shell QDs used to fabricate solar cell devices in this work were synthesized in similar ways as in our previous work [21]. TiO_2 nanorod arrays were grown via hydrothermal technique [22]. In the process, FTO glass substrates were placed in a 23 ml Teflon cup and 12 ml of precursor solution, which was prepared by dissolving 1 ml of titanium(IV) butoxide in a mixture of 20 ml of pure water and 20 ml of concentrated HCl (ca. 37%) was added. The Teflon cup was then sealed tightly inside a stainless steel autoclave and heated at 150 °C for 3 hours to obtain TiO_2 nanorods. The autoclave was then cooled and the TiO_2 nanorod arrays were washed with dilute HCl solution and pure water. The nanorods were finally dried under airflow and at 80 °C in an oven.

PbS/CdS core-shell QDs were synthesised via cation exchange [23, 24] from PbS QDs, which had been synthesised via hot injection technique [25, 26]. The PbS QDs were synthesized by mixing 760 mg of $\text{Pb}(\text{OAc})_2 \cdot 3\text{H}_2\text{O}$, 2.4 ml of OA and 15 ml of ODE in a three neck round bottom flask followed by heating to 150 °C for 1 h while stirring and purging with N_2 flow. The content was then cooled to 130 °C under vacuum and the N_2 flow was restored. Then, 2 ml of bis(trimethylsilyl) sulfide in trioctylphosphine (1 : 10 volume ratio) was quickly injected into the Pb precursor solution and cooled abruptly down to 100 °C, at which temperature the reaction was run

for 5 minutes. The reaction was stopped by quickly cooling the flask via dipping in cold water. The QDs were then dispersed in toluene, kept at 4 °C for two days and purified using methanol. The purified PbS QDs were dispersed in toluene ready for synthesis of PbS/CdS core-shell QDs. For the synthesis of PbS/CdS core-shell QDs, Cd precursor was first prepared by heating a mixture of CdO (25 mg), OA (24 mL) and ODE (40 mL) to 255 °C under N₂ flow for 20 min while stirring followed by cooling to 155 °C under vacuum for 15 min and the N₂ flux was restored. In a separate round bottom flask, 150 mL of PbS QDs solution in toluene (~350 mg PbS) was bubbled with N₂ for 30 min and heated rapidly to 90 °C. The Cd/OA mixture was injected while stirring and the reaction was carried out at 90 °C and stopped by quenching in cold water. The PbS/CdS core-shell QDs were then purified 3 times using alcohol and dissolved in mixture of octane and decane (3:1 volume ratio) for solar cell fabrication.

Au nanostars were synthesized via chemical reduction with a modified procedure from references [27-29]. In this procedure, Au seed solution was first prepared and used as precursor for the synthesis of the Au nanostars. First, 1.058 mL of 104 mM HAuCl₄ aqueous solution was diluted by adding 125 mL of water in three neck round bottom flask and heated to boiling while stirring. This was followed by injection of a separate solution prepared by dissolving 0.32 g trisodium citrate in 32 mL water. The mixture solution was kept boiling for 15 min and then cooled to room temperature. After the addition of 3.2 g of PVP, the solution was continuously stirred overnight at room temperature, which resulted in Au seed formation. The PVP coated Au seed solution was then centrifuged and re-dispersed in ethanol with concentration adjusted to about 4 mM based on absorption measurements. The Au nanostars were prepared from the Au seed solution. Accordingly, 0.1 mL of HAuCl₄ solution in DMF (104 mM) was mixed with 30 mL PVP solution in DMF (10 mM) in a three neck round bottom flask. Then 0.1 mL of PVP coated Au seed solution (about 4 mM) was added rapidly and stirred for 3 hours at room temperature. Finally the Au nanostars were sedimented by centrifugation and redispersed in anhydrous ethanol.

2.3. Fabrication of Solar Cell Devices

Solar cell devices were fabricated via layer-by-layer spin coating of PbS/CdS core-shell QDs on TiO₂ nanorod arrays films followed by ligand exchange in ambient air. Each layer of QDs was spin coated by dispensing 200 µl of the QD suspension on a 1 inch by 1 inch FTO/TiO₂ nanorod array substrate and rotating at 2500 rpm for 20 seconds. The ligand exchange was carried out three

times for each layer of QDs by treating it with 10 % v/v solution of 3-mercaptopropionic acid in methanol for 1 min followed by washing with methanol and hexane. For devices involving Au nanostars, they were deposited on a QD film, which was formed following 2, 3 or 4 spin coating cycles, by spin coating different concentrations of Au nanostars in ethanol at 1000 rpm for 1 min. Then the QD spin coating and ligand exchange processes were continued until the desired final number of layers of QDs was reached. About 20 nm thick MoO₃ hole extracting layer was deposited on the QD film by thermal evaporation. It was then followed by thermal evaporation of about 40 nm thick Au back electrode through a shadow mask of 4 by 4 circular arrays with circular aperture of 4 mm in diameter, resulting in photoactive area of about 0.13 cm². The pressure in the vacuum chamber was set at < 10⁻⁶ mbar.

2.4. Characterizations

A JEOL JSM-6300F scanning electron microscope (SEM) and a JEOL 2100F transmission electron microscope (TEM) were used to study the morphology of Au nanostars, core-shell QDs and TiO₂ nanorods, and to characterize the device structure. A Philips X'pert diffractometer with Cu-K α radiation source was used to acquire X-ray diffraction (XRD) pattern of the TiO₂ nanorod arrays. A Cary 5000 spectrophotometer (Varian) including integrating sphere accessory was used for the acquisition of extinction and absorption spectra. The extinction spectra were measured using a standard sample holder. The absorption spectra of the films were obtained from the transmission plus scattering and reflection, which were acquired using an integrating sphere; Absorption = 100 - (reflection + transmission + scattering). The reflection was measured by placing the samples at the port opposite to the input port without the back-reflector. The baseline was obtained by using a back-reflector and by blocking the light at the input port; the difference was set to 100 %. The sum of transmission and scattering was measured by placing the sample at the input port and placing the back-reflector at the port opposite to the input port so that all the transmitted light is back reflected and detected. The baseline was obtained using a back-reflector and quartz film at the input port, and by blocking the light at the input port; the difference was set to 100 %. A Fluorolog®-3 system (Horiba Jobin Yvon) was used to record photoluminescence (PL) emission spectrum of QDs with excitation wavelength of 670 nm. The concentration of the Au nanostars was determined by neutron activation analysis using a SLOWPOKE nuclear reactor. Solar cell devices were characterized by performing current density – voltage (J-V) measurements using an Agilent B2901A instrument in dark and under AM 1.5 simulated sun light, which was

provided by an Oriel Sol3A Class AAA Solar Simulator (Oriel Instruments, Newport Corporation). EQE measurements of the solar cell devices were carried out using an Oriel® IQE-200™ quantum efficiency measurement system.

2.5. Theoretical Calculations

Optiwave finite-difference time-domain (FDTD) simulation was used to calculate the extinction, absorption, scattering of an Au nanostar, electric field distribution around an Au nanostar embedded in the QD film and electric field induced absorption enhancement of the QD film as a function of distance from the Au nanostar tip. An Au nanostar with five tips in each of two orthogonal planes was modelled. The refractive index of Au was extracted from the data of Palik [30]. The simulation cell was created with a grid size resolution of 1 nm. For the simulation of the electric field distribution around the Au nanostar in the QD film, a polarized Gaussian modulated continuous wave centered at 980 nm (close to the first excitonic absorption peak of the QD film) was used as the input light source.

3. Results and Discussion

Based on our previous work [21] TiO₂ nanorod arrays of optimum length hydrothermally grown on clean FTO substrate (about 450 nm) and similar PbS/CdS core-shell QDs are used in this work for fabrication and investigation of the BH solar cell devices. The SEM images and the XRD

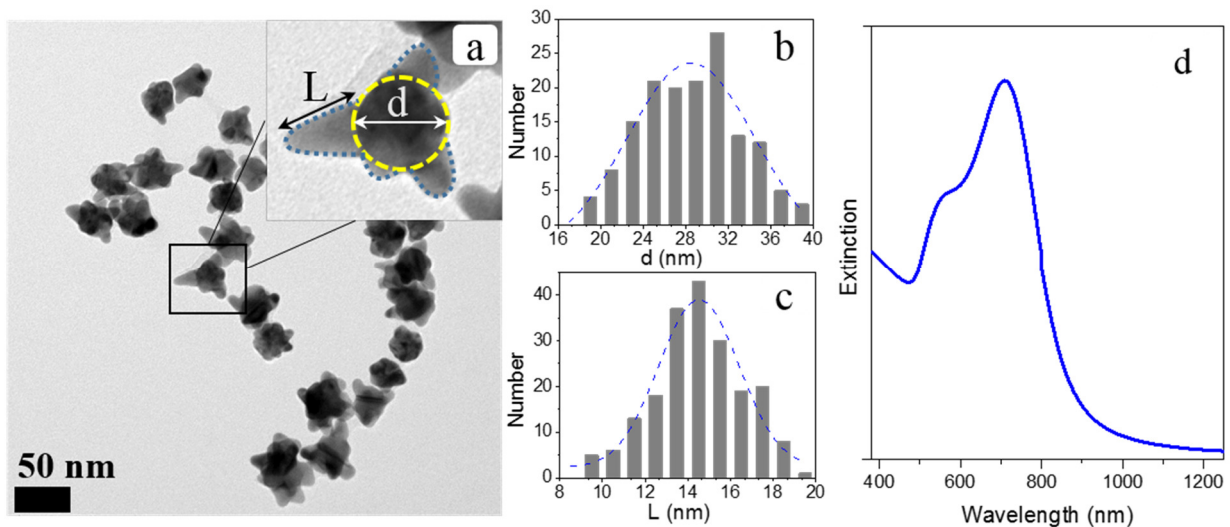


Figure 1. (a) TEM image, (b) size distribution of the core (diameter) and (c) tip (length) of the Au nanostars, and (d) extinction spectrum of Au nanostars in ethanol.

pattern of the TiO₂ nanorod arrays are shown in Figure S1. The PbS/CdS core-shell QDs used have average PbS core diameter of about 3.0 nm and CdS shell thickness of about 0.1 nm. They were synthesized via the cation exchange reaction of PbS QDs (~3.2 nm in diameter) with Cd²⁺ ions. The average CdS shell thickness was obtained by subtracting the average PbS core radius from the average radius of the parent PbS QDs, which were both determined from the position of their first excitonic absorption peaks [21, 31]. As reported in our previous work, the size of PbS QDs estimated from their optical spectra was quite consistent with that from TEM observations [23, 24]. The visible-NIR extinction and photoluminescence (PL) emission spectra of the PbS/CdS core-shell QDs as well as the TEM image are shown in Figure S2.

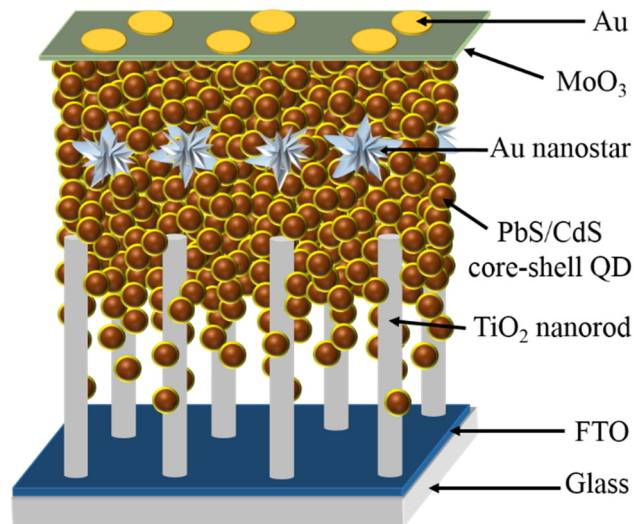


Figure 2. Schematic illustration of the structure of plasmonic bulk heterojunction solar cell device.

TEM images of the Au nanostars used for fabricating plasmonic bulk heterojunction solar cells are shown in Figure 1 a. The Au nanostars have average core diameter of about 27.5 nm and tip length of 13.6 nm. The distribution of the core diameter and tip length of the Au nanostars are shown in Figure 1 b and c respectively. The extinction spectrum of the Au nanostars dispersed in ethanol is shown in Figure 1d. The resonance pattern was composed of a peak centered at ~710 nm and a shoulder at ~560 nm, in line with literature reports for similar plasmonic nanostructures [27, 29, 32]. The shoulder at ~560 nm was assigned to the transverse mode of the Au core, whereas the strong resonance peak arose from the formation of tips. A diluted Au nanostars solution in ethanol with an absorbance of about 3.0 at the center of the resonance band of the Au nanostars (~710 nm) was found to have a concentration of 171 ppm, with uncertainty of $\pm 5\%$ according to the neutron activation analysis.

The structure of the bulk heterojunction solar cell devices investigated herein is schematically illustrated in Figure 2. Basically the solar cell device consisted of the Au nanostars embedded in the PbS/CdS core-shell QD film, which was deposited onto hydrothermally grown TiO₂ nanorod

arrays via layer-by-layer spin coating and ligand exchange technique. The QDs partially infiltrated into the gaps of the TiO₂ nanorod arrays, and thus forming the bulk heterojunction as previously reported by our group [21]. The Au nanostars were introduced into the PbS/CdS core-shell QD film at different locations by spin coating their ethanol solution onto the QD film prepared following different spin coating cycles. The devices were completed by thermal evaporation of a hole extracting layer of MoO₃ and Au back electrode.

Figure 3a shows the cross-sectional SEM image of the bulk heterojunction device involving Au nanostars. The TiO₂ nanorod length is ~ 450 nm and the QDs seem to infiltrate into the gaps between the TiO₂ nanorods and the QD film thickness above the nanorods is ~ 300 nm. Figure 3b is an SEM image showing the distribution of Au nanostars on the QD film surface following their spin coating deposition. In this specific case, the Au nanostar concentration of 6.84 mg/ml was used for the spin coating process. The Au nanostars can be clearly identified from the background QD film and they seemed to be more or less sparsely distributed over the QD film with a few aggregations observed.

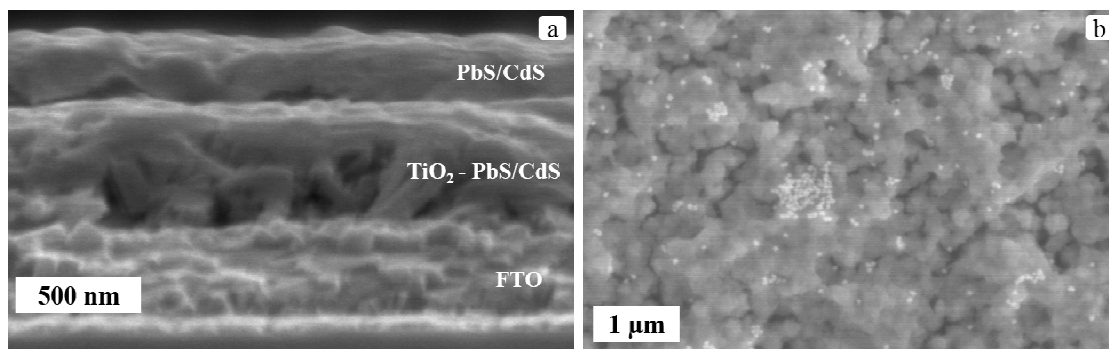


Figure 3. (a) Cross-sectional SEM image of the solar cell device involving PbS/CdS core-shell QDs, TiO₂ nanorod arrays and Au nanostars, and (b) SEM image of Au nanostars spin coated on QDs film before depositing next cycle of QDs.

In order to study the effect of the density of the Au nanostars and their location in the QD film on device performance, different concentrations of Au nanostars were used for deposition onto the QD film of different thickness. The highest AM 1.5 PCE of about 4.16 % was achieved by spin coating the Au nanostar ethanol solution at the concentration of 6.84 mg/ml on 3 spin-coated layers (thickness: ~ 170 nm) of PbS/CdS core-shell QDs (Figure 3b). This represented an increase of

about 16 % compared to that (PCE: 3.59 %) of the control device without Au nanostars. The J-V characteristics of these two devices under AM 1.5 illumination are shown in Figure 4. It can be clearly seen that the enhancement in the PCE after the incorporation of the Au nanostars was

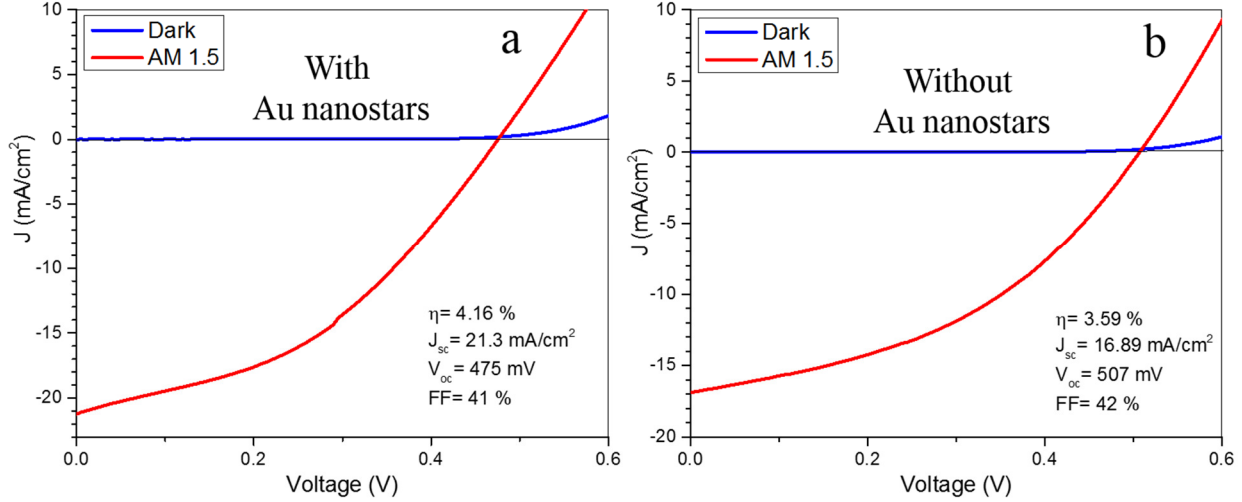


Figure 4. J-V curves of bulk heterojunction devices (a) with and (b) without Au nanostars.

mainly due to the increase in J_{sc} (about 26 % in this case) suggesting that the presence of Au nanostars enhanced charge carrier generation via improving photon absorption. The enhancement in photon absorption could be in general attributed to the combined effects of both increased effective optical path length in the QD film due to enhanced scattering with the presence of Au nanostars and improved exciton generation in the QDs in the proximity of the Au nanostars due to the local electric field enhancement. However, the introduction of the Au nanostars simultaneously resulted in slight decrease of open circuit voltage (V_{oc}) and fill factor (FF) by about 6.3 % and 2.4 % respectively, which was considered to be due to the introduction of charge carrier recombination centers. This shows the increase in J_{sc} overcomes the decrease in V_{oc} and FF resulting in increase in overall PCE.

In order to better understand the plasmonic contribution to device performance, EQE of devices with the Au nanostars and without was measured. As shown in Figure 5a, EQE enhancement took place almost over the whole spectral range measured, from 380 nm to 1200 nm. This is in agreement with the observed increase in J_{sc} . Indeed this evident enhancement in photoresponse over the whole measured spectral range from NIR to ultraviolet is also observed in other report [33]. Meanwhile, the absorption of QD films with and without Au nanostars was also measured.

The absorption spectra of the PbS/CdS core-shell QD films (without Au nanostars and with optimum amount of Au nanostars at optimum location in the QD film (Figure 5b)) correspond to the EQE spectra of the devices extending in the NIR part of the solar spectrum reaching up to 1200 nm. The enhancement in absorption (Figure 5c) was obtained by subtracting the absorption spectrum of the QD film without Au nanostars from that of the QD film with the Au nanostars. The spectrum of the absorption enhancement overlaps very well with the extinction of the Au nanostars film with a slight red shift, which is due to the high refractive index of the QD film [19,

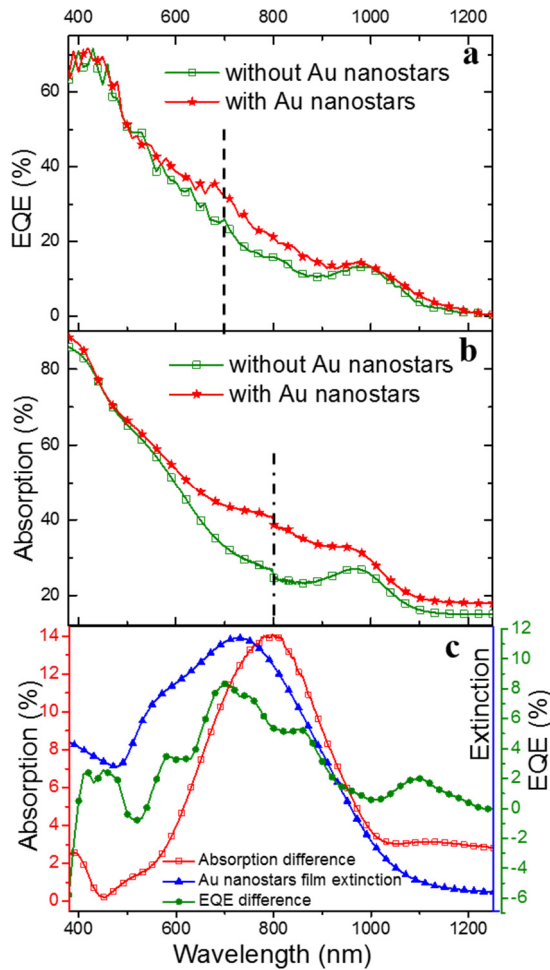


Figure 5. (a) EQE spectra of devices with and without Au nanostars, (b) absorption spectra of PbS/CdS core-shell QD film with and without Au nanostars and (c) comparison of difference in absorption and difference in EQE spectra along with the extinction spectrum of Au nanostar film.

29, 34] surrounding the Au nanostars. This clearly shows the observed increase in absorption is because of the presence of the Au nanostars. The close overlap of the wavelengths over which EQE and absorption enhancement occurred suggests that the considerably increased photoresponse is closely related to the increase of absorption in the photoactive layer due to incorporation of the Au nanostars into the QD film. The correlation can be seen more clearly in Figure 5c, where we plot the LSPR of Au nanostars, the difference in absorption and difference in EQE together for comparison.

The enhancement of absorption could be due to the scattering of light, field enhanced absorption in the QD film nearby and absorption of light by the Au nanostars themselves. While the first two processes are advantageous in enhancing the performance of the devices, the latter is undesired. These

properties of the Au nanostars were elucidated using theoretical calculation by FDTD simulation. The calculated absorption, scattering and extinction of the Au nanostars as well as the electric field distribution around an Au nanostar embedded in the QD film by using refractive index of 2.6 [34] and dielectric constant of 14 [35] belonging to PbS QD film plotted at excitonic absorption peak of the PbS/CdS core-shell QD film, ~980 nm are shown in Figure 6 a and b. The scattering-to-absorption ratio of the Au nanostars is significantly higher than that of spherical Au nanoparticles of similar size [36]. This makes the Au nanostars better candidates for QD based solar cells, since a higher scattering-to-absorption ratio and less parasitic absorption are always desired. Although spherical Au nanoparticles can also be designed to display similar scattering to absorption ratio, much larger particle sizes are required. This is less attractive since the integration of smaller particles in the QD film displaces less amounts of the photoactive material (QDs herein) and are thus preferred.

The LSPR-induced electric field enhancement is concentrated at the tips of the Au nanostars extending farther up to about 40 nm from the tip while decreasing in intensity (Figure 6b); i.e, the field enhancement is above 1 up to a distance of 40 nm from the tip of the Au nanostar. This electric field enhancement results in enhancement of absorption in the QD film, which is directly proportional to the square of the electric field [37, 38]. The experimentally observed enhancement in absorption of QD film due to incorporation of the Au nanostars should have mainly come from the combination of the scattering and field enhancement. This is highly probable especially

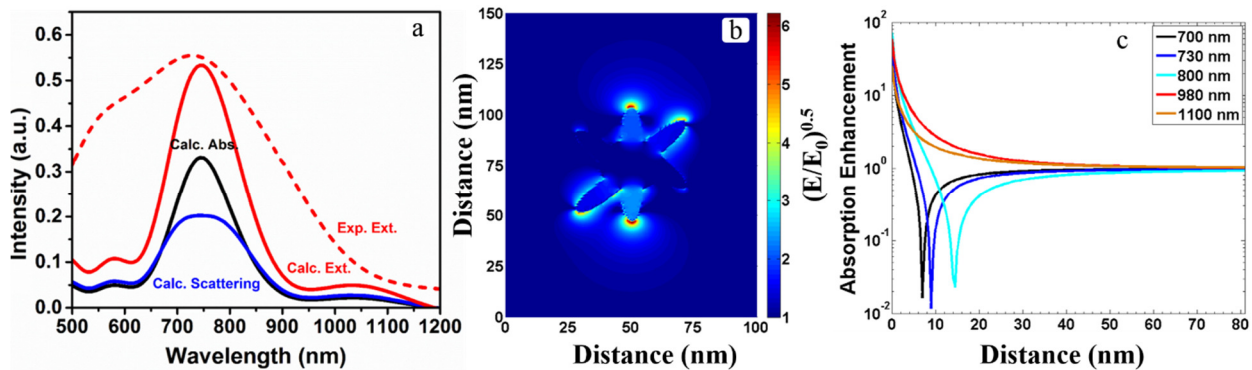


Figure 6. (a) Calculated absorption, scattering and extinction spectra of Au nanostars compared with the experimental extinction spectrum, (b) calculated electromagnetic field distribution surrounding an Au nanostar under excitation with wavelength of 980 nm, The intensity scale is normalized as $(E/E_0)^{0.5}$, and (c) absorption enhancement in the QD film as a function of distance from an Au nanostar tip at different excitation wavelengths.

considering the observation of enhancement in EQE of the devices. The contributions to enhancement in absorption and thus EQE due to field enhanced absorption and scattering is higher than the parasitic absorption by the Au nanostars. Figure 6 c shows the calculated enhancement of absorption of different wavelengths of photons in the QD film around the Au nanostar as the function of distance from the tip of the Au nanostar. The wavelengths at which the absorption enhancement was calculated were chosen based on Figure 5c. These are 700 nm (where highest increase in EQE is observed), 730 nm (at the centre of LSPR band of the Au nanostars), 800 nm (where the highest increase in absorption is observed), 980 nm (near the excitonic absorption peak of the QD film) and 1100 nm (where the highest increase in EQE above the QD excitonic absorption peak is observed). The absorption enhancement at longer wavelengths, including the highest absorption enhancement observed at the wavelength of 980 nm and at the wavelength of 1100 nm, is more than one time for longer distance from the nanostar tip than the shorter wavelengths of 700 nm, 730 nm and 800 nm. This suggests that the observed increase in absorption, hence the EQE, at the longer wavelengths (980 nm and 1100 nm) is mainly due to field enhanced absorption. While at shorter wavelengths (700 nm, 730 nm and 800 nm) it could be mainly due to the combination of the three different contributions – scattering, field enhanced absorption and absorption in the Au nanostars themselves though the contribution from the latter is minimal.

All the above experimental and theoretical results are related to the optimal device. In the following part, we present the effect of different density and location of the Au nanostars in the QD film on device performance in detail. The adjustment of the density was realized by tuning the Au nanostar concentration during the deposition process. It was found that the PCE and J_{sc} of the solar cell devices reached the maximum at optimum density of the Au nanostars in the QD film (6.84 mg/ml of Au spin coated). However, V_{oc} decreased monotonically with the increase in the density of the Au nanostars. The FF fluctuated at the beginning when the concentration of the Au nanostars was increased and then decreased monotonically as the concentration of the Au nanostars was further increased. The trends are plotted in Figure 7a. The introduction of the plasmonic nanoparticles into the QDs film can in general result in two antagonistic effects with respect to the device performance. The beneficial effect arises from improved light absorption via enhanced light scattering and local field enhancement, directly leading to increased charge carrier generation, mostly relevant to the value of J_{sc} . However, when there are too many plasmonic nanoparticles,

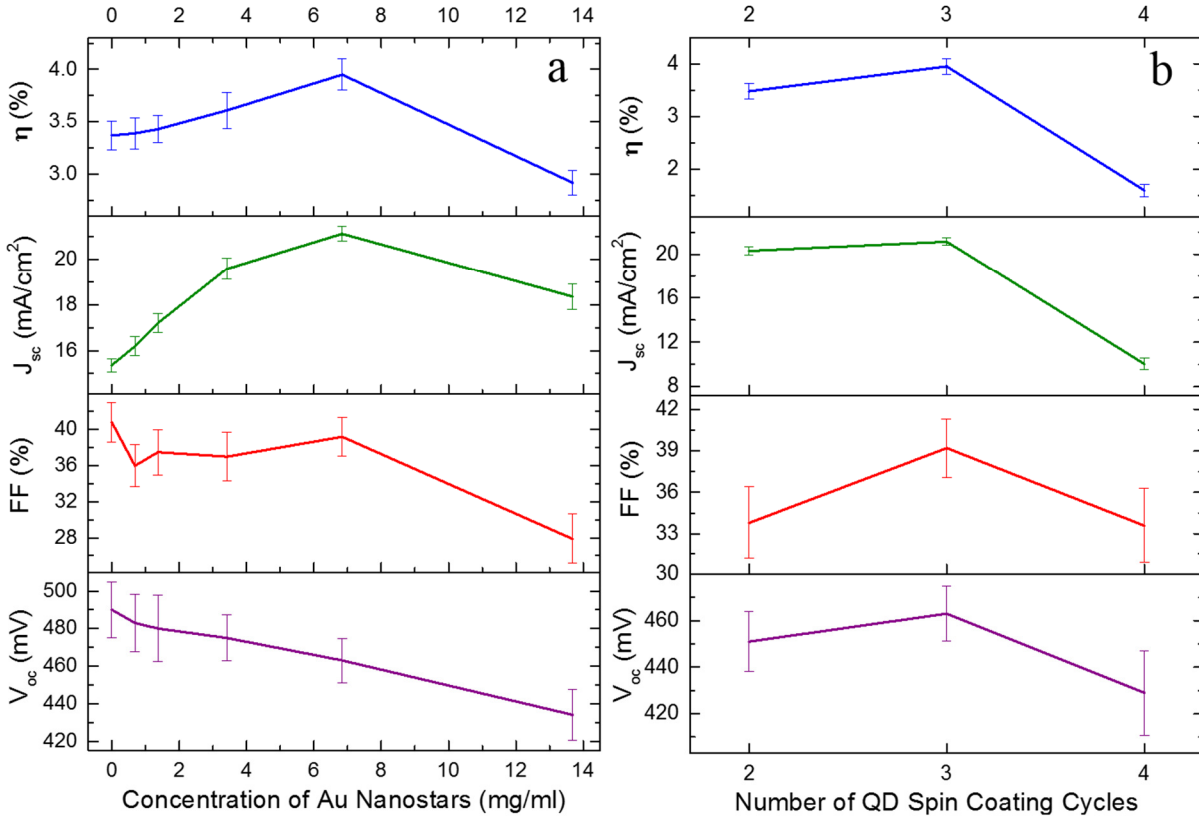


Figure 7. Dependence of the performance parameters of solar cell devices on (a) the concentration of Au nanostars spin coated and (b) their location in QDs film.

high fraction of lights will be absorbed by them, rather than by the QDs [39]. In addition, the number of nearby QDs may be too low to significantly benefit from the positive plasmonic effects. Therefore, in the latter case, charge carrier generation may be even decreased. This reasonably explains why J_{sc} , which is most directly related to charge carrier generation, showed initial increase and then decrease with increasing Au nanostar concentration. The unwanted effect consists of the introduction of charge carrier recombination centers, which negatively affects the device performance, as evidenced by consistently similar or lower V_{oc} and FF, whatever Au nanostars concentrations, as compared to the control device without any Au nanostars. Straightforwardly, the higher the density of the Au nanostars is, the more recombination sites are introduced. The observed variation of the overall PCE with the concentration of Au nanostars was essentially the result of the interplay of all these factors. As the negative effect can outweigh at relatively high Au nanostar density, the concentration optimization is important in realizing plasmon-enhanced solar cells.

All the parameters, PCE, J_{sc} , V_{oc} , and FF reached maximum at an optimum location of the Au nanostars, deposited after 3 cycles of QDs are spin coated (Figure 7b). When the Au nanostars are too close to the QDs-TiO₂ junction, they may shadow the QD film behind resulting in reduced absorption. This resulted in slight decrease in the PCE. Whereas the decrease in the PCE is higher when the Au nanostars are too close to the back electrode. In this case the charge carriers extraction is less efficient as the photogenerated charge carriers due to field enhanced absorption occurs far from the QDs-TiO₂ junction resulting in more recombinations, which decreases not only the J_{sc} but also the V_{oc} and FF. The scattering of light might also be reduced as the intensity of light reaching there is weak after passing through much of the QD film. The volume of the QDs that can benefit from the field enhanced absorption is also less as the field enhancement is effective to a distance of about 40 nm from the tip of the Au nanostar.

4. Conclusions

Ambient air processed plasmonic bulk heterojunction solar cell devices involving TiO₂ nanorod arrays, NIR PbS/CdS core-shell QDs and Au nanostars processed from solution have been investigated in this work. After optimizing the devices with respect to the density of Au nanostars in the QD film and their location in the cross-section of the QD film, a PCE as high as 4.16 % has been achieved. The effect of the Au nanostars on the performance of the devices is evident from an increase in J_{sc} of the devices and enhanced photoresponse evidenced from the EQE measurements. This is attributed to the experimentally observed enhancement of optical absorption of the QD film due to the incorporation of the Au nanostars. It is inferred from theoretical calculation results that the absorption enhancement is due to both near field enhancement and scattering. This work demonstrated the importance of plasmonic nanoparticles integration into QD based solar cells in improving the performance and paves a way for further investigation of plasmonic nanoparticles in improvement of the performance of QD based solar cells. Further optimization would be able to improve the performance of the devices. For example, utilizing seed layer for the growth TiO₂ nanorod arrays and surface modification of the Au nanostars may help to overcome the decrease in performance due to charge carriers recombination.

Acknowledgements

Financial support from the Natural Sciences and Engineering Research Council (NSERC) of Canada, Canadian Solar Inc. and OLA Display Corp. in the context of the NSERC-Strategic grant

is greatly appreciated. The authors also acknowledge the financial support from the FRQNT (Le Fonds de Recherche du Québec-Nature et Technologies) through its strategic Network “Plasma-Québec”, and from Nano-Québec (the Québec Organization for the promotion of nanoscience and nanotechnologies).

Appendix A. Supporting Information

Supplementary data of this article including SEM images and XRD pattern of TiO₂ nanorod arrays, absorption and PL emission spectra as well as TEM image of PbS/CdS core-shell QDs are given in supporting information. This material is available via the Internet.

References

1. I.J. Kramer and E.H. Sargent, *The Architecture of Colloidal Quantum Dot Solar Cells: Materials to Devices*. Chem. Rev., 2014. **114**(1):863-882.
2. A. Zaban, O.I. Micic, B.A. Gregg, and A.J. Nozik, *Photosensitization of Nanoporous TiO₂ Electrodes With InP Quantum Dots*. Langmuir, 1998. **14**(12):3153-3156.
3. G.H. Carey, L. Levina, R. Comin, O. Voznyy, and E.H. Sargent, *Record Charge Carrier Diffusion Length in Colloidal Quantum Dot Solids via Mutual Dot-To-Dot Surface Passivation*. Adv. Mater., 2015. **27**(21):3325–3330.
4. A.J. Labelle, S.M. Thon, S. Masala, M.M. Adachi, H.P. Dong, M. Farahani, A.H. Ip, A. Fratilocchi, and E.H. Sargent, *Colloidal Quantum Dot Solar Cells Exploiting Hierarchical Structuring*. Nano Lett., 2015. **15**(2):1101-1108.
5. C.H.M. Chuang, P.R. Brown, V. Bulovic, and M.G. Bawendi, *Improved Performance and Stability in Quantum Dot Solar Cells Through Band Alignment Engineering*. Nat. Mater., 2014. **13**(8):796-801.
6. M.R. Kim and D. Ma, *Quantum-Dot-Based Solar Cells: Recent Advances, Strategies, and Challenges*. J. Phys. Chem. Lett., 2015. **6**(1):85-99.
7. X. Lan, S. Masala, and E.H. Sargent, *Charge-Extraction Strategies for Colloidal Quantum Dot Photovoltaics*. Nat. Mater., 2014. **13**(3):233-240.
8. M.A. Green and S. Pillai, *Harnessing Plasmonics For Solar Cells*. Nature Photon., 2012. **6**(3):130-132.

9. K.A. Willets and R.P. Van Duyne, *Localized Surface Plasmon Resonance Spectroscopy and Sensing*. *Annu. Rev. Phys. Chem.*, 2007. **58**(1):267-297.
10. K.R. Catchpole and A. Polman, *Design Principles for Particle Plasmon Enhanced Solar Cells*. *Appl. Phys. Lett.*, 2008. **93**(19):191113 (3pp).
11. Y. Nishijima, K. Ueno, Y. Yokota, K. Murakoshi, and H. Misawa, *Plasmon-Assisted Photocurrent Generation from Visible to Near-Infrared Wavelength Using a Au-Nanorods/TiO₂ Electrode*. *J. Phys. Chem. Lett.*, 2010. **1**(13):2031-2036.
12. H.A. Atwater and A. Polman, *Plasmonics for Improved Photovoltaic Devices*. *Nat. Mater.*, 2010. **9**(3):205-213.
13. J.L. Wu, F.C. Chen, Y.S. Hsiao, F.C. Chien, P.L. Chen, C.H. Kuo, M.H. Huang, and C.S. Hsu, *Surface Plasmonic Effects of Metallic Nanoparticles on the Performance of Polymer Bulk Heterojunction Solar Cells*. *ACS Nano*, 2011. **5**(2):959-967.
14. Y. Takeda, T. Motohiro, D. Konig, P. Aliberti, Y. Feng, S. Shrestha, and G. Conibeer, *Practical Factors Lowering Conversion Efficiency of Hot Carrier Solar Cells*. *Appl. Phys. Express*, 2010. **3**(10):104301 (3pp).
15. M.D. Brown, T. Suteewong, R.S.S. Kumar, V. D'Innocenzo, A. Petrozza, M.M. Lee, U. Wiesner, and H.J. Snaith, *Plasmonic Dye-Sensitized Solar Cells Using Core-Shell Metal-Insulator Nanoparticles*. *Nano Lett.*, 2011. **11**(2):438-445.
16. Q.Q. Gan, F.J. Bartoli, and Z.H. Kafafi, *Plasmonic-Enhanced Organic Photovoltaics: Breaking the 10% Efficiency Barrier*. *Adv. Mater.*, 2013. **25**(17):2385-2396.
17. A.Y. Mahmoud, J.M. Zhang, D.L. Ma, R. Izquierdo, and V.V. Truong, *Optically-Enhanced Performance of Polymer Solar Cells with Low Concentration of Gold Nanorods in The Anodic Buffer Layer*. *Org. Electron.*, 2012. **13**(12):3102-3107.
18. D. Paz-Soldan, A. Lee, S.M. Thon, M.M. Adachi, H. Dong, P. Maraghechi, M. Yuan, A.J. Labelle, S. Hoogland, K. Liu, E. Kumacheva, and E.H. Sargent, *Jointly Tuned Plasmonic-Excitonic Photovoltaics Using Nanoshells*. *Nano Lett.*, 2013. **13**(4):1502-1508.

19. T. Kawawaki, H. Wang, T. Kubo, K. Saito, J. Nakazaki, H. Segawa, and T. Tatsuma, *Efficiency Enhancement of PbS Quantum Dot/ZnO Nanowire Bulk-Heterojunction Solar Cells by Plasmonic Silver Nanocubes*. ACS Nano, 2015. **9**(4):4165-4172.
20. B.A. Gonfa, H. Zhao, J.T. Li, J.X. Qiu, M. Saidani, S.Q. Zhang, R. Izquierdo, N.Q. Wu, M.A. El Khakani, and D. Ma, *Air-Processed Depleted Bulk Heterojunction Solar Cells Based on PbS/CdS Core-shell Quantum Dots and TiO₂ Nanorod Arrays*. Sol. Energ. Mat. Sol. Cells, 2014. **124**:67-74.
21. B.A. Gonfa, M.R. Kim, N. Deegan, A.C. Tavares, R. Izquierdo, N. Wu, M.A. El Khakani, and D. Ma, *Towards High Efficiency Air-Processed Near-Infrared Responsive Photovoltaics: Bulk Heterojunction Solar Cells Based on PbS/CdS Core-Shell Quantum Dots and TiO₂ Nanorod Arrays*. Nanoscale, 2015. **7**(22):10039-10049.
22. B. Liu and E.S. Aydil, *Growth of Oriented Single-Crystalline Rutile TiO₂ Nanorods on Transparent Conducting Substrates for Dye-Sensitized Solar Cells*. J. Am. Chem. Soc., 2009. **131**(11):3985-3990.
23. H. Zhao, M. Chaker, and D. Ma, *Effect of CdS Shell Thickness on the Optical Properties of Water-Soluble, Amphiphilic Polymer-Encapsulated PbS/CdS Core/Shell Quantum Dots*. J. Mater. Chem., 2011. **21**(43):17483-17491.
24. H. Zhao, M. Chaker, N.Q. Wu, and D. Ma, *Towards Controlled Synthesis and Better Understanding of Highly Luminescent PbS/CdS Core/shell Quantum Dots*. J. Mater. Chem., 2011. **21**(24):8898-8904.
25. M.A. Hines and G.D. Scholes, *Colloidal PbS Nanocrystals With Size-Tunable Near-Infrared Emission: Observation of Post-Synthesis Self-Narrowing of the Particle Size Distribution*. Adv. Mater., 2003. **15**(21):1844-1849.
26. T. Zhang, H. Zhao, D. Riabinina, M. Chaker, and D. Ma, *Concentration-Dependent Photoinduced Photoluminescence Enhancement in Colloidal PbS Quantum Dot Solution*. J. Phys. Chem. C, 2010. **114**(22):10153-10159.
27. M. Li, J.M. Zhang, S. Suri, L.J. Sooter, D.L. Ma, and N.Q. Wu, *Detection of Adenosine Triphosphate with an Aptamer Biosensor Based on Surface-Enhanced Raman Scattering*. Anal. Chem., 2012. **84**(6):2837-2842.

28. G. Frens, *Controlled Nucleation for Regulation of Particle-Size in Monodisperse Gold Suspensions*. Nature-Phys. Sci., 1973. **241**(105):20-22.
29. P.S. Kumar, I. Pastoriza-Santos, B. Rodriguez-Gonzalez, F.J. Garcia de Abajo, and L.M. Liz-Marzan, *High-Yield Synthesis and Optical Response of Gold Nanostars*. Nanotechnology, 2008. **19**(1):015606 (6pp).
30. E.D. Palik, *Handbook of Optical Constants of Solids*. 1985, Orlando: Academic Press.
31. I. Moreels, K. Lambert, D. Smeets, D. De Muynck, T. Nollet, J.C. Martins, F. Vanhaecke, A. Vantomme, C. Delerue, G. Allan, and Z. Hens, *Size-Dependent Optical Properties of Colloidal PbS Quantum Dots*. Acs Nano, 2009. **3**(10):3023-3030.
32. M. Li, S.K. Cushing, J.M. Zhang, J. Lankford, Z.P. Aguilar, D. Ma, and N.Q. Wu, *Shape-Dependent Surface-Enhanced Raman Scattering in Gold-Ramanprobe-Silica Sandwiched Nanoparticles for Biocompatible Applications*. Nanotechnology, 2012. **23**(11):115501 (10pp).
33. J. Wu, S.C. Mangham, V.R. Reddy, M.O. Manasreh, and B.D. Weaver, *Surface Plasmon Enhanced Intermediate Band Based Quantum Dots Solar Cell*. Sol. Energ. Mat. Sol. Cells, 2012. **102**:44-49.
34. M.M. Adachi, A.J. Labelle, S.M. Thon, X. Lan, S. Hoogland, and E.H. Sargent, *Broadband Solar Absorption Enhancement via Periodic Nanostructuring Of Electrodes*. Sci. Rep., 2013. **3**:2928 (6pp).
35. P.R. Brown, R.R. Lunt, N. Zhao, T.P. Osedach, D.D. Wanger, L.-Y. Chang, M.G. Bawendi, and V. Bulović, *Improved Current Extraction from ZnO/PbS Quantum Dot Heterojunction Photovoltaics Using a MoO₃ Interfacial Layer*. Nano Lett., 2011. **11**(7):2955-2961.
36. P.K. Jain, K.S. Lee, I.H. El-Sayed, and M.A. El-Sayed, *Calculated Absorption and Scattering Properties of Gold Nanoparticles of Different Size, Shape, and Composition: Applications in Biological Imaging and Biomedicine*. J. Phys. Chem. B, 2006. **110**(14):7238-7248.
37. M.S. Mehata, *Enhancement of Charge Transfer and Quenching of Photoluminescence of Capped CdS Quantum Dots*. Sci. Rep., 2015. **5**:12056 (11pp).

38. T. Nakabayashi, R. Ohshima, and N. Ohta, *Electric Field Effects on Photoluminescence of CdSe Nanoparticles in a PMMA Film*. Crystals, 2014. **4**(2):152-167.
39. R.A. Pala, J. White, E. Barnard, J. Liu, and M.L. Brongersma, *Design of Plasmonic Thin-Film Solar Cells with Broadband Absorption Enhancements*. Adv. Mater., 2009. **21**(34):3504-3509.

Supporting Information for:

**Plasmonic Enhancement of the Performance of PbS/CdS Core-shell
Quantum Dots/TiO₂ Nanorod Arrays Bulk Heterojunction Solar
Cells**

Belete Atomsa Gonfa¹, Mee Rahn Kim¹, Peng Zheng², Nianqiang Wu², My Ali El Khakani¹, and Dongling Ma^{1,*}

¹Institut National de la Recherche Scientifique (INRS), Centre-Énergie, Matériaux et Télécommunications, 1650 Boulevard Lionel-Boulet, Varennes, QC, Canada J3X 1S2

²Department of Mechanical and Aerospace Engineering, West Virginia University, Morgantown, WV 26506-6106, USA

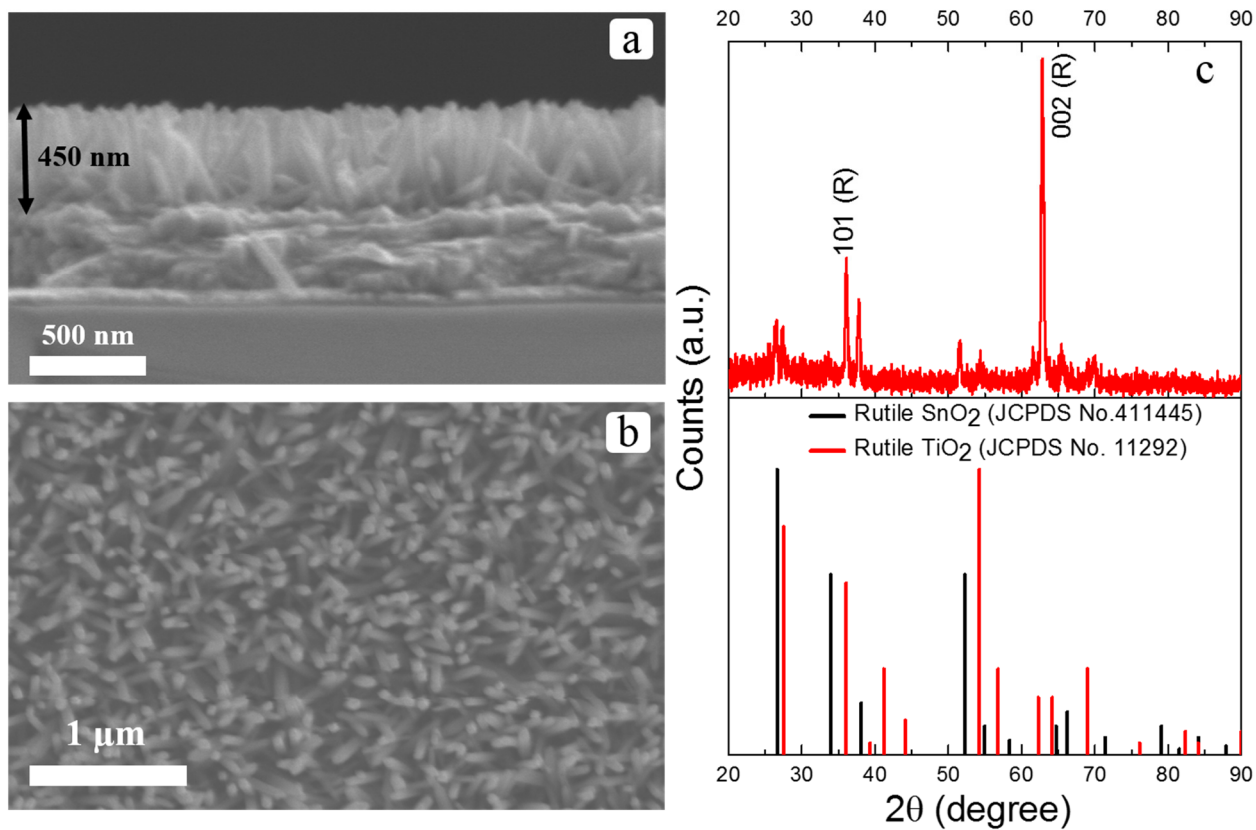


Figure S1. SEM images of 450 nm long TiO_2 nanorod arrays grown on FTO substrate (a) cross-sectional and (b) perspective view, and (c) XRD pattern of the 450 nm long TiO_2 nanorod arrays grown on FTO compared with the standard patterns of rutile SnO_2 and rutile TiO_2 . The peaks designated 'R' are ascribed to rutile TiO_2 .

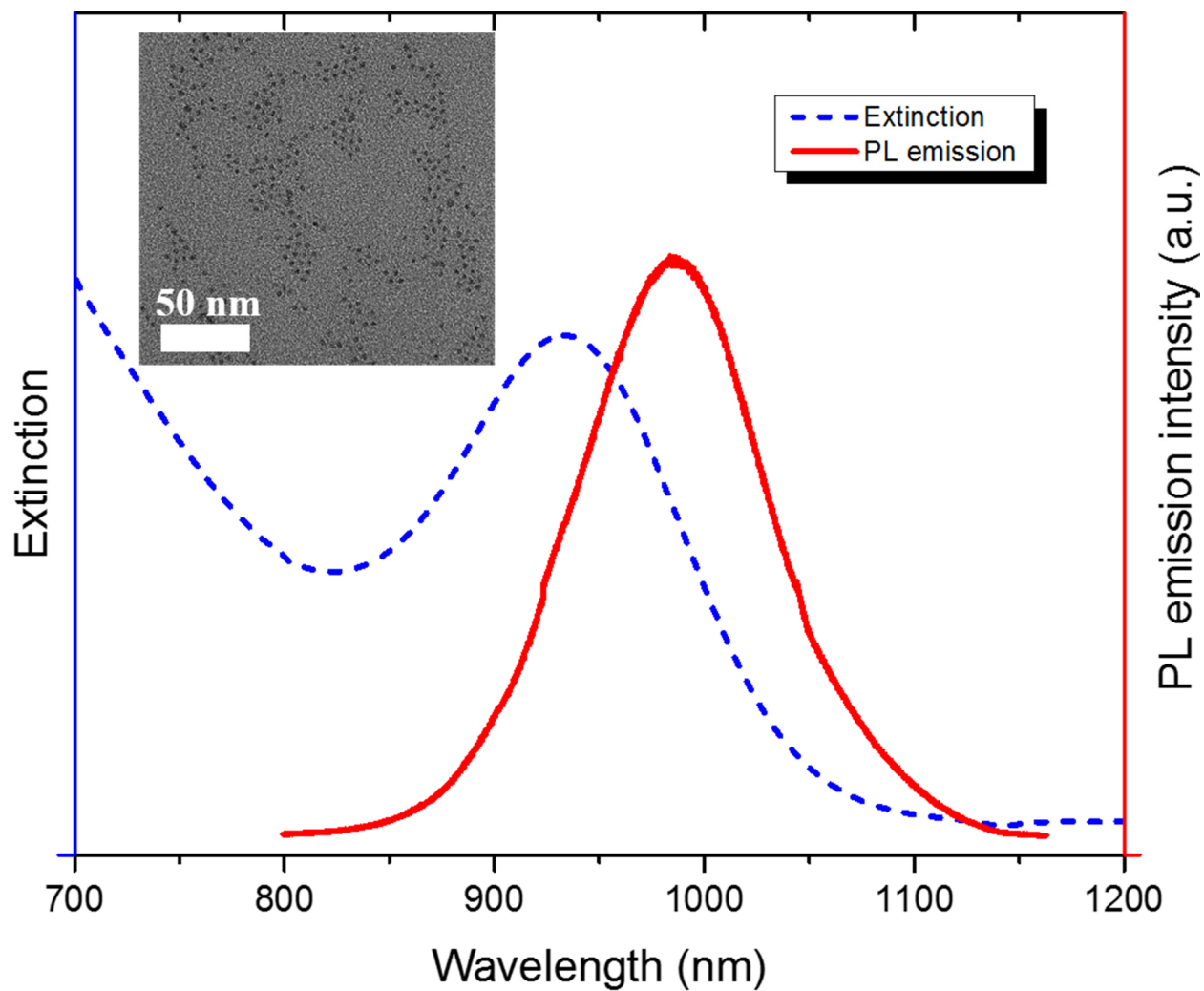


Figure S2. Visible-NIR extinction and PL emission spectra of the PbS/CdS core-shell QDs suspension in toluene, inset: TEM image of the PbS/CdS core-shell QDs.

CHAPTER 5 CONCLUSIONS AND PERSPECTIVES

5.1. Conclusions

Colloidal QDs have a promising future for application in solar cells due to their low cost synthesis, processing into devices from solution and their potential to be designed into high PCE devices. For enhanced performance, several factors are important. One of them is the architecture of the devices. Among different architectures of QD based solar cells studied so far, heterojunction solar cells involving the QDs and wide band gap semiconductors are the leading ones in terms of PCE.

Another factor is the quality of the QD film, which should be able to achieve the maximum absorption of photons, while still allow the efficient extraction of the photo-generated charge carriers. To this end, the QD film should have good charge carrier mobility and minimal charge carrier recombination centers. These can be achieved by surface engineering of the QDs via ligand exchange. The ligand exchange involves replacement of the long chain ligands capping the QDs with short chain ones or even ions like halides to bring the QDs closer, increasing the QD coupling that ultimately increases the charge carrier mobility in the QD film. Furthermore, the short chain ligands or ions, due to their reduced steric hindrance, may better passivate the surface defects of the QDs arising from the dangling bonds.

In this work, colloidal PbS/CdS core-shell QDs have been demonstrated to have a potential to be applied in solar cells by combining them with rutile TiO₂ nanorod arrays, which were synthesized by hydrothermal technique. It is of huge significance that both the PbS/CdS core-shell QDs and the rutile TiO₂ nanorod arrays are synthesized via low cost wet chemical approaches and the devices are processed from solutions. Moreover the PbS/CdS core-shell QDs enable the processing of the solar cells in ambient atmosphere, while yielding even better PCE (about 40 % higher) than the PbS QD solar cells fabricated inside a glove box under otherwise same fabrication conditions. In addition to the processing atmosphere, it has been found out that the interfacial hole transport layer between the QD film and the Au back electrode plays significant role in the performance of the devices.

Further optimizations of the PbS/CdS QDs – TiO₂ nanorod arrays devices have led to improved performance of the device. This was achieved by utilizing sputter-deposited TiO₂ seed layer on FTO substrate to improve the TiO₂ nanorod/FTO interface, optimizing TiO₂ nanorod length and performing mild thermal annealing of the QD film in N₂. Such optimizations have led to a PCE of 4.43 %.

It has also been demonstrated that the incorporation of Au nanostars in the PbS/CdS core-shell QD film can result in plasmonic enhancement of the performance of the DBH device. It has been found out that the density and the location of the Au nanostars in the QD film affect the performance of the devices.

This work in general paves a way for further investigation of colloidal QDs in solar cells towards improved performance. Especially, the demonstration of the importance of the utilization of core-shell QDs and plasmonic nanoparticles to extend light absorption into NIR region of the solar spectrum and the optimization of device architecture in improving the performance of QD based solar cells can trigger further research in this area.

5.2. Perspectives

Colloidal QDs, in general, and PbS/CdS core-shell QDs, in particular, look promising for solar cell applications in the future. However, the PCE of such devices needs to be further improved if they are to meet the requirements for commercialization competing with other energy technologies like fossil fuels and single crystalline silicon solar cells, which are the most widely commercialized solar cell technology so far. Improvement can be made on different aspects, which include photoelectrodes, QD films and even charge collecting electrodes.

In heterojunction solar cells, which have so far achieved the best PCE values among QD based solar cells of different architecture, the use of other semiconductors to form heterojunction with QDs needs to be explored. Improvement of the properties, such as electron mobility, of the wide band gap semiconductors (TiO₂ and ZnO) already in use by doping could also be one direction of increasing the performance of the solar cell devices. Further optimization of nanorod arrays in terms of controlled density and crystal quality are also necessary by the exploitation of different growth techniques. Related to this, it would also be possible to enhance the performance of solar cell devices by rationally designing photoelectrodes. Recently it has been reported that the use of

a hierarchically structured TiO₂ photoelectrode enables the use of thinner film of PbS QDs and enhances the PCE [162]. Combining TiO₂ or ZnO with high mobility semiconductors is also one option of improving the properties of photoelectrodes. Indeed it has been demonstrated in our recent work that incorporation of SWCNTs with TiO₂ nanorod arrays improves the performance of laser synthesized PbS QD based solar cells [138].

Further investigations on device architecture are necessary to realize the use of MEG and hot carriers in increasing the performance of the devices. Designing intermediate band solar cells involving QD superlattices through studying different techniques for QD film fabrication is also attractive. As these strategies have been theoretically predicted to be able to lead to devices surpassing the Shockley Quieser limits of single junction solar cells, it is worthwhile to explore their realization in QD based solar cells.

Similar to hierarchically structured photoelectrodes, which enhance absorption of photons by QD film through scattering, implementation of plasmonic nanostructures in QD based solar cells is quite attractive. This allows the use of a thinner QD film, which enhances charge carrier transport and collection efficiency, meanwhile with enhanced light absorption. Therefore, systematic investigation of plasmon enhanced QD solar cells is highly and urgently desired.

Although rapid progress has been made in the development of QD based solar cells, there still remains much room for further investigations for future commercial applications. Among these are the automatization and scaling up of QD synthesis and the scaling up of device fabrication.

REFERENCES

1. J. Poppe, S.G. Hickey, and A. Eychmüller, *Photoelectrochemical Investigations of Semiconductor Nanoparticles and Their Application to Solar Cells*. J. Phys. Chem. C, 2014. **118**(30):17123-17141.
2. E. Yablonovitch, O.D. Miller, and S.R. Kurtz. *The Opto-electronic Physics that Broke the Efficiency Limit in Solar Cells*. in *Photovoltaic Specialists Conference (PVSC), 2012 38th IEEE*. 2012.
3. PV magazine. *Soitec Achieves 46% Multi-Junction Cell for CPV*. 2014 January 26, 2015; Available from: http://www.pv-magazine.com/news/details/beitrag/soitec-achieves-46-multi-junction-cell-for-cpv_100017342/.
4. CaltechAUTHORS, *Basic Research Needs for Solar Energy Utilization*. 2005: Renée M. Nault, Argonne National Laboratory.
5. C. Wadia, A.P. Alivisatos, and D.M. Kammen, *Materials Availability Expands the Opportunity for Large-Scale Photovoltaics Deployment*. Environ. Sci. Technol., 2009. **43**(6):2072-2077.
6. *Renewables 2014 Global Status Report*. 2014, Renewable Energy Policy Network for 21st Century.
7. Wikimedia Commons. *World Energy Consumption*. 2014; Available from: http://commons.wikimedia.org/wiki/File:Total_World_Energy_Consumption_by_Source_2013.png.
8. P.V. Kamat, *Meeting the Clean Energy Demand: Nanostructure Architectures for solar Energy conversion*. J. Phys. Chem. C, 2007. **111**(7):2834-2860.
9. The McGraw-Hill Companies. *Nuclear Fission and Fusion*. 2001 February 04, 2015; Available from: http://www.mhhe.com/physsci/chemistry/chang7/ssg/chap23_5sg.html.
10. M. Gratzel, *Photoelectrochemical Cells*. Nature, 2001. **414**(6861):338-344.
11. M.S. Dresselhaus and I.L. Thomas, *Alternative Energy Technologies*. Nature, 2001. **414**(6861):332-337.
12. C. Silvi, *History and Future of Renewable Solar Energy*. Development, 2008. **51**(3):409-414.

13. February 03, 2015; Available from: <http://www.pvresources.com/Terminology/UnitsandMeasures.aspx>.
14. G. Lanzani, *The Photophysics Behind Photovoltaics And Photonics*. 2012: WILEY-VCH Verlag GmbH & Co. KGaA.
15. C.E. Fritts, *On A New Form of Selenium Cell, And Some Electrical Discoveries Made By Its Use*. *AJS*, 1883. **26**(156):465-472.
16. R.S. Ohl, *Light-Sensitive Electric Device*. 1946, Google Patents.
17. D.M. Chapin, C.S. Fuller, and G.L. Pearson, *A New Silicon p-n Junction Photocell for Converting Solar Radiation into Electrical Power*. *J. Appl. Phys.*, 1954. **25**(5):676-677.
18. MIT Technology Review. *Record-Breaking Solar Cell Points the Way to Cheaper Power*. 2014 February 01, 2015; Available from: <http://www.technologyreview.com/news/528351/record-breaking-solar-cell-points-the-way-to-cheaper-power/>.
19. S.E. Habas, H.A.S. Platt, M.F.A.M. van Hest, and D.S. Ginley, *Low-Cost Inorganic Solar Cells: From Ink To Printed Device*. *Chem. Rev.*, 2010. **110**(11):6571-6594.
20. H.W. Hillhouse and M.C. Beard, *Solar Cells from Colloidal Nanocrystals: Fundamentals, Materials, Devices, and Economics*. *Current Opinion in Colloid & Interface Science*, 2009. **14**(4):245-259.
21. G.F. Brown and J.Q. Wu, *Third Generation Photovoltaics*. *Laser & Photonics Reviews*, 2009. **3**(4):394-405.
22. M.A. Green, *Third Generation Photovoltaics: Ultra-High Conversion Efficiency at Low Cost*. *Progress in Photovoltaics: Research and Applications*, 2001. **9**(2):123-135.
23. Y. Liu, C.-C. Chen, Z. Hong, J. Gao, Y. Yang, H. Zhou, L. Dou, G. Li, and Y. Yang, *Solution-Processed Small-Molecule Solar Cells: Breaking the 10% Power Conversion Efficiency*. *Sci. Rep.*, 2013. **3**:3356 (8pp).
24. NREL. *Research Cell Efficiency Records*. 2015 January 26, 2015; Available from: http://www.nrel.gov/ncpv/images/efficiency_chart.jpg
25. S.M. Reimann and M. Manninen, *Electronic Structure of Quantum Dots*. *Rev. Mod. Phys.*, 2002. **74**(4):1283-1342.
26. Royal Society of Chemistry. *A quantum Paintbox*. 2003 January 31, 2015; Available from: <http://www.rsc.org/chemistryworld/Issues/2003/September/paintbox.asp>.

27. P.V. Kamat, *Quantum Dot Solar Cells. Semiconductor Nanocrystals as Light Harvesters*. J. Phys. Chem. C, 2008. **112**(48):18737-18753.
28. R.J. Ellingson, M.C. Beard, J.C. Johnson, P.R. Yu, O.I. Micic, A.J. Nozik, A. Shabaev, and A.L. Efros, *Highly Efficient Multiple Exciton Generation in Colloidal PbSe and PbS Quantum Dots*. Nano Lett., 2005. **5**(5):865-871.
29. A.J. Nozik, M.C. Beard, J.M. Luther, M. Law, R.J. Ellingson, and J.C. Johnson, *Semiconductor Quantum Dots and Quantum Dot Arrays and Applications of Multiple Exciton Generation to Third-Generation Photovoltaic Solar Cells*. Chem. Rev., 2010. **110**(11):6873-6890.
30. V.I. Klimov, J.A. McGuire, J. Joo, J.M. Pietryga, and R.D. Schaller, *New Aspects of Carrier Multiplication in Semiconductor Nanocrystals*. Acc. Chem. Res., 2008. **41**(12):1810-1819.
31. O.E. Semonin, J.M. Luther, S. Choi, H.Y. Chen, J.B. Gao, A.J. Nozik, and M.C. Beard, *Peak External Photocurrent Quantum Efficiency Exceeding 100% via MEG in a Quantum Dot Solar Cell*. Science, 2011. **334**(6062):1530-1533.
32. Y.N. Gao, E. Talgorn, M. Aerts, M.T. Trinh, J.M. Schins, A.J. Houtepen, and L.D.A. Siebbeles, *Enhanced Hot-Carrier Cooling and Ultrafast Spectral Diffusion in Strongly Coupled PbSe Quantum-Dot Solids*. Nano Lett., 2011. **11**(12):5471-5476.
33. R. Patterson, M. Kirkengen, B.P. Veettil, D. Konig, M.A. Green, and G. Conibeer, *Phonon Lifetimes in Model Quantum Dot Superlattice Systems with Applications to the Hot Carrier Solar Cell*. Sol. Energ. Mat. Sol. Cells, 2010. **94**(11):1931-1935.
34. A. Luque, A. Marti, and C. Stanley, *Understanding Intermediate-Band Solar Cells*. Nature Photon., 2012. **6**(3):146-152.
35. I. Moreels, Y. Justo, B. De Geyter, K. Haustraete, J.C. Martins, and Z. Hens, *Size-Tunable, Bright, and Stable PbS Quantum Dots: A Surface Chemistry Study*. ACS Nano, 2011. **5**(3):2004-2012.
36. E.H. Sargent, *Colloidal Quantum Dot Solar Cells*. Nature Photon., 2012. **6**(3):133-135.
37. J.A. Tang and E.H. Sargent, *Infrared Colloidal Quantum Dots for Photovoltaics: Fundamentals and Recent Progress*. Adv. Mater., 2011. **23**(1):12-29.
38. F.W. Wise, *Lead Salt Quantum Dots: The Limit of Strong Quantum Confinement*. Acc. Chem. Res., 2000. **33**(11):773-780.

39. A.G. Pattantyus-Abraham, I.J. Kramer, A.R. Barkhouse, X.H. Wang, G. Konstantatos, R. Debnath, L. Levina, I. Raabe, M.K. Nazeeruddin, M. Gratzel, and E.H. Sargent, *Depleted-Heterojunction Colloidal Quantum Dot Solar Cells*. *ACS Nano*, 2010. **4**(6):3374-3380.
40. M.A. Hines and G.D. Scholes, *Colloidal PbS Nanocrystals with Size-Tunable Near-Infrared Emission: Observation of Post-Synthesis Self-Narrowing of the Particle Size Distribution*. *Adv. Mater.*, 2003. **15**(21):1844-1849.
41. J.M. Luther, J. Gao, M.T. Lloyd, O.E. Semonin, M.C. Beard, and A.J. Nozik, *Stability Assessment on a 3% Bilayer PbS/ZnO Quantum Dot Heterojunction Solar Cell*. *Adv. Mater.*, 2010. **22**(33):3704-3707.
42. P. Reiss, M. Protiere, and L. Li, *Core/Shell Semiconductor Nanocrystals*. *Small*, 2009. **5**(2):154-168.
43. F.Q. Ren, H.G. Zhao, F. Vetrone, and D.L. Ma, *Microwave-Assisted Cation Exchange Toward Synthesis of Near-Infrared Emitting PbS/CdS Core/shell Quantum Dots with Significantly Improved Quantum Yields Through a Uniform Growth Path*. *Nanoscale*, 2013. **5**(17):7800-7804.
44. W.H. Guo, J.J. Li, Y.A. Wang, and X.G. Peng, *Luminescent CdSe/CdS Core/shell Nanocrystals in Dendron Boxes: Superior Chemical, Photochemical and Thermal Stability*. *J. Am. Chem. Soc.*, 2003. **125**(13):3901-3909.
45. J.J. Li, Y.A. Wang, W.Z. Guo, J.C. Keay, T.D. Mishima, M.B. Johnson, and X.G. Peng, *Large-scale Synthesis of Nearly Monodisperse CdSe/CdS Core/shell Nanocrystals Using Air-Stable Reagents via Successive Ion Layer Adsorption and Reaction*. *J. Am. Chem. Soc.*, 2003. **125**(41):12567-12575.
46. X.G. Peng, M.C. Schlamp, A.V. Kadavanich, and A.P. Alivisatos, *Epitaxial Growth of Highly Luminescent CdSe/CdS Core/shell Nanocrystals with Photostability and Electronic Accessibility*. *J. Am. Chem. Soc.*, 1997. **119**(30):7019-7029.
47. B. De Geyter, Y. Justo, I. Moreels, K. Lambert, P.F. Smet, D. Van Thourhout, A.J. Houtepen, D. Grodzinska, C.D. Donega, A. Meijerink, D. Vanmaekelbergh, and Z. Hens, *The Different Nature of Band Edge Absorption and Emission in Colloidal PbSe/CdSe Core/Shell Quantum Dots*. *ACS Nano*, 2011. **5**(1):58-66.
48. A. Sashchiuk, D. Yanover, A. Rubinfeld, G.I. Maikov, R.K. Capek, R. Vaxenburg, J. Tilchin, G. Zaiats, and E. Lifshitz, *Tuning of Electronic Properties in IV-VI Colloidal*

- Nanostructures by Alloy Composition and Architecture*. *Nanoscale*, 2013. **5**(17):7724-7745.
49. C.M. Cirloganu, L.A. Padilha, Q.L. Lin, N.S. Makarov, K.A. Velizhanin, H.M. Luo, I. Robel, J.M. Pietryga, and V.I. Klimov, *Enhanced Carrier Multiplication in Engineered Quasi-Type-II Quantum Dots*. *Nat. Commun.*, 2014. **5**:4148 (8pp).
 50. H.G. Zhao, M. Chaker, N.Q. Wu, and D.L. Ma, *Towards Controlled Synthesis and Better Understanding of Highly Luminescent PbS/CdS Core/shell Quantum Dots*. *J. Mater. Chem.*, 2011. **21**(24):8898-8904.
 51. H.G. Zhao, H.Y. Liang, **B.A. Gonfa**, M. Chaker, T. Ozaki, P. Tijssen, F. Vidal, and D.L. Ma, *Investigating Photoinduced Charge Transfer in Double- and Single-Emission PbS@CdS Core@shell Quantum Dots*. *Nanoscale*, 2014. **6**(1):215-225.
 52. L. Dworak, V.V. Matylitsky, V.V. Breus, M. Braun, T. Basche, and J. Wachtveitl, *Ultrafast Charge Separation at the CdSe/CdS Core/Shell Quantum Dot/Methylviologen Interface: Implications for Nanocrystal Solar Cells*. *J. Phys. Chem. C*, 2011. **115**(10):3949-3955.
 53. H. Zhao, Z. Fan, H. Liang, G.S. Selopal, **B.A. Gonfa**, L. Jin, A. Soudi, D. Cui, F. Enrichi, M.M. Natile, I. Concina, D. Ma, A.O. Govorov, F. Rosei, and A. Vomiero, *Controlling Photoinduced Electron Transfer from PbS@CdS Core@shell Quantum Dots to Metal Oxide Nanostructured Thin Films*. *Nanoscale*, 2014. **6**(12):7004-7011.
 54. **B.A. Gonfa**, M.R. Kim, N. Deegan, A.C. Tavares, R. Izquierdo, N. Wu, M.A. El Khakani, and D. Ma, *Towards High Efficiency Air-Processed Near-Infrared Responsive Photovoltaics: Bulk Heterojunction Solar Cells Based on PbS/CdS Core-Shell Quantum Dots and TiO₂ Nanorod Arrays*. *Nanoscale*, 2015. **7**(22):10039-10049.
 55. **B.A. Gonfa**, H.G. Zhao, J.T. Li, J.X. Qiu, M. Saidani, S.Q. Zhang, R. Izquierdo, N.Q. Wu, M.A. El Khakani, and D.L. Ma, *Air-Processed Depleted Bulk Heterojunction Solar Cells Based on PbS/CdS Core-shell Quantum Dots and TiO₂ Nanorod Arrays*. *Sol. Energ. Mat. Sol. Cells*, 2014. **124**:67-74.
 56. D.C.J. Neo, C. Cheng, S.D. Stranks, S.M. Fairclough, J.S. Kim, A.I. Kirkland, J.M. Smith, H.J. Snaith, H.E. Assender, and A.A.R. Watt, *Influence of Shell Thickness and Surface Passivation on PbS/CdS Core/Shell Colloidal Quantum Dot Solar Cells*. *Chem. Mater.*, 2014. **26**(13):4004-4013.

57. Z.J. Ning, H.N. Tian, C.Z. Yuan, Y. Fu, H.Y. Qin, L.C. Sun, and H. Agren, *Solar Cells Sensitized With Type-I ZnSe-CdS Core/Shell Colloidal Quantum Dots*. Chem. Commun. (Camb.), 2011. **47**(5):1536-1538.
58. N. McElroy, R.C. Page, D. Espinbarro-Valazquez, E. Lewis, S. Haigh, P. O'Brien, and D.J. Binks, *Comparison of Solar Cells Sensitized by CdTe/CdSe and CdSe/CdTe Core/shell Colloidal Quantum Dots with and without a CdS Outer Layer*. Thin Solid Films, 2014. **560**:65-70.
59. S. Itzhakov, H. Shen, S. Buhbut, H. Lin, and D. Oron, *Type-II Quantum-Dot-Sensitized Solar Cell Spanning the Visible and Near-Infrared Spectrum*. J. Phys. Chem. C, 2012. **117**(43):22203-22210.
60. J. Bang, J. Park, J.H. Lee, N. Won, J. Nam, J. Lim, B.Y. Chang, H.J. Lee, B. Chon, J. Shin, J.B. Park, J.H. Choi, K. Cho, S.M. Park, T. Joo, and S. Kim, *ZnTe/ZnSe (Core/Shell) Type-II Quantum Dots: Their Optical and Photovoltaic Properties*. Chem. Mater., 2010. **22**(1):233-240.
61. Z.L. Chen, H. Zhang, Q.S. Zeng, Y. Wang, D.D. Xu, L. Wang, H.Y. Wang, and B. Yang, *In Situ Construction of Nanoscale CdTe-CdS Bulk Heterojunctions for Inorganic Nanocrystal Solar Cells*. Adv. Energy Mater., 2014. **4**(10):1400235 (5pp).
62. L. Etgar, D. Yanover, R.K. Capek, R. Vaxenburg, Z.S. Xue, B. Liu, M.K. Nazeeruddin, E. Lifshitz, and M. Gratzel, *Core/Shell PbSe/PbS QDs TiO₂ Heterojunction Solar Cell*. Adv. Funct. Mater., 2013. **23**(21):2736-2741.
63. Z. Pan, I. Mora-Seró, Q. Shen, H. Zhang, Y. Li, K. Zhao, J. Wang, X. Zhong, and J. Bisquert, *High-Efficiency "Green" Quantum Dot Solar Cells*. J. Am. Chem. Soc., 2014. **136**(25):9203-9210.
64. W.L. Ma, S.L. Swisher, T. Ewers, J. Engel, V.E. Ferry, H.A. Atwater, and A.P. Alivisatos, *Photovoltaic Performance of Ultrasmall PbSe Quantum Dots*. ACS Nano, 2011. **5**(10):8140-8147.
65. K.W. Johnston, A.G. Pattantyus-Abraham, J.P. Clifford, S.H. Myrskog, D.D. MacNeil, L. Levina, and E.H. Sargent, *Schottky-Quantum Dot Photovoltaics for Efficient Infrared Power conversion*. Appl. Phys. Lett., 2008. **92**(15):151115 (3pp).
66. D. Wang, J.K. Baral, H. Zhao, **B.A. Gonfa**, V.V. Truong, M.A. El Khakani, R. Izquierdo, and D. Ma, *Controlled Fabrication of PbS Quantum-Dot/Carbon-Nanotube*

- Nanoarchitecture and its Significant Contribution to Near-Infrared Photon-to-Current Conversion*. Adv. Funct. Mater., 2011. **21**(21):4010-4018.
67. Freiburg Materials Research Center. *Development of Bulk-Heterojunction Solar Cells Based on Quantum Dot - Polymer Hybrid Materials*. January 28, 2015; Available from: https://www.fmf.uni-freiburg.de/projects/pg_anorg_en/AKKrueger/projects/photovoltaics?set_language=en.
68. J.M. Luther, J.B. Gao, M.T. Lloyd, O.E. Semonin, M.C. Beard, and A.J. Nozik, *Stability Assessment on a 3% Bilayer PbS/ZnO Quantum Dot Heterojunction Solar Cell*. Adv. Mater., 2010. **22**(33):3704-3707.
69. J.B. Gao, J.M. Luther, O.E. Semonin, R.J. Ellingson, A.J. Nozik, and M.C. Beard, *Quantum Dot Size Dependent J-V Characteristics in Heterojunction ZnO/PbS Quantum Dot Solar Cells*. Nano Lett., 2011. **11**(3):1002-1008.
70. L.-Y. Chang, R.R. Lunt, P.R. Brown, V. Bulović, and M.G. Bawendi, *Low-Temperature Solution-Processed Solar Cells Based on PbS Colloidal Quantum Dot/CdS Heterojunctions*. Nano Lett., 2013. **13**(3):994-999.
71. N. Zhao, T.P. Osedach, L.-Y. Chang, S.M. Geyer, D. Wanger, M.T. Binda, A.C. Arango, M.G. Bawendi, and V. Bulovic, *Colloidal PbS Quantum Dot Solar Cells with High Fill Factor*. ACS Nano, 2010. **4**(7):3743-3752.
72. C.H.M. Chuang, P.R. Brown, V. Bulovic, and M.G. Bawendi, *Improved Performance and Stability in Quantum Dot Solar Cells Through Band Alignment Engineering*. Nat. Mater., 2014. **13**(8):796-801.
73. D.A.R. Barkhouse, R. Debnath, I.J. Kramer, D. Zhitomirsky, A.G. Pattantyus-Abraham, L. Levina, L. Etgar, M. Gratzel, and E.H. Sargent, *Depleted Bulk Heterojunction Colloidal Quantum Dot Photovoltaics*. Adv. Mater., 2011. **23**(28):3134-3138.
74. J. Jean, S. Chang, P.R. Brown, J.J. Cheng, P.H. Rekemeyer, M.G. Bawendi, S. Gradečak, and V. Bulović, *ZnO Nanowire Arrays for Enhanced Photocurrent in PbS Quantum Dot Solar Cells*. Adv. Mater., 2013. **25**(20):2790-2796.
75. I.J. Kramer, D. Zhitomirsky, J.D. Bass, P.M. Rice, T. Topuria, L. Krupp, S.M. Thon, A.H. Ip, R. Debnath, H.C. Kim, and E.H. Sargent, *Ordered Nanopillar Structured Electrodes for Depleted Bulk Heterojunction Colloidal Quantum Dot Solar Cells*. Adv. Mater., 2012. **24**(17):2315-2319.

76. X.Z. Lan, S. Masala, and E.H. Sargent, *Charge-Extraction Strategies for Colloidal Quantum Dot Photovoltaics*. Nat. Mater., 2014. **13**(3):233-240.
77. H.B. Wang, T. Kubo, J. Nakazaki, T. Kinoshita, and H. Segawa, *PbS-Quantum-Dot-Based Heterojunction Solar Cells Utilizing ZnO Nanowires for High External Quantum Efficiency in the Near-Infrared Region*. J. Phys. Chem. Lett., 2013. **4**(15):2455-2460.
78. X. Lan, J. Bai, S. Masala, S.M. Thon, Y. Ren, I.J. Kramer, S. Hoogland, A. Simchi, G.I. Koleilat, D. Paz-Soldan, Z. Ning, A.J. Labelle, J.Y. Kim, G. Jabbour, and E.H. Sargent, *Self-Assembled, Nanowire Network Electrodes for Depleted Bulk Heterojunction Solar Cells*. Adv. Mater., 2013. **25**(12):1769-1773.
79. H.A. Atwater and A. Polman, *Plasmonics for Improved Photovoltaic Devices*. Nat. Mater., 2010. **9**(3):205-213.
80. Y. Takeda, T. Motohiro, D. Konig, P. Aliberti, Y. Feng, S. Shrestha, and G. Conibeer, *Practical Factors Lowering Conversion Efficiency of Hot Carrier Solar Cells*. Applied Physics Express, 2010. **3**(10):104301 (3pp).
81. Y. Zhang, N. Stokes, B. Jia, S. Fan, and M. Gu, *Towards Ultra-Thin Plasmonic Silicon Wafer Solar Cells with Minimized Efficiency Loss*. Sci. Rep., 2014. **4**:4939 (6pp).
82. X. Chen, B. Jia, J.K. Saha, B. Cai, N. Stokes, Q. Qiao, Y. Wang, Z. Shi, and M. Gu, *Broadband Enhancement in Thin-Film Amorphous Silicon Solar Cells Enabled by Nucleated Silver Nanoparticles*. Nano Lett., 2012. **12**(5):2187-2192.
83. H. Choi, J.P. Lee, S.J. Ko, J.W. Jung, H. Park, S. Yoo, O. Park, J.R. Jeong, S. Park, and J.Y. Kim, *Multipositional Silica-Coated Silver Nanoparticles for High-Performance Polymer Solar Cells*. Nano Lett., 2013. **13**(5):2204-2208.
84. J.L. Wu, F.C. Chen, Y.S. Hsiao, F.C. Chien, P.L. Chen, C.H. Kuo, M.H. Huang, and C.S. Hsu, *Surface Plasmonic Effects of Metallic Nanoparticles on the Performance of Polymer Bulk Heterojunction Solar Cells*. ACS Nano, 2011. **5**(2):959-967.
85. C. Andrei, E. Lestini, S. Crosbie, C. de Frein, T. O'Reilly, and D. Zerulla, *Plasmonic Enhancement of Dye Sensitized Solar Cells via a Tailored Size-Distribution of Chemically Functionalized Gold Nanoparticles*. PLoS ONE, 2014. **9**(10):109836 (12pp).
86. C. Hagglund, M. Zach, and B. Kasemo, *Enhanced Charge Carrier Generation in Dye Sensitized Solar Cells by Nanoparticle Plasmons*. Appl. Phys. Lett., 2008. **92**(1):013113 (3pp).

87. W. Zhang, M. Saliba, S.D. Stranks, Y. Sun, X. Shi, U. Wiesner, and H.J. Snaith, *Enhancement of Perovskite-Based Solar Cells Employing Core-Shell Metal Nanoparticles*. Nano Lett., 2013. **13**(9):4505-4510.
88. **B.A. Gonfa**, M.R. Kim, M.A. El Khakani, and D. Ma, *Plasmonic Enhancement of the Performance of PbS/CdS Core-shell Quantum Dots/TiO₂ Nanorod Arrays Bulk Heterojunction Solar Cells*. , in preparation.
89. T. Kawawaki, H. Wang, T. Kubo, K. Saito, J. Nakazaki, H. Segawa, and T. Tatsuma, *Efficiency Enhancement of PbS Quantum Dot/ZnO Nanowire Bulk-Heterojunction Solar Cells by Plasmonic Silver Nanocubes*. ACS Nano, 2015. **9**(4):4165-4172.
90. D. Paz-Soldan, A. Lee, S.M. Thon, M.M. Adachi, H. Dong, P. Maraghechi, M. Yuan, A.J. Labelle, S. Hoogland, K. Liu, E. Kumacheva, and E.H. Sargent, *Jointly Tuned Plasmonic-Excitonic Photovoltaics Using Nanoshells*. Nano Lett., 2013. **13**(4):1502-1508.
91. **B.A. Gonfa**, M.A. El Khakani, and D. Ma, *Quantum Dot/Carbon Nanotube Nanohybrids for Novel Nanostructured Photovoltaic Devices*. Rev. Nanosci. Nanotechnol., 2012. **1**(1):22-39.
92. B. Aissa and M.A. El Khakani, *The ChannelLength Effect on the Electrical Performance of Suspended Single-wall Carbon Nanotube Based Field Effect Transistors*. Nanotechnology, 2009. **20**(17):175203 (9pp).
93. T. Durkop, S.A. Getty, E. Cobas, and M.S. Fuhrer, *Extraordinary Mobility in Semiconducting Carbon Nanotubes*. Nano Lett., 2004. **4**(1):35-39.
94. K.H. Yu and J.H. Chen, *Enhancing Solar Cell Efficiencies Through 1-D Nanostructures*. Nanoscale Res. Lett., 2009. **4**(1):1-10.
95. J.M. Haremza, M.A. Hahn, and T.D. Krauss, *Attachment of Single CdSe Nanocrystals to Individual Single-Walled Carbon Nanotubes*. Nano Lett., 2002. **2**(11):1253-1258.
96. X.H. Peng and S.S. Wong, *Controlling Nanocrystal Density and Location on Carbon Nanotube Templates*. Chem. Mater., 2009. **21**(4):682-694.
97. S. Ravindran, S. Chaudhary, B. Colburn, M. Ozkan, and C.S. Ozkan, *Covalent Coupling of quantum Dots to Multiwalled Carbon Nanotubes for Electronic Device Applications*. Nano Lett., 2003. **3**(4):447-453.

98. X.H. Peng, M.Y. Sfeir, F. Zhang, J.A. Misewich, and S.S. Wong, *Covalent Synthesis and Optical Characterization of Double-Walled Carbon Nanotube-Nanocrystal Heterostructures*. J. Phys. Chem. C, 2010. **114**(19):8766-8773.
99. B.F. Pan, D.X. Cui, R. He, F. Gao, and Y.F. Zhang, *Covalent Attachment of Quantum Dot on Carbon nanotubes*. Chem. Phys. Lett., 2006. **417**(4-6):419-424.
100. S. Banerjee and S.S. Wong, *Synthesis and Characterization of Carbon Nanotube-Nanocrystal Heterostructures*. Nano Lett., 2002. **2**(3):195-200.
101. G.Z. Zou, *Highly Conjugated Water Soluble CdSe Quantum Dots to Multiwalled Carbon Nanotubes*. Chinese Chemical Letters, 2009. **20**(3):356-357.
102. Y.P. Sun, K.F. Fu, Y. Lin, and W.J. Huang, *Functionalized Carbon Nanotubes: Properties and Applications*. Acc. Chem. Res., 2002. **35**(12):1096-1104.
103. B.J. Landi, S.L. Castro, H.J. Ruf, C.M. Evans, S.G. Bailey, and R.P. Raffaele, *CdSe Quantum Dot-Single Wall Carbon Nanotube Complexes for Polymeric Solar Cells*. Sol. Energ. Mat. Sol. Cells, 2005. **87**(1-4):733-746.
104. L. Chen, X.W. Pan, D.X. Zheng, Y. Gao, X.X. Jiang, M.S. Xu, and H.Z. Chen, *Hybrid Solar Cells Based on P3HT and Si@MWCNT Nanocomposite*. Nanotechnology, 2010. **21**(34):345201 (9pp).
105. S.Q. Ren, L.Y. Chang, S.K. Lim, J. Zhao, M. Smith, N. Zhao, V. Bulovic, M. Bawendi, and S. Gradecak, *Inorganic-Organic Hybrid Solar Cell: Bridging Quantum Dots to Conjugated Polymer Nanowires*. Nano Lett., 2011. **11**(9):3998-4002.
106. F. Li, D.I. Son, T.W. Kim, E. Ryu, S.W. Kim, S.K. Lee, and Y.H. Cho, *Photovoltaic Cells Fabricated Utilizing Core-shell CdSe/ZnSe Quantum Dot/Multiwalled Carbon Nanotube Heterostructures*. Appl. Phys. Lett., 2009. **95**(6):061911 (3pp).
107. C. Entrakul, Y.H. Kim, J.M. Nedeljkovic, S.P. Ahrenkiel, K.E.H. Gilbert, J.L. Alleman, S.B. Zhang, O.I. Micic, A.J. Nozik, and M.J. Heben, *Self-Assembly of Linear Arrays of Semiconductor Nanoparticles on Single-Walled Carbon Nanotubes*. J. Phys. Chem. B, 2006. **110**(50):25153-25157.
108. R. Ahmad, U. Soni, R. Srivastava, V.N. Singh, S. Chand, and S. Sapra, *Investigation of the Photophysical and Electrical Characteristics of CuInS₂ QDs/SWCNT Hybrid Nanostructure*. J. Phys. Chem. C, 2014. **118**(21):11409-11416.

109. K.S. Leschkies, A.G. Jacobs, D.J. Norris, and E.S. Aydil, *Nanowire-Quantum-Dot Solar Cells and the Influence of Nanowire Length on the Charge Collection Efficiency*. Appl. Phys. Lett., 2009. **95**(19):193103 (3pp).
110. X.W. Sun, J. Chen, J.L. Song, D.W. Zhao, W.Q. Deng, and W. Lei, *Ligand Capping Effect for Dye Solar Cells with a CdSe Quantum Dot Sensitized ZnO Nanorod Photoanode*. Opt. Express, 2010. **18**(2):1296-1301.
111. J. Chen, C. Li, D.W. Zhao, W. Lei, Y. Zhang, M.T. Cole, D.P. Chu, B.P. Wang, Y.P. Cui, X.W. Sun, and W.I. Milne, *A Quantum Dot sensitized Solar Cell Based on Vertically Aligned Carbon Nanotube Templated ZnO Arrays*. Electrochem. Commun., 2010. **12**(10):1432-1435.
112. S. Jeong, H.C. Shim, S. Kim, and C.S. Han, *Efficient Electron Transfer in Functional Assemblies of Pyridine-Modified NQDs on SWNTs*. ACS Nano, 2010. **4**(1):324-330.
113. Q.W. Li, B.Q. Sun, I.A. Kinloch, D. Zhi, H. Siringhaus, and A.H. Windle, *Enhanced Self-Assembly, of Pyridine-Capped CdSe Nanocrystals on Individual Single-Walled Carbon Nanotubes*. Chem. Mater., 2006. **18**(1):164-168.
114. C. Schulz-Drost, V. Sgobba, C. Gerhards, S. Leubner, R.M.K. Calderon, A. Ruland, and D.M. Guldi, *Innovative Inorganic-Organic Nanohybrid Materials: Coupling Quantum Dots to Carbon Nanotubes*. Angew. Chem. Int. Ed., 2010. **49**(36):6425-6429.
115. J.E. Weaver, M.R. Dasari, A. Datar, S. Talapatra, and P. Kohli, *Investigating Photoinduced Charge Transfer in Carbon Nanotube-Perylene-Quantum Dot Hybrid Nanocomposites*. ACS Nano, 2010. **4**(11):6883-6893.
116. L. Hu, Y.L. Zhao, K. Ryu, C. Zhou, J.F. Stoddart, and G. Gruner, *Light-Induced Charge Transfer in Pyrene/CdSe-SWNT Hybrids*. Adv. Mater., 2008. **20**(5):939-946.
117. B.J. Landi, C.M. Evans, J.J. Worman, S.L. Castro, S.G. Bailey, and R.P. Raffaele, *Noncovalent Attachment of CdSe Quantum Dots to Single Wall Carbon Nanotubes*. Mater. Lett., 2006. **60**(29-30):3502-3506.
118. C.G. Lu, A. Akey, W. Wang, and I.P. Herman, *Versatile Formation of CdSe Nanoparticle-Single Walled Carbon Nanotube Hybrid Structures*. J. Am. Chem. Soc., 2009. **131**(10):3446-3447.
119. Y.A. Kim, H. Muramatsu, K.C. Park, D. Shimamoto, Y.C. Jung, J.H. Kim, T. Hayashi, Y. Saito, M. Endo, M. Terrones, and M.S. Dresselhaus, *CdSe Quantum Dot-Decorated*

- Double Walled Carbon Nanotubes: The Effect of Chemical Moieties*. Appl. Phys. Lett., 2008. **93**(5):051901 (3pp).
120. B.F. Pan, D.X. Cui, C.S. Ozkan, M. Ozkan, P. Xu, T. Huang, F.T. Liu, H. Chen, Q. Li, R. He, and F. Gao, *Effects of Carbon Nanotubes on Photoluminescence Properties of Quantum Dots*. J. Phys. Chem. C, 2008. **112**(4):939-944.
121. H.Y. Si, C.H. Liu, H. Xu, T.M. Wang, and H.L. Zhang, *Shell-Controlled Photoluminescence in CdSe/CNT Nanohybrids*. Nanoscale Res. Lett., 2009. **4**(10):1146-1152.
122. Z. Li, L.B. Yu, Y.B. Liu, and S.Q. Sun, *CdS/CdSe Quantum Dots Co-Sensitized TiO₂ Nanowire/Nanotube Solar Cells with Enhanced Efficiency*. Electrochimica Acta, 2014. **129**:379-388.
123. Y. Li, L. Wei, X. Chen, R. Zhang, X. Sui, Y. Chen, J. Jiao, and L. Mei, *Efficient PbS/CdS Co-Sensitized Solar Cells Based on TiO₂ Nanorod Arrays*. Nanoscale Res. Lett., 2013. **8**(1):67 (7pp).
124. S.Y. Yang, A.S. Nair, R. Jose, and S. Ramakrishna, *Electrospun TiO₂ Nanorods Assembly Sensitized by CdS Quantum Dots: A Low-Cost Photovoltaic Material*. Energy & Environmental Science, 2010. **3**(12):2010-2014.
125. C. Liu, Y.T. Li, L. Wei, C.C. Wu, Y.X. Chen, L.M. Mei, and J. Jiao, *CdS Quantum Dot-Sensitized Solar Cells Based on Nano-Branched TiO₂ Arrays*. Nanoscale Res. Lett., 2014. **9**:107 (8pp).
126. D.S. Yu, Y.J. Chen, B.J. Li, X.D. Chen, and M.Q. Zhang, *Fabrication and Characterization of PbS/Multiwalled Carbon Nanotube Heterostructures*. Appl. Phys. Lett., 2007. **90**(16):161103 (6pp).
127. S.K. Pillai, N. Moloto, and S.S. Ray, *CoS-Carbon Nanotube Heterostructure: One-Step Synthesis and Optical Properties*. J. Nanosci. Nanotechnol., 2010. **10**(7):4279-4285.
128. Y.J. Na, H.S. Kim, and J. Park, *Morphology-Controlled Lead Selenide Nanocrystals and Their In Situ Growth on Carbon Nanotubes*. J. Phys. Chem. C, 2008. **112**(30):11218-11226.
129. M. Li, F.Y. Shao, Q.Q. Ban, and J.W. Yang, *CdS Quantum Dots Sensitized Single-Crystalline TiO₂ Nanowire Array Films: Photovoltaic Performance And Photoelectron Transport Properties*. J. Ovonic Res., 2013. **9**(6):157-165.

130. S. Banerjee and S.S. Wong, *In Situ Quantum Dot Growth on Multiwalled Carbon Nanotubes*. J. Am. Chem. Soc., 2003. **125**(34):10342-10350.
131. F.S. Li, S.H. Cho, D.I. Son, T.W. Kim, S.K. Lee, Y.H. Cho, and S.H. Jin, *UV photovoltaic cells based on conjugated ZnO quantum dot/multiwalled carbon nanotube heterostructures*. Appl. Phys. Lett., 2009. **94**(11).
132. P. Sudhagar, T. Song, D.H. Lee, I. Mora-Sero, J. Bisquert, M. Laudenslager, W.M. Sigmund, W.I. Park, U. Paik, and Y.S. Kang, *High Open Circuit Voltage Quantum Dot Sensitized Solar Cells Manufactured with ZnO Nanowire Arrays and Si/ZnO Branched Hierarchical Structures*. J. Phys. Chem. Lett., 2011. **2**(16):1984-1990.
133. M. Seol, H. Kim, Y. Tak, and K. Yong, *Novel Nanowire Array Based Highly Efficient Quantum Dot Sensitized Solar Cell*. Chem. Commun. (Camb.), 2010. **46**(30):5521-5523.
134. Y.X. Chen, L. Wei, G.H. Zhang, and J. Jiao, *Open Structure ZnO/CdSe Core/shell Nanoneedle Arrays for Solar Cells*. Nanoscale Res. Lett., 2012. **7**:516 (6pp).
135. C. Li, J. Xia, Q.L. Wang, J. Chen, C. Li, W. Lei, and X.B. Zhang, *Photovoltaic Property of a Vertically Aligned Carbon Nanotube Hexagonal Network Assembled with CdS Quantum Dots*. ACS Appl. Mater. Interfaces, 2013. **5**(15):7400-7404.
136. F. Xu, J. Benavides, X. Ma, and S.G. Cloutier, *Interconnected TiO₂ Nanowire Networks for PbS Quantum Dot Solar Cell Applications*. Journal of Nanotechnology, 2012. **2012**:709031(6pp).
137. F. Tan, S. Qu, Q. Jiang, J. Liu, Z. Wang, F. Li, G. Yue, S. Li, C. Chen, W. Zhang, and Z. Wang, *Interpenetrated Inorganic Hybrids for Efficiency Enhancement of PbS Quantum Dot Solar Cells*. Adv. Energy Mater., 2014. **4**(17):1400512 (8pp).
138. I. Ka, **B. Gonfa**, V. Le Borgne, D. Ma, and M.A. El Khakani, *Pulsed Laser Ablation Based Synthesis of PbS-Quantum Dot-Decorated One-Dimensional Nanostructures and Their Direct Integration into Highly Efficient Nanohybrid Heterojunction-Based Solar Cells*. Adv. Funct. Mater., 2014. **24**(26):4042-4050.
139. I. Ka, V. Le Borgne, D. Ma, and M.A. El Khakani, *Pulsed Laser Ablation based Direct Synthesis of Single-Wall Carbon Nanotube/PbS Quantum Dot Nanohybrids Exhibiting Strong, Spectrally Wide and Fast Photoresponse*. Adv. Mater., 2012. **24**(47):6289-6294.

140. N.P. Dasgupta, H.J. Jung, O. Trejo, M.T. McDowell, A. Hryciw, M. Brongersma, R. Sinclair, and F.B. Prinz, *Atomic Layer Deposition of Lead Sulfide Quantum Dots on Nanowire Surfaces*. Nano Lett., 2011. **11**(3):934-940.
141. Z.H. Chen, C.P. Liu, H.E. Wang, Y.B. Tang, Z.T. Liu, W.J. Zhang, S.T. Lee, J.A. Zapien, and I. Bello, *Electronic Structure at the Interfaces of Vertically Aligned Zinc Oxide Nanowires and Sensitizing Layers in Photochemical Solar Cells*. J. Phys. D: Appl. Phys., 2011. **44**(32):325108 (6pp).
142. R.S. Aga, D. Jowhar, A. Ueda, Z. Pan, W.E. Collins, R. Mu, K.D. Singer, and J. Shen, *Enhanced Photoresponse in ZnO Nanowires Decorated with CdTe Quantum Dot*. Appl. Phys. Lett., 2007. **91**(23):232108 (3pp).
143. M. Liu, G.H. Lu, and J.H. Chen, *Synthesis, Assembly, and Characterization of Si Nanocrystals and Si Nanocrystal Carbon Nanotube Hybrid Structures*. Nanotechnology, 2008. **19**(26):265705 (5pp).
144. D. Bera, L. Qian, T. Tseng, and P. Holloway, *Quantum Dots and Their Multimodal Applications: A Review*. Materials, 2010(3):2260-2345.
145. I. Robel, B.A. Bunker, and P.V. Kamat, *Single-Walled Carbon Nanotube-CdS Nanocomposites as Light-Harvesting Assemblies: Photoinduced Charge-Transfer Interactions*. Adv. Mater., 2005. **17**(20):2458-2463.
146. F. Li, D.I. Son, S.H. Cho, W.T. Kim, and T.W. Kim, *Flexible Photovoltaic Cells Fabricated Utilizing ZnO Quantum Dot/Carbon Nanotube Heterojunctions*. Nanotechnology, 2009. **20**(15):155202 (4pp).
147. D. Wang, H. Zhao, N.Q. Wu, M.A. El Khakani, and D. Ma, *Tuning the Charge-Transfer Property of PbS-Quantum Dot/TiO₂-Nanobelt Nanohybrids via Quantum Confinement*. J. Phys. Chem. Lett., 2010. **1**(7):1030-1035.
148. D. Tafen and O.V. Prezhdo, *Size and Temperature Dependence of Electron Transfer between CdSe Quantum Dots and a TiO₂ Nanobelt*. J. Phys. Chem. C, 2015. **119**(10):5639-5647.
149. M. Olek, T. Busgen, M. Hilgendorff, and M. Giersig, *Quantum Dot Modified Multiwall Carbon Nanotubes*. J. Phys. Chem. B, 2006. **110**(26):12901-12904.

150. M. Grzelczak, M.A. Correa-Duarte, V. Salgueirino-Maceira, M. Giersig, R. Diaz, and L.M. Liz-Marzan, *Photoluminescence Quenching Control in Quantum Dot-Carbon Nanotube Composite Colloids Using a Silica-Shell Spacer*. *Adv. Mater.*, 2006. **18**(4):415-+.
151. J.Z. Zhang, *Optical Properties and Spectroscopy of Nanomaterials*. Singapore: World Scientific Publishing Co. Pte. Ltd., 2009:261-304.
152. D.M. Guldi, G.M.A. Rahman, V. Sgobba, N.A. Kotov, D. Bonifazi, and M. Prato, *CNT-CdTe Versatile Donor-Acceptor Nanohybrids*. *J. Am. Chem. Soc.*, 2006. **128**(7):2315-2323.
153. E.S. Aydil and B. Liu, *Growth of Oriented Single-Crystalline Rutile TiO₂ Nanorods on Transparent Conducting Substrates for Dye-Sensitized Solar Cells*. *J Am Chem Soc*, 2009. **131**(11):3985-3990.
154. C.W. Zhou, A. Kumar, and A.R. Madaria, *Growth of Aligned Single-Crystalline Rutile TiO₂ Nanowires on Arbitrary Substrates and Their Application in Dye-Sensitized Solar Cells*. *J. Phys. Chem. C*, 2010. **114**(17):7787-7792.
155. J.T. Li, M.W.G. Hoffmann, H. Shen, C. Fabrega, J.D. Prades, T. Andreu, F. Hernandez-Ramirez, and S. Mathur, *Enhanced Photoelectrochemical Activity of an Excitonic Staircase in CdS@TiO₂ and CdS@anatase@rutile TiO₂ Heterostructures*. *J Mater Chem*, 2012. **22**(38):20472-20476.
156. T. Zhang, H. Zhao, D. Riabinina, M. Chaker, and D. Ma, *Concentration-Dependent Photoinduced Photoluminescence Enhancement in Colloidal PbS Quantum Dot Solution*. *J. Phys. Chem. C*, 2010. **114**(22):10153-10159.
157. H.G. Zhao, M. Chaker, and D.L. Ma, *Effect of CdS Shell Thickness on the Optical Properties of Water-Soluble, Amphiphilic Polymer-Encapsulated PbS/CdS Core/shell Quantum Dots*. *J. Mater. Chem.*, 2011. **21**(43):17483-17491.
158. M. Li, J.M. Zhang, S. Suri, L.J. Sooter, D.L. Ma, and N.Q. Wu, *Detection of Adenosine Triphosphate with an Aptamer Biosensor Based on Surface-Enhanced Raman Scattering*. *Anal. Chem.*, 2012. **84**(6):2837-2842.
159. G. Frens, *Controlled Nucleation for Regulation of Particle-Size in Monodisperse Gold Suspensions*. *Nature-Physical Science*, 1973. **241**(105):20-22.

160. P.S. Kumar, I. Pastoriza-Santos, B. Rodriguez-Gonzalez, F.J. Garcia de Abajo, and L.M. Liz-Marzan, *High-Yield Synthesis and Optical Response of Gold Nanostars*. *Nanotechnology*, 2008. **19**(1):015606 (6pp).
161. E.D. Palik, *Handbook of optical constants of solids*. 1985, Orlando: Academic Press.
162. A.J. Labelle, S.M. Thon, S. Masala, M.M. Adachi, H.P. Dong, M. Farahani, A.H. Ip, A. Fratolocchi, and E.H. Sargent, *Colloidal Quantum Dot Solar Cells Exploiting Hierarchical Structuring*. *Nano Lett.*, 2015. **15**(2):1101-1108.

RÉSUMÉ

Introduction

Le soleil est l'énergie la plus viable, la plus abondante, la plus propre et la source la plus renouvelable pour répondre aux demandes d'une population mondiale en expansion [11]. Pour pouvoir l'exploiter, elle doit être convertie et stockée sous une forme utilisable, par exemple sous forme de courant électrique. La technologie des cellules solaires permet de collecter et de convertir l'énergie solaire en courant électrique en offrant un important rendement de conversion en puissance (RCP). Pour que les technologies exploitant l'énergie solaire soient utilisables en pratique, elles doivent être compétitives face aux autres sources d'énergies en termes de coût économique.

Depuis la découverte en 1839 de l'effet photovoltaïque par le français Alexandre-Edmond Becquerel [1], différents matériaux et structures ont été étudiés conduisant ainsi à la mise au point de dispositifs à fort RCP, et ensuite à leur commercialisation. Parmi les réalisations remarquables, on peut citer par exemple les dispositifs à jonctions simples qui peuvent atteindre une RCP de 28,3% [2] et les dispositifs à jonctions multiples (4 jonctions) qui ont montré un RCP de 46 % [3]. En comparaison, les cellules solaires les plus largement commercialisées, faites à base de silicium monocristallin atteignent au mieux un RCP de 25,6 %, alors que des modules à base de silicium poly-cristallin délivrent un RCP pouvant atteindre 19,3% [18-20]. Toutefois, ces cellules solaires ont un coût de production relativement élevé. Il est donc nécessaire de développer de nouveaux dispositifs produits à des coûts moindres avec des RCPs raisonnables, leur permettant de concurrencer avec les technologies plus onéreuses.

Les cellules solaires qui ont été étudiées jusqu'à présent sont classées en différentes générations selon leur RCP, leur coût, le type de dispositif et les matériaux utilisés. Ainsi, la première génération, basée sur les cellules solaires à base de silicium monocristallin offre à la fois un RCP élevé mais avec des coûts élevés également. La deuxième génération offre de meilleurs prix au détriment d'un RCP inférieur. L'idée de la troisième génération est donc de proposer des cellules solaires à fort RCP et à prix modéré. Les cellules solaires à base de boîtes quantiques (BQs) constituent des candidats prometteurs au sein de la troisième génération. Parmi les nombreuses

techniques de fabrication de BQs, la synthèse par voie colloïdale est fort intéressante grâce à la simplicité de sa mise en œuvre et ses bas coût de production [27].

De plus, les BQs possèdent des propriétés uniques qui expliquent leur fort potentiel pour des applications solaires. Les BQs présentent une forte absorption due à leur coefficient d'extinction élevé, permettant leur utilisation sous forme de films minces. En outre, grâce au confinement quantique des excitons dans les BQs, il est possible d'ajuster leur absorption en modifiant leurs tailles. En particulier, les BQs actives dans le proche infrarouge (NIR) sont d'un grand intérêt puisque qu'elles permettent de profiter de la partie infrarouge du spectre solaire qui représente près de 50% des photons du spectre solaire. Les BQs offrent également la possibilité de générer des excitons multiples [28-30] et d'extraire des porteurs de charges chaudes [32, 33] et cellules solaires de la bande intermédiaire [34]. Tous ces avantages permettent la possibilité de dépasser la limite de Shockley-Queisser pour les cellules solaires à jonctions simples (RCP de 31%) [21]. Alors que les BQs colloïdales n'offrent pas la stabilité désirée, leur encapsulation par une coquille inorganique plus stable permet d'améliorer significativement leur stabilité et résistance à l'oxydation. De telles BQs cœur/coquille constituent ainsi une alternative prometteuse pour des applications photovoltaïques (PVs) [50].

Afin de mieux intégrer les BDs dans des dispositifs photovoltaïques, certains points doivent être pris en compte. Parmi ceux-ci, lorsque des films continus de BQs sont fabriqués, les BQS doivent être peu éloignées pour ne pas nuire à la mobilité des porteurs de charges au travers du film et le nombre de sites de recombinaison de charges doit être minimisé. Pour surmonter ces difficultés, il est possible d'adjoindre une structure uni-dimensionnelle (1D) aux BQs, cette structure 1D jouant alors le rôle de transporteur de charges [8, 91]. Une autre solution applicable aux films épais de BQs consiste en l'insertion de nanoparticules plasmoniques au sein de films de BQs plus minces pour accroître l'absorption optique tout en conservant une extraction des porteurs de charges efficace.

Objectif de la Thèse

Les principaux objectifs de la thèse sont :

1. la fabrication et l'étude de cellules solaires composées de hétérojonctions (HJs) à base de BQs actives dans l'infrarouge (PbS et PbS/CdS coeur-coquille) et de structures 1D (i.e., des nano bâtonnets de TiO_2 (NBs- TiO_2) fabriqués par croissance hydrothermale;

2. Étudier l'effet des traitements de surface des BQs de PbS et de PbS/CdS coeur/coquille dans des cellules solaires;
3. Optimiser l'architecture des dispositifs impliquant des BQs PbS/CdS coeur/coquille pour ensuite améliorer les performances des cellules solaires à HJs. L'optimisation inclue : (i) l'étude de l'effet de la déposition par pulvérisation d'une couche germinale ultramince de TiO_2 sur le FTO afin de favoriser la croissance subséquente des NBs- TiO_2 , (ii) l'effet de la taille des NBs- TiO_2 , et (iii) l'effet du recuit des BQs PbS/CdS coeur/coquille sous atmosphère inerte sur les performances des cellules solaires à HJs ;
4. L'intégration de nanoparticules plasmoniques de nano-étoiles d' Au dans des cellules solaires à base de BQs PbS/CdS coeur/coquille et étudier leurs effets sur les performances PVs.

Dans la première partie de ce travail, des cellules solaires ont été fabriquées à partir de BQs colloïdales de PbS et PbS/CdS coeur/coquille combinées à des réseaux de NBs- TiO_2 rutile (2 et 4

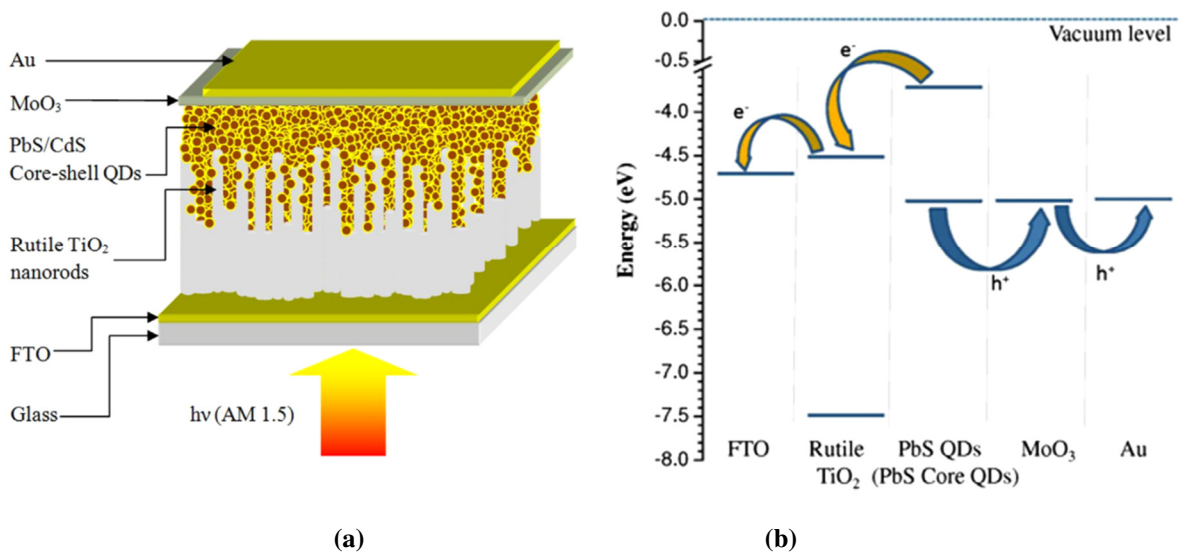


Figure R1. (a) Diagramme schématique de la vue en transverse d'une cellule solaire à base de FTO/NBs- TiO_2 /BQs/PbS/CdS/MoO₃/Au; (b) diagramme des bandes d'énergies de la cellule solaire.

μm de long), synthétisés par la technique hydrothermale. La structure générale des dispositifs étudiés est (FTO)/ TiO_2 /BQs/couche d'interface/Au (la coupe transverse schématisée ainsi que le diagramme de bandes d'énergies des différents composants sont présentés dans la Figure R1). Deux types de BQs (PbS et PbS/CdS coeur/coquille) ainsi que deux types de couche d'interface (PEDOT:PSS et MoO_3) entre le film de BQs et l'électrode inférieure ont été étudiés. L'effet de

l'atmosphère (inerte ou ambiante) sous laquelle la dispersion par centrifugation des BQs et l'échange des ligands sont effectuées a également été étudié.

Nous avons trouvé que l'atmosphère ainsi que la couche interfaciale (MoO_3) extractrice de trous entre le film de BQs et l'électrode inférieure d'au affectent significativement les performances des cellules solaires. Un RCP maximal de 2.14% a été atteint sous illumination solaire (AM 1.5) pour des dispositifs utilisant des BQs PbS/CdS coeur/coquille, des NBs de TiO_2 de 2 μm de long avec une couche d'interface de MoO_3 . Par ailleurs, ces dispositifs sont traités sous atmosphère ambiante et ont montré de meilleures performances (jusqu'à plus de 40%) que les dispositifs à base de BQs de PbS traités sous atmosphère inerte (RCP maximal de 1.53%), toutes les autres

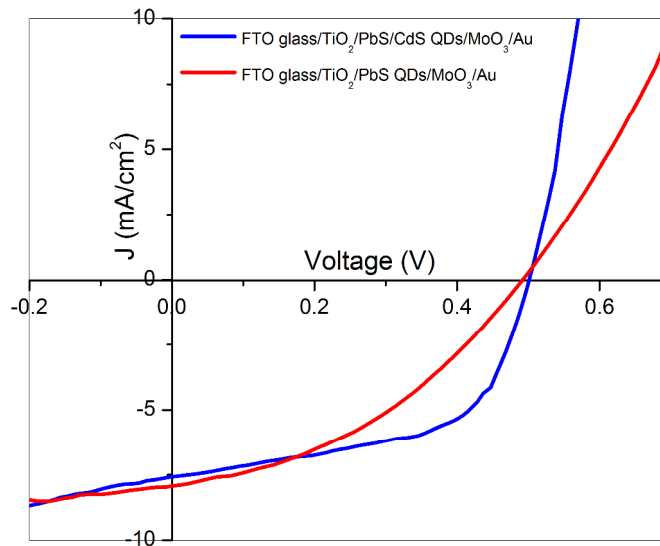


Figure R2. Courbes J-V du dispositif à HJS : (bleue) verre FTO/NBs- TiO_2 /BQs (PbS/CdS)/ MoO_3 /Au, la dispersion par centrifugation et l'échange de ligand des BQs de PbS/CdS QDs ont été faits sous atmosphère ambiante; (rouge) verre FTO /NBs de TiO_2 /BQs PbS/ MoO_3 /Au, la dispersion par centrifugation et l'échange de ligands des BQs de PbS QDs ont été faits sous atmosphère contrôlé.

conditions de fabrication étant équivalentes. La comparaison des courbes courant-tension (J-V) des deux dispositifs sont présentés sur la Figure R2. Il est à noter qu'aussi bien les BQs PbS/CdS coeur/coquille que les NBs de TiO_2 rutile ont été synthétisés par des techniques de fabrication chimiques en solution avec des coûts relativement bas.

Les résultats extraits de cette partie sont présentés dans la publication [55]:

[55] Gonfa, B.A., H.G. Zhao, J.T. Li, J.X. Qiu, M. Saidani, S.Q. Zhang, R. Izquierdo, N.Q. Wu, M.A. El Khakani, and D.L. Ma, Sol. Energ. Mat. Sol. Cells, 2014. **124**: p. 67-74.

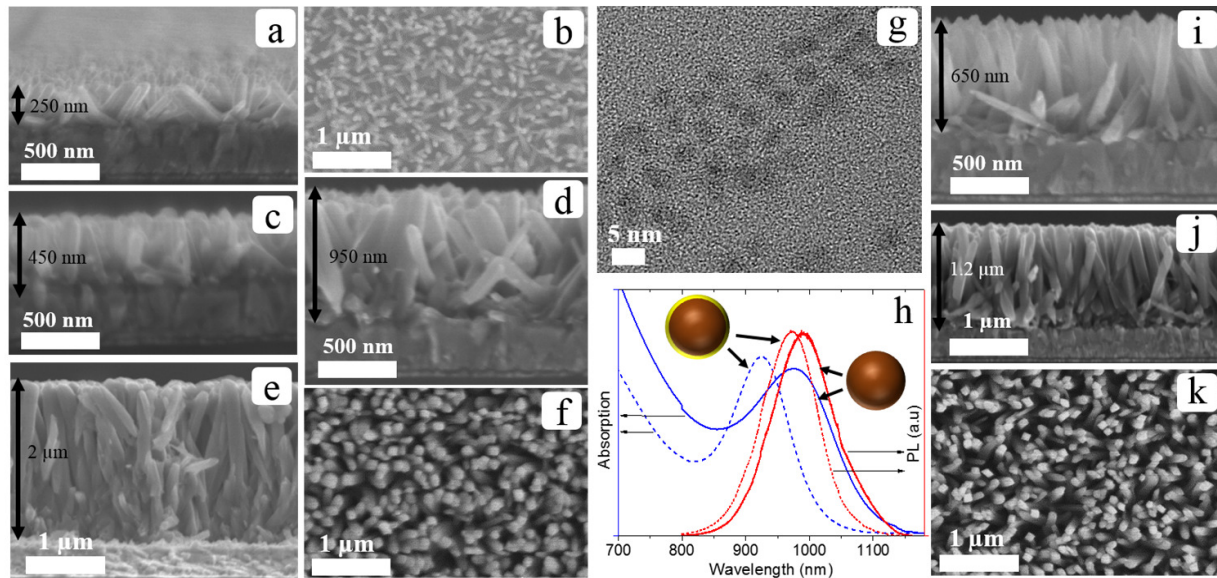


Figure R3. (a,c,d et e) Image MEB de vue en transverse de NBs de TiO_2 de différentes longueurs sur couche germinale/substrat de FTO, (g) Image MET type de BQs-PbS/CdS, (h) spectre d'absorption Vis-NIR (bleu) et de photoluminescence (rouge) de BQs de PbS/CdS en solution (courbes en pointillés) et BQs de PbS en solution (courbes pleines), (i et j) images MEB de vue en transverse de NBs de TiO_2 de tailles différentes synthétisées sur substrat de FTO et vue de dessus par MEB de NBs de TiO_2 de longueurs (b) 250 nm et (f) 2 μm synthétisés sur couche germinale/substrat de FTO, et (k) NBs de TiO_2 de longueur 2 μm sur substrat de FTO.

Il était important de démontrer les performances accrues de cellules solaires composées de BQs PbS/CdS coeur/coquille synthétisés par des procédés de fabrication simples sous atmosphère ambiante en comparaison des cellules à base de BQs de PbS qui nécessitent l'utilisation de boîtes à gants sous atmosphère inerte. Toutefois, il reste de nombreuses optimisations à effectuer en vue d'améliorer encore significativement les performances. C'est ainsi que dans la seconde partie de ce travail, des dispositifs de cellules solaires à base de BQs PbS/CdS coeur/coquille ont été développés en optimisant les matériaux et les structures utilisées, permettant d'atteindre un RCP aussi élevé que 4.43% (sous simulateur solaire AM 1.5). Ce RCP a été obtenu en utilisant une couche germinale de TiO_2 déposée par pulvérisation cathodique sur une verre de FTO avant de

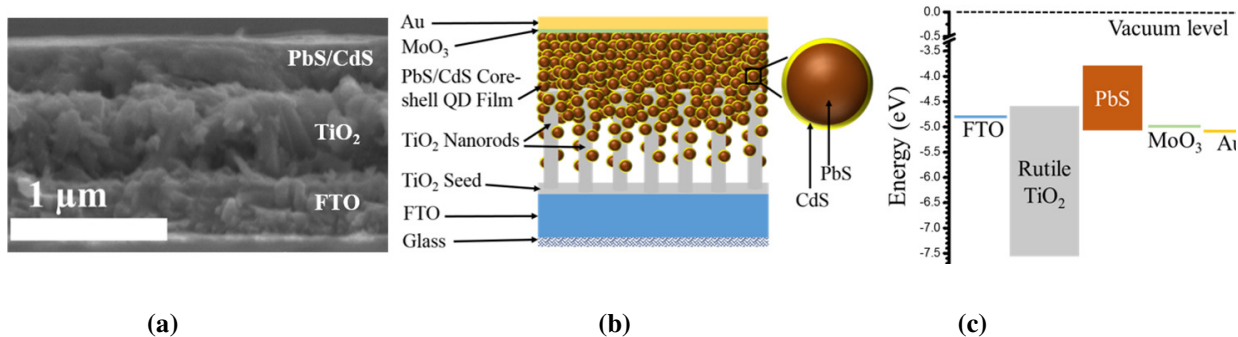


Figure R4. (a) Image MEB de coupe transverse de BQs de PbS/CdS dispersées sur NBs de TiO₂ long de 450 nm sur couche germinale/verre FTO, (b) représentation schématique de l'architecture en coupe transverse d'une cellule solaire à HJS et (c) alignement des bandes d'énergies des composants utilisés.

faire croître un réseau de NBs de TiO₂ de longueur optimisée et d'un film de BQs PbS/CdS coeur/coquille recuit sous atmosphère inerte. Des images par microscopie électronique à balayage (MEB) des NBs de TiO₂ avec et sans couche germinale (vue en transverse et vue en perspective) sont présentées dans la Figure R3 ainsi qu'une image par microscopie électronique en transmission (MET) des BQs PbS/CdS coeur/coquille et des spectres de photoluminescence (PL) et

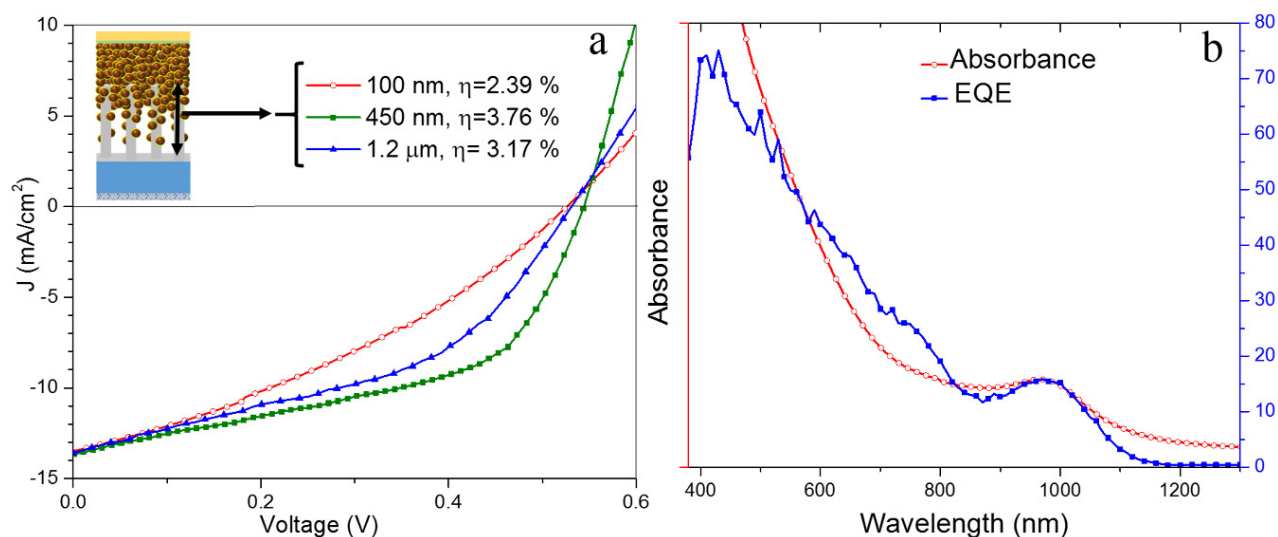


Figure R5. (a) Courbes J-V du dispositif à HJs fait de NBs TiO₂ de 100 nm, 450 nm et 1.2 μm sur couche germinale/verre FTO sous illumination AM1.5, et (b) spectre EQE du dispositif à NBs de TiO₂ long de 450 nm sur couche germinale/verre FTO comparé avec le spectre d'absorption UV-Vis-NIR de film de BQs de PbS/CdS coeur-coquille sur quartz.

d'absorption dans le visible et l'infrarouge proche (Vis-NIR) des BQs PbS/CdS coeur/coquille et PbS en solution. L'image de vue en transverse du film de BQs déposé sur des NBs de TiO₂ par MEB, le schéma des dispositifs ainsi que les diagrammes de bandes d'énergies des composants utilisés sont présentés dans la Figure R4. Nous avons trouvé que les performances des cellules solaires dépendent de la taille des NBs-TiO₂ et que celle-ci est optimale à une longueur de 450 nm pour laquelle le RCP vaut 3.76%. À titre d'illustration, les courbes J-V de trois dispositifs à longueur de NBs de 100 nm, 450 nm et 1.2 μm sous illumination AM 1.5, avec la présence d'une couche germinale sont présentés sur la Figure R5. Le RCP croît dans un premier temps avec la longueur des NBs de TiO₂ avant de décroître. La photoréponse s'étend à des longueurs d'ondes ≥1200 nm comme le montre le spectre d'absorption du film de BQs et le spectre d'efficacité quantique externe (EQE) (Figure R5b). En comparaison des dispositifs sans couche germinale, un RCP maximal de 3.56% est également atteint pour une longueur de NBs de 450 nm. Les dispositifs sans couche germinale de TiO₂ présentent des tendances similaires aux systèmes avec couche dans les variations de J_{sc}, V_{oc} et FF selon la taille des NBs. Des différences plus importantes ont été constatées pour des NBs de TiO₂ plus longs. Il n'y a alors plus de décroissance monotone des courbes J-V lorsque les bâtonnets croissent de 450 nm à 2 μm mais une chute de V_{oc} en absence

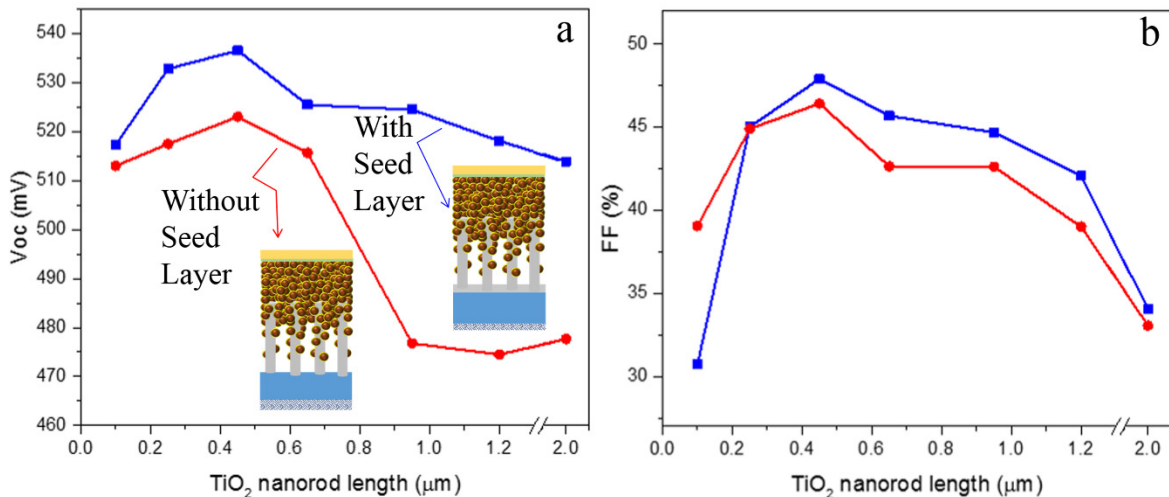


Figure R6. Comparaison de la dépendance de la longueur des NBs du (a) V_{oc} et du (b) FF des dispositifs à HJs à base de NBs de TiO₂ sur couche germinale/ verre FTO et sur verre FTO seul.

de couche germinale qui s'effectue en deux étapes (Figure R6). Une forte décroissance lorsque la longueur varie de 650 nm à 950 nm et ensuite une décroissance plus modérée. Ceci met en évidence l'effet bénéfique de la déposition par pulvérisation de couche germinale de TiO₂ pour atteindre une meilleure adhésion interfaciale des NBs de TiO₂ sur le substrat de FTO, favoriser le transport des charges à l'interface et ainsi réduire les sites de recombinaison de photocharges.

Le recuit à 110 °C sous atmosphère saturée en N₂ des dispositifs après dépôt du film BQs accroît grandement le RCP qu'ils contiennent une couche germinale ou non. La Figure R7 présente les courbes J-V de dispositifs avec et sans couche germinale après recuit, le RCP des dispositifs ayant une couche germinale et des NBs-TiO₂ de longueur optimisée à 450 nm atteignent la valeur de

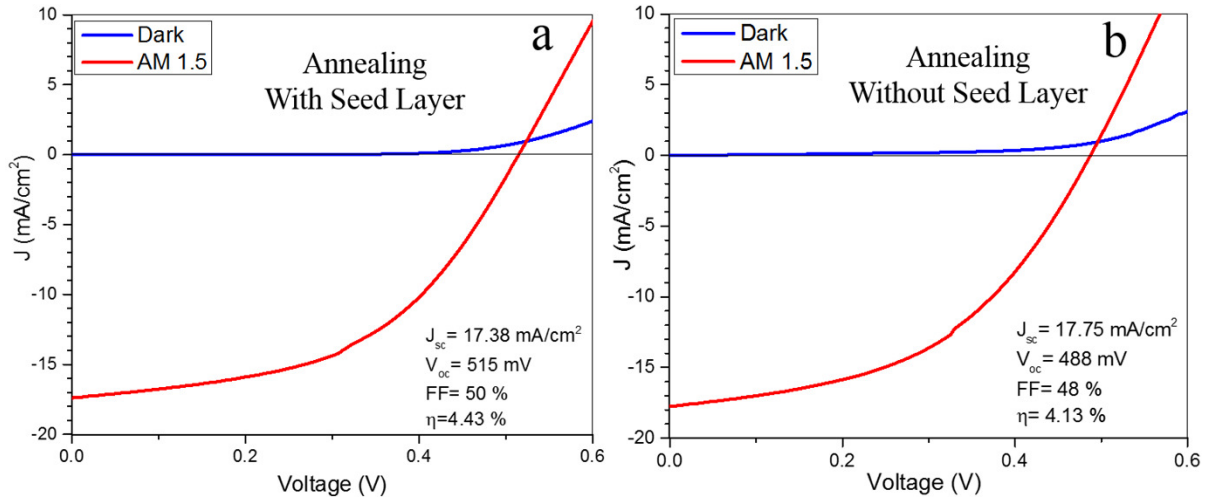


Figure R7. Courbes J-V de dispositifs recuit sous atmosphère saturée de N₂ avec NBs de TiO₂ de 450 nm sur (a) couche germinale/ verre FTO et (b) verre FTO seul.

4.43%, correspondant à une amélioration du RCP de ~18%. Le système sans couche a quant à lui un RCP qui croît de 16% pour atteindre 4.13%. L'augmentation du RCP est principalement due à une augmentation de J_{sc}, le transport des charges est donc amélioré par le meilleur couplage des BQs qui se trouvent plus proches les uns des autres et par la réduction de l'énergie d'activation de pièges peu profonds.

Les résultats extraits de cette partie sont présentés dans la publication [54]:

[54] Gonfa, B.A., M.R. Kim, N. Delegan, A.C. Tavares, R. Izquierdo, N. Wu, M.A. El Khakani, and D. Ma, *Nanoscale*, 2015. 7(22): p. 10039-10049.

En vue d'augmenter l'absorption de la lumière, l'insertion de nanoparticules plasmoniques dans

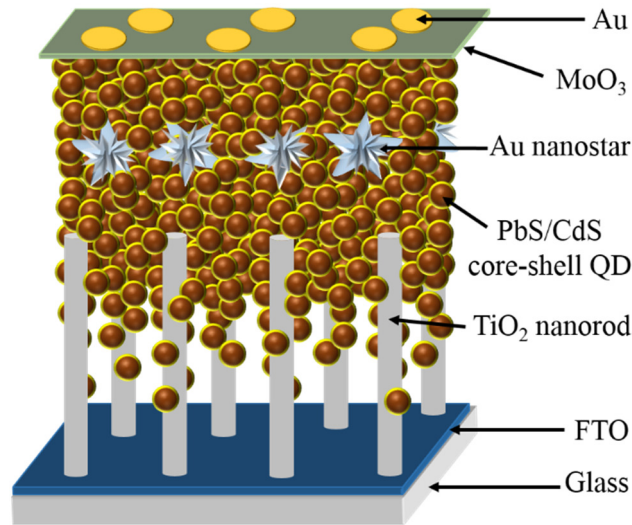


Figure R8. Représentation schématique de la coupe transverse de dispositifs plasmoniques à HJs.

nos dispositifs PVs a été étudié la troisième partie de ma thèse. En effet, nous avons particulièrement étudié l'intégration de nano-étoiles d' Au dans nos cellules solaires à HJs utilisant des BQs PbS/CdS coeur/coquille. La coupe transverse schématisée de ce dispositif est représentés sur la Figure R8. Nous avons trouvé que la densité de nano-étoiles d' Au ainsi que leurs positions

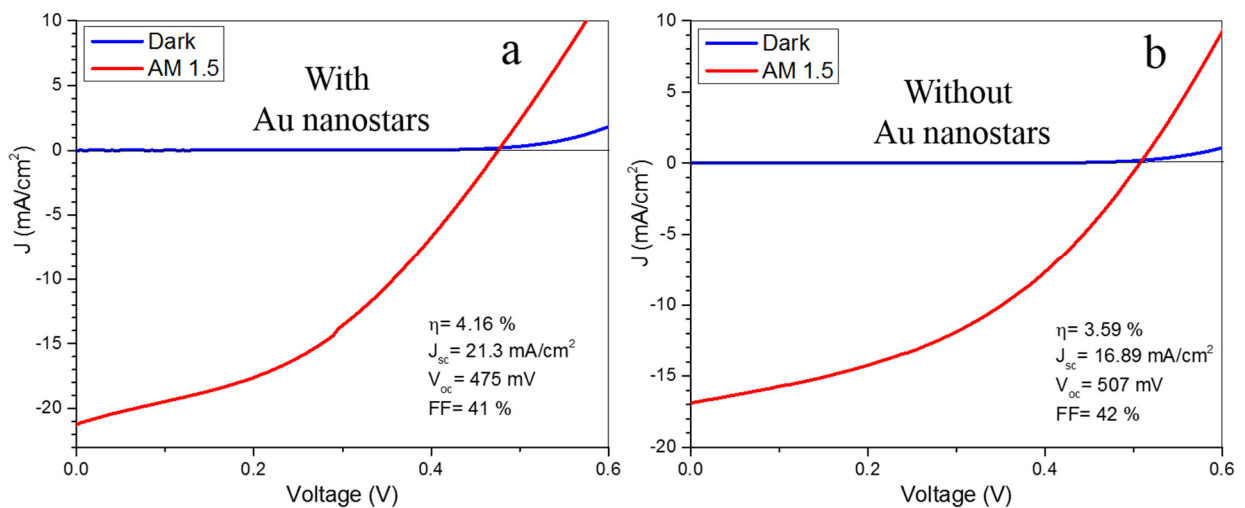


Figure R9. Courbes J-V de dispositifs à HJs (a) avec et (b) sans nano-étoiles d' Au.

au sein du film de BQs affectent les performances des dispositifs. En optimisant ces paramètres, un RCP de 4.16% a été obtenu, soit une augmentation de 16% en comparaison des systèmes sans nano-étoiles d’Au qui ont un RCP de 3.59%. La Figure R9 montre les courbes J-V de dispositifs avec et sans nanoparticules d’Au. Cet accroissement du RCP est attribué à l’exaltation du champ électrique à proximité des nanoparticules plasmoniques, qui augmente l’absorption de lumière et la génération de porteur de charges dans le film de BQs, tel que démontré par l’augmentation du courant de court-circuit (26%) et de l’EQE. La comparaison des EQEs des deux dispositifs est présentée sur la Figure R10. Les spectres d’absorption des films avec ou sans nano-étoiles d’Au ainsi que les spectres d’absorption et d’extinction de films de nano-étoiles d’Au sont également

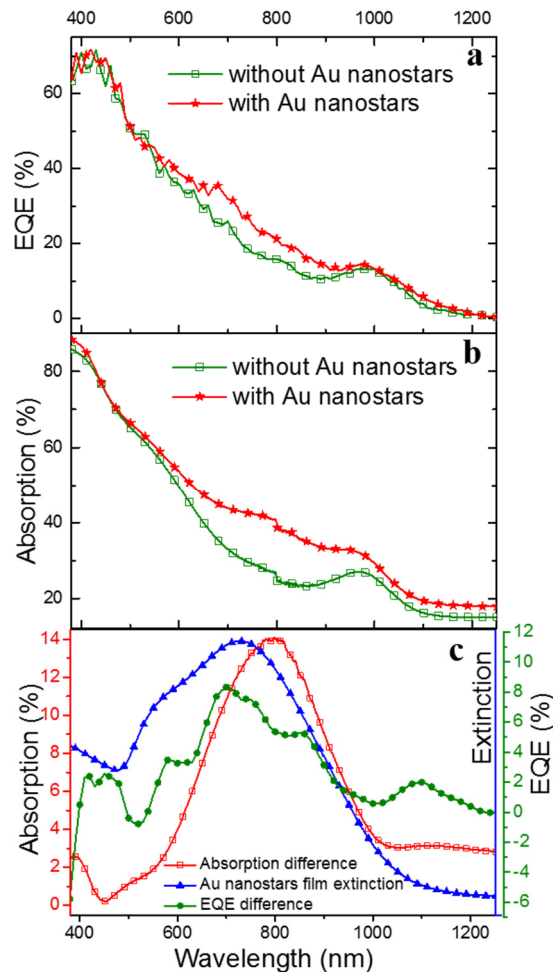


Figure R10. (a) Spectres EQE de dispositifs à HJS avec et sans nano-étoiles d’Au, (b) spectres d’absorption de films de BQs PbS/CdS coeur-coquille avec et sans nano-étoiles d’Au et (c) comparaison des différence de spectres d’absorption et différence de EQE avec spectres d’absorption de film de nano-étoiles d’Au.

présentés dans la Figure R10. Dans cette partie de la thèse, nous avons pu démontrer que l'incorporation des nanoparticules d'Or dans des films de BQs de PbS/CdS coeur/coquille peut conduire à une exaltation plasmonique des performances des dispositifs à HJs.

Les résultats extraits de cette partie sont présentés dans la publication [88].

[88] Gonfa, B.A., M.R. Kim, M.A. El Khakani, and D. Ma, *Plasmonic Enhancement of the Performance of PbS/CdS Core-shell Quantum Dots/TiO₂ Nanorod Arrays Bulk Heterojunction Solar Cells.* , être soumis.

En résumé, ce travail de thèse a démontré la possibilité de concevoir des cellules solaires de haute efficacité à base de BQs colloïdales, en particulier des BQs de PbS/CdS coeur/coquille. En effet, nous avons non seulement démontré la faisabilité de telles cellules, mais surtout leur capacité de fournir un RPC dépassant les 4%. Même si un tel RPC peut paraître modeste, il est néanmoins significatif pour des dispositifs fabriqués pour la première fois à l'échelle du laboratoire. Il est clair que le RCP de tels dispositifs doit encore être amélioré pour devenir commercialement compétitif avec les technologies établies. Les améliorations concernent différents aspects, parmi lesquels on peut mentionner : les photoélectrodes, les films de BQs et les électrodes de collection de charges. Ce travail ouvre donc la voie pour des recherches à venir sur des cellules solaires à BQs à haut rendement. Celles-ci devraient en particulier se baser sur la démonstration de principe faite dans le cadre de cette thèse qui souligne l'importance des BQs coeur/coquille et des nanoparticules plasmoniques pour étendre le spectre d'absorption vers le NIR tout en améliorant l'absorption des photons du soleil.